Neutrinos and Glashow Resonance

Auteur : Michel, Thomas
Promoteur(s) : Cudell, Jean-Rene; Bhattacharya, Atri
Faculté : Faculté des Sciences
Diplôme : Master en sciences spatiales, à finalité approfondie
Année académique : 2019-2020
URI/URL : http://hdl.handle.net/2268.2/9347

Université de Liège

Master in Space Sciences

AGO Department

Neutrinos and Glashow Resonance

Author
Thomas Michel

Supervisors
Jean-René Cudell
Atri Bhattacharya

Academic year 2019-2020

Acknowledgement

I would like to thank Pr. Jean-René Cudell for having given me the opportunity to work with him during this master thesis, always available whenever I ran into a problem, and for his kindness and patience with all my questions.

I would also like to thank Dr. Atri Bhattacharya for all his advices and guidance he showed throughout the year, during our many and pleasant meetings. Moreover, I would like to thank him for all the challenges he helped me overcome.

I would also like to thank Mister Justin Janquart without whom these 5 years would not as been as fun (especially the breaks).
Finally, I would like to thank my family, in particular my parents, my Nonno and Nonna, and Céline for providing me with unfailing support and continuous encouragement throughout my years of study and through the process of writing this thesis.

Abstract

Recent observations of ultrahigh-energy neutrinos at the km^3-volume, South Pole based detector IceCube have revealed interesting discrepancies between sets of observations distinguished only by experimental cuts but ostensibly looking at the same incoming flux of particles. The High-Energy Starting Events (HESE) sampling over 2078 days looks only at events which have their first interaction inside the detector volume and finds an event spectrum supported by a soft incoming neutrino flux ($\propto E^{-2.91}$). In contrast, the Through-going muons (Thμ) sampling, collected over 8 years, identifies only those events which have originated outside the detector but have part of their resulting tracks cutting across the detector volume and finds support for a much harder incoming flux ($\propto E^{-2.19}$). The sharp differences of these 2 spectra are brought to the forefront by the different numbers of Glashow Resonance events they predict. The Glashow Resonance is an enhancement of the electron antineutrino cross section at around 6.3 PeV within the paradigm of Standard Model physics, which should lead to a sharp spike in event rates seen around this energy. Only a single cascade at these energies has been observed — that too only when enhancing the effective detector volume beyond its instrumented one by including partially contained cascades.

We first investigate if these two disparate flux shapes and their very different predictions for the number of Glashow Resonance events can be explained — despite originating from similar sources — by standard physics alone, and find that unlikely. Therefore, we examine non-standard physics, focusing on neutrino decay, a scheme in which heavier neutrinos are not stable particles and decay into their lighter siblings. The goal is to consider an incoming neutrino flux consistent with the best-fit from the Thμ sampling and see if the effects of neutrino decay modify it in such a way that we are able to reproduce the event rates of the HESE sampling. With that objective in mind, we find that although the normal and inverted neutrino mass hierarchies lead to the same event rates when considering only standard physics, they differ widely once we include non-standard physics in the propagation of neutrinos. We find for the neutrino decay that the normal hierarchy fails to provide enough of an effect on the hard flux, and thus cannot explain the HESE event rate. The inverted hierarchy, on the other hand, proves more promising, allowing the reconciliation of the two best-fit fluxes as well as explaining the single Glashow Resonance event. We also consider the influence of the θ_{13} mixing angle and the CP violating phase δ_{CP} by taking their 3σ interval into account. These effects do not alter our qualitative conclusions.

We also note that the interactions leading to the production of neutrinos at sources are not experimentally confirmed. Therefore, we consider two different cases: 1) photo-hadronic interactions ($p\gamma$) leading to neutrinos and 2) neutrinos from high-energy neutron decay as representative examples to explore what differences to our results that would entail.

Contents

1 Introduction **1**
- 1.1 Neutrino: the little neutral one . . . 3
- 1.2 Sources of neutrinos . . . 4
  - 1.2.1 Relic neutrinos . . . 4
  - 1.2.2 Solar neutrinos . . . 5
  - 1.2.3 Supernova burst (1987A) . . . 5
  - 1.2.4 Terrestrial anti-neutrino . . . 5
  - 1.2.5 Background from old supernovae . . . 5
- 1.3 Neutrino oscillations . . . 6
  - 1.3.1 Neutrino oscillations in vacuum . . . 6
  - 1.3.2 Neutrino oscillations in matter . . . 9
- 1.4 Neutrino mass hierarchies . . . 10
- 1.5 Neutrino interactions . . . 12
  - 1.5.1 Neutrino-electron elastic scattering . . . 13
  - 1.5.2 Neutrino quasi-elastic scattering . . . 13
  - 1.5.3 Elastic neutral-current interactions . . . 14
  - 1.5.4 Deep(ly) inelastic scattering . . . 14
  - 1.5.5 Neutrino production . . . 15

2 Sources of ultrahigh-energy ν and detection **16**
- 2.1 Flux of ultrahigh-energy neutrinos . . . 16
  - 2.1.1 Atmospheric neutrinos . . . 16
  - 2.1.2 Neutrinos from extragalactic sources . . . 18
  - 2.1.3 Cosmogenic neutrinos . . . 19
- 2.2 The Waxman-Bahcall bound: an upper limit to the astrophysical neutrino flux . 20
- 2.3 IceCube: a detector for astrophysical neutrinos . . . 21
- 2.4 Neutrino detection at IceCube . . . 22
- 2.5 Types of neutrino-induced events . . . 24
  - 2.5.1 Neutral current . . . 24
  - 2.5.2 Charged current . . . 24
- 2.6 Reconstruction of the neutrino energy . . . 27
  - 2.6.1 Muon tracks . . . 28
  - 2.6.2 Cascades . . . 28
- 2.7 Expected number of events . . . 30
  - 2.7.1 Cross section: a fully theoretical framework . . . 30
  - 2.7.2 Effective area: a more realistic approach . . . 31
  - 2.7.3 Model of flux . . . 32
  - 2.7.4 Event rates and expected number of events . . . 33
  - 2.7.5 Neutrino flavour ratio . . . 33

3 The Glashow Resonance: the long sought process **35**
3.1 Cross section . . . 35
3.1.1 An introduction to resonance . . . 35
3.1.2 The Glashow Resonance . . . 37
3.2 High Energy Starting Events . . . 37
3.2.1 Cross section and effective area . . . 38
3.2.2 Fraction of $\bar{\nu}_e$ at the Earth . . . 38
3.2.3 Event rates as a function of $\bar{\nu}_e$ . . . 39
3.2.4 Event rates as a function of the spectral index γ . . . 40
3.3 PeV Energy Partially Contained Events . . . 42
3.3.1 Event rates as a function of ζ . . . 43

4 Non-standard physics in neutrino oscillations **47**
4.1 Flavour selection at the source: spectral averaging . . . 47
4.2 Flavour selection at Earth . . . 48
4.3 Flavour selection during neutrino propagation . . . 49
4.3.1 Neutrino decay: a Standard Model extension . . . 49
4.3.2 CP violating phase and θ_{13} variation . . . 57
4.4 IceCube flux: refitting the flux after decay . . . 62
4.4.1 Another neutrino production mechanism: neutron decay . . . 66

Summary and conclusions **71**

Appendices **74**

A Feynman rules **75**
A.1 Vertex of quantum electrodynamics . . . 75
A.2 Vertex of weak interaction . . . 76
A.3 Propagator . . . 76

B Neutrino mixing and flavour ratio **77**
B.1 Flavour ratio after mixing . . . 77
B.2 Flavour ratio $\nu_e : \nu_\mu : \nu_\tau = 1 : 1 : 1$ . . . 79

C Narrow-Width Approximation **80**

D Glashow resonance cross section **81**

Chapter 1

Introduction

For a long time, humanity has studied the Universe using visible light coming from the stars. During the last century, Science has progressed, allowing us to look at the Cosmos from different perspectives: infrared, X-rays, γ rays, and through other parts of the electromagnetic spectrum as well, leading to the discovery of new phenomena such as Gamma Ray Bursts and Active Galactic Nuclei. Similarly to using gravitational waves to probe the Universe, using another particle would open a new window. This other particle could be the neutrino. However, as opposed to others such as photons, which were and are still used, neutrinos interact very feebly with matter. Thus, there are still many mysteries surrounding them. Important questions such as their origins are still open.
This feeble interaction must not be seen as a disadvantage. Rather, when observing a neutrino, it can be assumed it arrived unscathed, as opposed to protons that would be completely scattered by intergalactic magnetic fields, or photons that would interact with matter. This elementary particle is thus an ideal astronomical messenger on the scale of cosmological distances. The downside is, of course, the difficulty to detect them.

Why are neutrinos important for astronomy? As just written, they allow to obtain information unaffected by the interstellar medium, *i.e.* information almost completely intrinsic to the source. Photons might undergo reddening due to interstellar dust. In that case, the observation will be affected, but still possible. However, the optical depth at a given place and time in the Universe can such that said place is simply opaque to photons. This is where neutrinos are useful: there are places, opaque to photons, but transparent to neutrinos. This enables us to observe previously unseen part of the Cosmos. This was confirmed in 2013, when the first high-energy astrophysical neutrino was detected, confirming that extraterrestrial neutrinos are key astronomical messengers when it comes to observing regions of the Universe that were opaque at certain wavelength [1]. Indeed, this was he first detection of neutrino with energy higher than 1 MeV, *i.e.* a high-energy neutrino, that in addition was coming from outside our Solar System. This must however not be seen as a random success due to hope of observing neutrinos from regions in which photons cannot travel. At the time, cosmic rays were already well studied. If their models were right, neutrinos were expected to be produced by the reactions occurring within the cosmic rays generator. The observation mentioned above is a first clue that neutrinos are indeed tightly linked to cosmic rays generator.

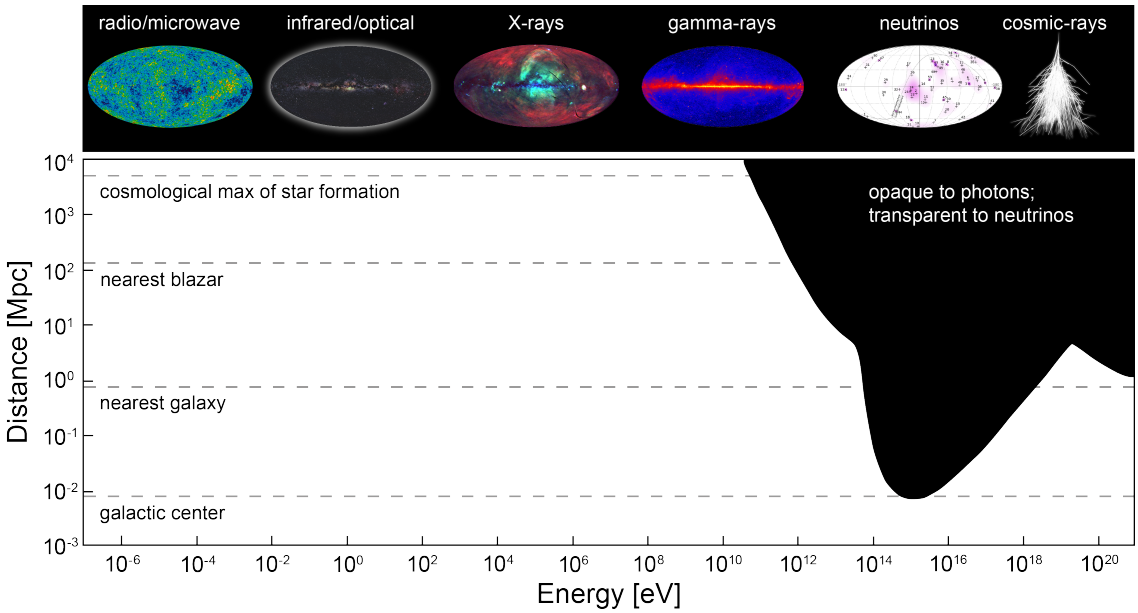

Figure 1.1: Figure showing the region transparency for photons and neutrinos as a function of the distance and the energy. The grey region is transparent to both, whereas the black region only lets neutrinos pass through. Before the development of neutrino astronomy, it was impossible to observe regions of the Universe at large distance and high energy. For instance, the sources of cosmic rays could not be observed. The wavelength domains corresponding to the energy axis are shown on top. The horizontal dashed lines represent the typical distance of different objects, extracted from [2].

The since-then measured neutrino flux implies that an important fraction, if not all, of the energy in the non-thermal Universe comes from powerful hadronic generators, such as neutron star or black hole. This was further confirmed in July 2018, when the simultaneous detection of neutrinos by IceCube and photons by Fermi, MAGIC and other experiments, from blazar TXS 0506+056. This was the first identification of a likely extragalactic neutrinos and high-energy cosmic ray source. The consequences of this breakthrough detection were important. Firstly, it simply confirms the relation between neutrinos and cosmic rays discussed above. Secondly, a multimessenger collaboration with detector and scientists was set up to do follow-up observations by optical, X-ray and gamma-ray telescope triggered by real-time neutrino alerts from IceCube. This collaboration has begun on September 22, in 2017. In practice, the alert is sent within one minute of neutrino(s) detection. The goal is to allow the observation of rapidly fading electromagnetic source, or gravitational waves [2].

In the first chapter of this work, the neutrinos will be presented. Their potential sources will be discussed. Neutrino oscillations will then be explained, followed by a presentation of the neutrinos mass hierarchies. Finally, their interactions will be detailed. This will lead us to a high-energy phenomenon called the Glashow Resonance, which although is clear from a theoretical point of view, is still undetected. The mystery of this resonant phenomenon, which will be at the heart of this thesis, can be summarised as follows: being resonant implies that it is expected to be observed quite often, of the order of once per year. However, during several years of observation, while more than ten events were expected, only 1 was found. In the second chapter, the possible sources of high-energy neutrinos will be analysed in details. Their means of detection will be explained. Afterwards, several types of events with their corresponding topologies will be

described. At that point, all the cards necessary to compute the expected number of events will be in our hand. The third chapter will focus on the Glashow Resonance that will be introduced in the first chapter. The influence of parameters such as the initial electron antineutrino fraction on the number of events will be considered. The notion of partially contained event as well as its importance in the problem studied in this thesis will then be presented. At that point, we will have encountered the second key problem of this thesis: the discrepancy between the HESE and Thμ fit fluxes.
The fourth and last chapter will present non-standard physics interactions to try to explain the partial disappearance of Glashow Resonance event as well as the previously mentioned discrepancy. Processes at the source, during propagation and at the Earth will be considered, with a focus on neutrino decay, to try to modify the neutrino spectra. The result will be a new refitted flux, taking into account non-standard physics, and trying to explain as well as possible the observed rate of events.

1.1 Neutrino: the little neutral one

Neutrinos were predicted by Pauli in 1931 in order to "fix" the apparent violation of energy conservation in β^- decays. The name was given later by Fermi, in 1934: the neutrino, symbolised by the Greek letter ν. In Italian, "neutrino" means "little neutral one". A neutrino should be a massless particle that interacts poorly with matter, otherwise it would have been detected before. The new particle was only discovered in 1959 by C. Cowan and F. Reines by studying particles created near a nuclear power plant [3]. The neutrino that was found seemed to be somehow linked to the electron. A few years later, in 1962, another neutrino was detected. This time, it seemed to be linked to muon. When the tau particle was discovered, as it is like a heavier version of the electron and the muon, a tau neutrino was predicted, then detected. To detect them, neutrino detectors such as the Homestake experiment [4] were built. It could detect electron neutrinos from the Sun. The experimental device worked, but only one-third of the expected number of neutrinos were detected. This problem was known as the "solar neutrino problem" and was confirmed by a later experiment in Japan, Kamiokande. The lack of detection was explained by considering that neutrinos can oscillate between different flavour: a neutrino created as an electron neutrino might be observed as a muon neutrino because of this. These oscillations can be obtained from a quantum point of view, as will be shown later. An important consequence is that for these to happen, the mass of the neutrino should be non-zero [5]. As a reminder, the particle was understood to be massless initially. However, this non-zero mass should not be too high in order not to invalidate the problems it had previously solved, such as the energy conservation in β^- decays. An announcement by the Japanese experiment was made to confirm this statement. At the time, the scale of mass was measured to be less than one-millionth of the electron mass [6].

Let us come back te the fact that neutrinos do not interact a lot with matter. In the Universe, there are four fundamental interactions. By order of decreasing strength, these are: the nuclear force, electromagnetism, the weak interaction and gravity. The first one acts on hadrons, which have a non-zero strong hypercharge. The same way electromagnetism acts on particles with a non-zero electrical charge, the strong hypercharge can be seen as the equivalent of the electrical one, for another type of interactions. The second one acts only on charged particles, as it was just written. The last two act on everything. Gravity is especially weaker than the others.
As neutrinos have no electrical nor strong hypercharge, they are not affected by either of the two strongest interactions. As their mass is very weak, one can consider that they are not affected a lot by gravity either. Thus, the only remaining interaction is the weak one. These are the only elementary particles to interact that way [7].

	Gravitation	Weak	Electromagnetic	Strong
Strength relative to electromagnetic interaction for two u quarks at 10^{-18} m	10^{-41}	0.8	1	25

Table 1.1: Table showing the strength of different interaction, normalised by the the electromagnetic force between two u quarks separated by 10^{-18} m, from [8]

There are about 100 trillion neutrinos that pass through our body every second [9]. Due to their feeble interaction, this goes unnoticed. However, it does not change the fact that they do. Thus, an important yet not completely answered question is where do all these neutrinos come from.

1.2 Sources of neutrinos

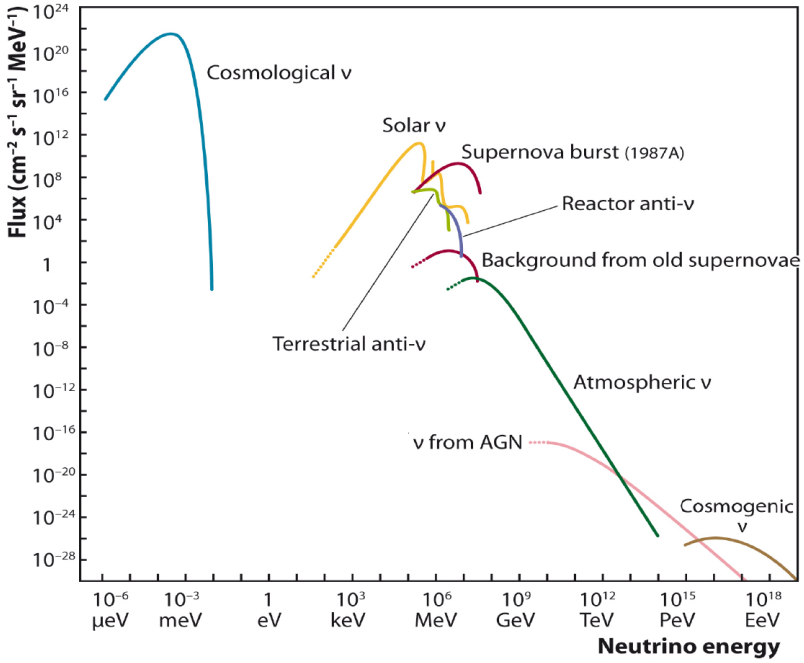

Figure 1.2: Measured and predicted flux of neutrinos, from natural sources, or reactors, as a function of the neutrino energy, from [10].

Neutrinos can come from several sources. As was mentioned above, they interact only weakly with matter. Thus, their detection is hard. A consequence is that determining the flux is also challenging. It is hard to tell at a first glance if it is isotropic, continuous, how it depends on energy, and so on. It is nonetheless still possible to combine theoretical predictions with measurements to have an idea of the flux of neutrinos as a function of their energy, as it was done on Fig.1.2. Please consider that the plot does not distinguish between the three neutrino flavours.

1.2.1 Relic neutrinos

The lowest energy neutrinos that are expected are called cosmological or relic neutrinos. They come from the cooling down of the Universe. They were the first particles to freeze out, *i.e.* to decouple, amongst Standard Model particles. It happened at a temperature of 1 MeV [11],

but due to the expansion of the Universe, these kinds of neutrinos have an energy spectrum that ranges only from the scale of μeV to meV. Moreover, these are only theoretical predictions. They are not detected experimentally, as the range of energy is quite small. There is a gap in the energy spectrum before the next sources of neutrinos. This part of the spectrum is still unknown, and no usable method exists to measure it yet [10].

1.2.2 Solar neutrinos

After a gap in which no neutrino are known so far come those of solar origins. One can note that whereas for the cosmological ones, there was a single "spike", here there are several. This comes from the fact that there are several energies at which neutrinos are produced in the Sun, which corresponds to different reactions. A first one is during the first stage of nuclear burning. When two hydrogen nuclei (protons) fuse to form a helium nucleus, which is called the *pp* reaction, a neutrino is also emitted. Another is the proton-electron-proton reaction, or *pep*, which happens one time every 400 *pp* reaction. There is also the decay of an isotope of boron, ^8B, and the neutrinos from the CNO Cycle. Without going into the details, during each cycle, two neutrinos are produced: one from the decay of the ^{13}N, the other from the decay of ^{15}O [12]. There are also other sources, such as the interaction of ^7Be with an electron, which will give a ^7Li and a ν_e [13].

These are all well-understood Standard Model interactions. They can be detected. Their energies ranges from a few eV to MeV.

1.2.3 Supernova burst (1987A)

At the end of life of a massive star, when it collapses into a neutron star, almost all of the bonding energy is released in the form of neutrinos of all flavours. These are emitted in only several tens of second, whereas the photons take thousands of years to emerge from the star. Moreover, the neutrino luminosity is roughly 100 higher than the optical one [14]. As can be seen on the graph, their energy is just slightly higher than the ones coming from the Sun, hence they were detected with experiments that were initially used for the solar neutrinos. SN1987A is a supernova located in the Large Magellanic Cloud that was detected in the Super-Kamiokande, Baksan and IMB detector [15].

1.2.4 Terrestrial anti-neutrino

These are simply anti-neutrinos produced by nuclear decay, or byproducts of nuclear fission. Let us note that here, one speaks only of antineutrinos. However, all the other subsections speak of neutrinos, but should be understood as "neutrinos and antineutrinos".

1.2.5 Background from old supernovae

These are the neutrinos that come from previous supernovae and that reach us. They have the same energy as those from the supernova 1987A, but as they come from further, the flux is lower due to geometrical dilution.

If the energy of the neutrinos is above 100 MeV, one speaks of high-energy neutrinos [16]. If it is above 1 PeV, one speaks in this case of ultrahigh-energy neutrinos [17]. Both will be described in details in Chapter 2. The different ranges of energy for the neutrino sources are shown in the horizontal axis of Fig. 1.2, whereas the flux is represented on the vertical axis. The range of energy that is of interest in this work is from 100 TeV. It corresponds to the threshold of IceCube.

We explained that this plot does not take into account the three flavours. However, one can wonder what effect will these have on the propagation of a neutrino state.

1.3 Neutrino oscillations

As mentioned before, there are three flavours of neutrinos: ν_e, ν_μ and ν_τ, which are the three types of neutrinos that can play a role in the different standard model interactions. They can be expressed as combinations of mass eigenstates, *i.e.* eigenstates of the Hamiltonian that describes free neutrinos [18]. The fact that the neutrinos produced by standard model interactions are not the ones that are solutions of the evolution equation, coupled to the fact that it is this equation dictates the propagation of neutrino states will lead to a phenomenon known as neutrino oscillation.

1.3.1 Neutrino oscillations in vacuum

To understand where the neutrino oscillation phenomenon comes from, let us consider a situation where instead of the three flavours, there are only two of them, ν_e and ν_μ. The idea behind the development is the same, the maths are just simpler. One can relate the mass eigenstates to the flavour states by a unitary transform as follows:

$$\begin{pmatrix}\nu_e\\ \nu_\mu\end{pmatrix} = \begin{pmatrix}\cos\theta & \sin\theta\\ -\sin\theta & \cos\theta\end{pmatrix}\begin{pmatrix}\nu_1\\ \nu_2\end{pmatrix} \tag{1.1}$$

The mass eigenstates are such that $\mathcal{H}_0^m |\nu_i\rangle = E_i |\nu_i\rangle$, with $E_i = \sqrt{p^2 + m_i^2}$, with

$$\mathcal{H}_0^m = \begin{pmatrix}E_1 & 0\\ 0 & E_2\end{pmatrix} \text{ [19]}$$

the vacuum Hamiltonian in the mass basis, that will generate propagation of the neutrino state in time. However, the neutrinos produced by Standard Model interactions are the flavour eigenstates ν_l, $l = e, \mu, \tau$. Therefore, since we want to describe the evolution of these eigenstates rather than the mass ones, it is useful to reexpress the vacuum Hamiltonian in the flavour basis. Doing so results in

$$\mathcal{H}_0^f = \frac{\Delta m^2}{4E}\begin{pmatrix}-\cos 2\theta & \sin 2\theta\\ \sin 2\theta & \cos 2\theta\end{pmatrix} \text{ [20]}$$

Please note that the neutrinos are assumed to have approximately the same energy, hence the E without index. Its comes from the ultra-relativistic approximation that will be taken later, which can be written:

$$\begin{aligned} E_i = \sqrt{p^2 + m_i^2} &\approx\ p(1 + \frac{m_i^2}{2p^2}) \\ &= E + \frac{m_i^2}{2E} \end{aligned}$$

Since the second term is much smaller than the first one, one can write $E_1 \approx E_2 \approx E$. Switching from one basis to the other is done through a rotation matrix, more specifically the one that links the flavour and the mass eigenstates, given in (1.1). Let us first consider the evolution equation of a neutrino state. The relation between $\mathcal{H}_0^f$ and $\mathcal{H}_0^m$ will appear quite straightforwardly.

Let $(\nu(t)) \equiv (|\nu(t)_e\rangle, |\nu_\mu\rangle)^\dagger$ be a neutrino state in the 2-flavour framework. It will evolve according to the following equation:

$$i\frac{d}{dt}(\nu(t)) = \mathcal{H}_0^f(\nu(t))$$

We can express that state as a function of the mass eigenstate in the 2-flavour framework:

$$\begin{pmatrix} |\nu_e\rangle \\ |\nu_\mu\rangle \end{pmatrix} = U \begin{pmatrix} |\nu_1\rangle \\ |\nu_2\rangle \end{pmatrix}$$

where $U = \begin{pmatrix} \cos\theta & \sin\theta \\ -\sin\theta & \cos\theta \end{pmatrix}$ is the mixing matrix relating the mass and flavour eigenstates. Therefore, evolution equation can be rewritten

$$\begin{aligned} i\frac{d}{dt}\begin{pmatrix} |\nu_e\rangle \\ |\nu_\mu\rangle \end{pmatrix} &= iU\frac{d}{dt}\begin{pmatrix} |\nu_1\rangle \\ |\nu_2\rangle \end{pmatrix} \\ &= U\mathcal{H}_0^m \begin{pmatrix} |\nu_1\rangle \\ |\nu_2\rangle \end{pmatrix} \\ &= U\mathcal{H}_0^m U^\dagger \begin{pmatrix} |\nu_e\rangle \\ |\nu_\mu\rangle \end{pmatrix} \end{aligned}$$

One can then write $\mathcal{H}_0^f = U\mathcal{H}_0^m U^\dagger$ [19].
In the following, we will work in the ultra-relativistic approximation presented above. Inserting this into $\mathcal{H}_0^m$ yields

$$\begin{aligned} \mathcal{H}_0^m &= \begin{pmatrix} E_1 & 0 \\ 0 & E_2 \end{pmatrix} \\ &\approx \begin{pmatrix} p & 0 \\ 0 & p \end{pmatrix} + \frac{1}{2E}\begin{pmatrix} m_1^2 & 0 \\ 0 & m_2^2 \end{pmatrix} \end{aligned}$$

Since the first term will only give rise to a global phase factor, it can be dropped. Therefore, in the literature, the vacuum Hamiltonian in the mass basis is also written

$$\mathcal{H}_0^m = \frac{1}{2E}\begin{pmatrix} m_1^2 & 0 \\ 0 & m_2^2 \end{pmatrix}$$

Let us now consider neutrino oscillations. Let us assume that the initial neutrino state is a ν_e. It can be written:

$$|\nu(t=0)\rangle = |\nu_e\rangle = \cos\theta\,|\nu_1\rangle + \sin\theta\,|\nu_2\rangle$$

The neutrino state will evolve according to the evolution equation

$$i\frac{d}{dt}|\nu(t)\rangle = \mathcal{H}_0^f\,|\nu(t)\rangle$$

The solution as a function of time of this equation can be written:

$$|\nu(t)\rangle = \cos\theta\,|\nu_1\rangle\,e^{-iE_1 t} + \sin\theta\,|\nu_2\rangle\,e^{-iE_2 t}$$

Using an ultra-relativistic approximation, one has:

$$|\nu(t)\rangle \approx e^{-iE_1 t}\left(\cos\theta\,|\nu_1\rangle + \sin\theta\,|\nu_2\rangle\,e^{\frac{i\Delta m_{12}^2 t}{2p}}\right), \text{ with } \Delta m_{12}^2 = m_1^2 - m_2^2.$$

We can then compute the probability that, starting from the state $|\nu_e\rangle$, one observes $|\nu_\mu\rangle$. The result is

$$\begin{aligned} P(\nu_e \to \nu_\mu) &= |\,\langle\nu_\mu|\nu_e(t)\rangle\,|^2 \\ &= \sin^2(2\theta)\sin^2\left(\frac{1.27\Delta m_{12}^2 L}{E}\right) \end{aligned}$$

with L the travelled distance in m, Δm^2_{12} the difference of the squared masses of the two neutrino flavours in meV^2, and E the energy in MeV [4]. The evolution of this probability as a function of the ratio L/E is shown in Fig.1.3.

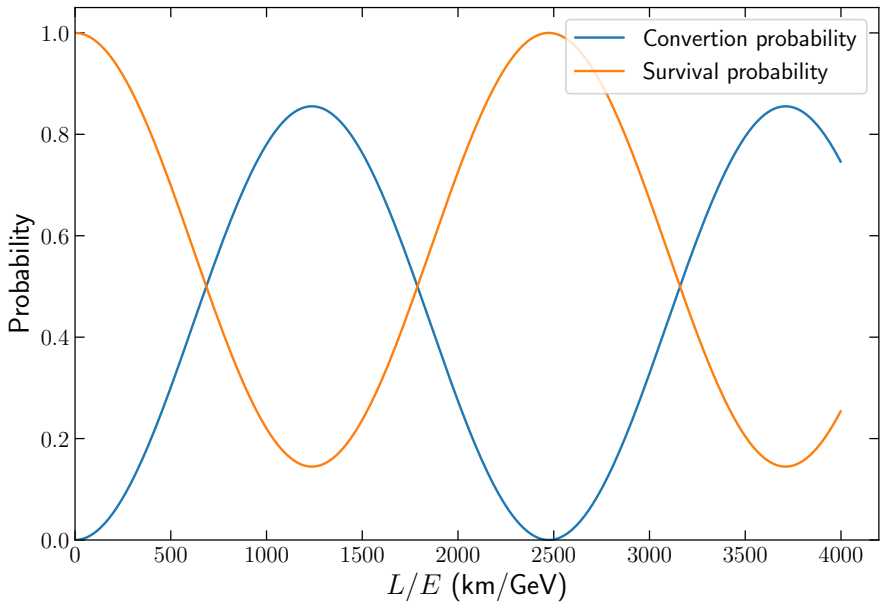

Figure 1.3: Probability to observe the ν_e or ν_μ generation, starting with an ν_e. As there are only two generations, the probabilities are dependant: $P(\nu_\alpha \to \nu_\beta) = 1 - P(\nu_\beta \to \nu_\alpha)$. If the oscillation is fast, the oscillating terms are averaged. Δm^2 was arbitrarily chosen as 1 eV^2, and θ as the current best fit given by [21], 33.82°, from [10].

In the case of three generations, there would be three Δm^2, but only two that are independent. One can see that if neutrinos were massless, or if they had the same mass, no oscillation would occur.

The two-flavour situation is useful to introduce the maths behind the oscillation phenomenon. In reality, there are three flavours, thus the previous model does not suffice. However, it is not completely irrelevant. As it will be shown later, the Δm^2 between the first and second mass eigenstates is of the order of 10^{-5} eV^2, whereas it is of the order of 10^{-3} for the second and third eigenstates. Therefore, the first two eigenstates being almost degenerated in mass, the 2-flavour model can be used as an approximation. The different coefficients that will describe the combination of the mass eigenstates in the 3-flavour scheme can be summed up in a matrix, called the Pontecorvo-Maki-Nakagawa-Sakata matrix, or PMNS matrix [22] such that:

$$\begin{pmatrix} \nu_e \\ \nu_\mu \\ \nu_\tau \end{pmatrix} = \begin{pmatrix} U_{e1} & U_{e2} & U_{e3} \\ U_{\mu 1} & U_{\mu 2} & U_{\mu 3} \\ U_{\tau 1} & U_{\tau 2} & U_{\tau 3} \end{pmatrix} \begin{pmatrix} \nu_1 \\ \nu_2 \\ \nu_3 \end{pmatrix}$$

Please note that this matrix is a generalisation to 3 flavours of the U matrix introduced above. For very long distance, when the oscillatory part will have averaged out, the probability to observe ν_β, starting with a ν_α, $\alpha, \beta = e, \mu, \tau$ is given by:

$$P(\nu_\alpha \to \nu_\beta) = \sum_j |U_{\alpha j}|^2 |U_{\beta j}|^2$$

When the sources of neutrinos were described, the expected ratio was $1:2:0$. This is only valid at the source. The ratio that one measures will be different due to the effect of neutrino mixing. For any initial ratio, the expected final one can be computed. Moreover, it can be shown analytically that starting with a $1:2:0$ ratio will result in roughly $1:1:1$ on Earth. One has to bear in mind that the initial and final flux ratios of $1:2:0$ and $1:1:1$ take into account both neutrinos and antineutrinos. As it will be explained later, IceCube, the biggest neutrino detector so far, does not distinguish them. However, when speaking of particular types of events such as the Glashow Resonance, it is important to distinguish between particles and anti-particles.
All mathematical details can be found in Appendix B.

1.3.2 Neutrino oscillations in matter

Let us now consider the oscillations of neutrinos in matter. Once again, a neutrino state can be described by a combination of mass eigenstates. The difference is that this time the Hamiltonian $\mathcal{H}$ is different. It can be written $\mathcal{H} = \mathcal{H}_0 + \mathcal{H}_1$ with $\mathcal{H}_0$ the vacuum Hamiltonian, and $\mathcal{H}_1 |\nu_\alpha\rangle = V_\alpha |\nu_\alpha\rangle$. V_α is the effective potential felt by ultra-relativistic neutrinos in the medium. It can be shown that $V_\alpha = V_{CC}\delta_{\alpha e} = \sqrt{2}G_F N_e \delta_{\alpha e}$ [23][20]. Thus, only V_e is non-zero. For simplification reasons, let us consider once again a situation where there are only two neutrino flavours, ν_e and ν_μ, as above. The Hamiltonian has the expression

$$\mathcal{H} = \frac{\Delta m^2}{4E}\begin{pmatrix} -\cos 2\theta & \sin 2\theta \\ \sin 2\theta & \cos 2\theta \end{pmatrix} + \begin{pmatrix} V_e & 0 \\ 0 & 0 \end{pmatrix}$$

where the first term is the vacuum Hamiltonian, the other term expresses the interaction in matter, and as there are mainly electrons and no tau or muon, only the first element is non-zero and the second term characterises the matter interaction. By using the expression of V_e and defining $A = \frac{2\sqrt{2}G_F N_e E}{\Delta m^2}$, the Hamiltonian becomes

$$\mathcal{H} = \frac{\Delta m^2}{4E}\begin{pmatrix} -\cos 2\theta + A & \sin 2\theta \\ \sin 2\theta & \cos 2\theta - A \end{pmatrix}$$

One can then define the effective mixing angle in matter θ_m as follow [24][20]:

$$\begin{aligned} \Delta m^2_m &= C\Delta m^2 \\ sin2\theta_m &= \frac{sin2\theta}{C} \\ C &= \sqrt{(\cos 2\theta - A)^2 + sin^2 2\theta} \end{aligned}$$

It allows to express the Hamiltonian in the same form as the vacuum one:

$$\mathcal{H} = \frac{\Delta m^2_m}{4E}\begin{pmatrix} -\cos 2\theta_m & sin2\theta_m \\ sin2\theta_m & \cos 2\theta_m \end{pmatrix}$$

As this operator has the same form as the vacuum Hamiltonian, it will lead to the same form of evolution of the neutrino state, this time in matter. The oscillation probability will also have the same form:

$$P(\nu_e \to \nu_\mu) = sin^2(2\theta_m) sin^2\left(\frac{1.27\Delta m^2_m L}{E}\right)$$

Once again, the neutrino oscillations depend on the difference of the squared masses. What differs from before is that the masses are not the ones of the eigenstates, but rather effective masses which depend on the medium.

The Mikheev-Smirnov-Wolfenstein effect

The Mikheev-Smirnov-Wolfenstein (MSW) effect is the name of the resonant phenomenon in which the mixing angle in matter will be maximum and equal to $\pi/4$. In other words, the mixing is maximal and can be significant, such that it is possible to observe a total transition between the two flavours, given that the resonance region is wide enough, even if the vacuum mixing angle θ is small. It happens when $A = \cos 2\theta$. It is possible to express the effective mixing angle as a function of the vacuum one:

$$tan2\theta_m = \frac{tan2\theta}{1 - \frac{A}{\cos 2\theta}}$$

Let us note that at the resonance, the difference of the squared effective masses is the smallest. The same reasoning can be done in a 2 flavours situation for antineutrinos. The difference is that there is a minus sign before every A. Thus, depending on the Δm^2, the behaviour of neutrino and anti-neutrino oscillations in matter can be different. For normal matter, A is positive, which can be used to constrain the mass hierarchy [24][20].

Whether one considers neutrino oscillations through vacuum or matter, the difference of the squared (effective) masses appears. As these oscillations happen, it implies that this difference is non-zero. In other words, the previously thought massless neutrinos do possess a mass, albeit very low. Moreover, not all the masses are equal. This leads us to the neutrino mass hierarchies and the associated problem regarding as to which one is the right one.

1.4 Neutrino mass hierarchies

Representing the neutrino masses as m_1, m_2, and m_3, only the differences of their square are directly measurable at oscillation experiments. This results in an ambiguity known as the "neutrino mass hierarchy problem". There exists two situations: either m_2 is lighter than m_3 and the hierarchy is called "normal", or it is the opposite, and the hierarchy is called "inverted".

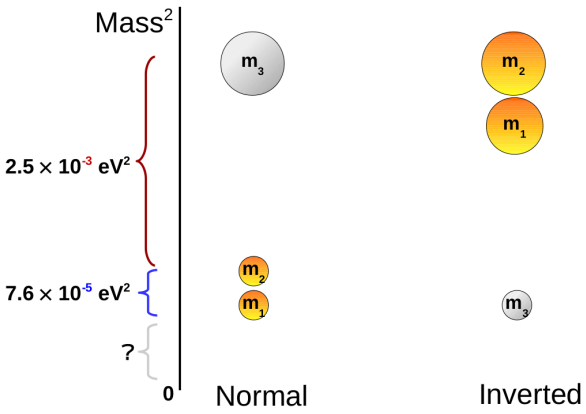

Figure 1.4: The two possible mass hierarchies. The coloured circles represent the mass eigenstate. The higher, the heavier. Depending on the position of m_3 with respect to the two others, one speaks of the normal or inverted mass hierarchy. Only the differences are known, not the absolute value of each mass. Taken from [25].

Apart from the study of neutrinos, the problem of the hierarchy is important as it has several implications. During the early stages of the cosmos, the four fundamental forces were believed to be unified. Several theories exist. Some predict a normal mass hierarchy, while others lead to an

inverted one. Thus, solving this problem can help us to understand better the early Universe, as it is not possible to recreate the conditions under which the interactions would unify yet. Solving this problem will play a role in the understanding of the present-day Universe as well. It is still not completely clear whether a neutrino and an antineutrino are two separate entities, or if a neutrino is its own antiparticle. Knowing which mass hierarchy is the actual one, and where it does come from might give us insights into this problem. If the latter is the reality, then the neutrino would be considered to be a Majorana particle. A neutrino and an antineutrino would just be two aspects of the same concept. The last important consequence of the mass hierarchy problem is the matter-antimatter imbalance. Right after the Big Bang, the Universe should have created equal amounts of matter and antimatter. After interaction, everything should have vanished, leaving only energy behind. If the leptonic number is not conserved, it could allow an asymmetry between matter and antimatter, thus explaining the world we see today. Such an explanation could be proven through neutrinoless double-beta decay. It is a process through which a nucleus decays into different nuclei, emitting two electrons and two antineutrinos. If the neutrino is its own antiparticle, two nuclei could decay, producing two electrons, without neutrinos, since one emitted neutrino will be absorbed by the other nucleus, meaning that the exchanged neutrinos are virtual. This process would favour matter over antimatter as no antimatter is created [26].

Finally, let us consider how the mass hierarchies are determined. Hyper-Kamiokande will observe atmospheric neutrinos. The ones that pass through the Earth, in other words, those coming from below the detector, will be influenced by the matter inside our planet. Some muon (anti)neutrinos will oscillate into electron (anti)neutrinos, and the opposite will be true as well. These effects depend on the mass hierarchy. Thus, by comparing the expected number of events with the observed one, the differences of the squared masses can be inferred. The discrepancy between the predicted rates of the two situations are of the order of 5 to 10%, but Hyper-Kamiokande is nonetheless able to measure it.

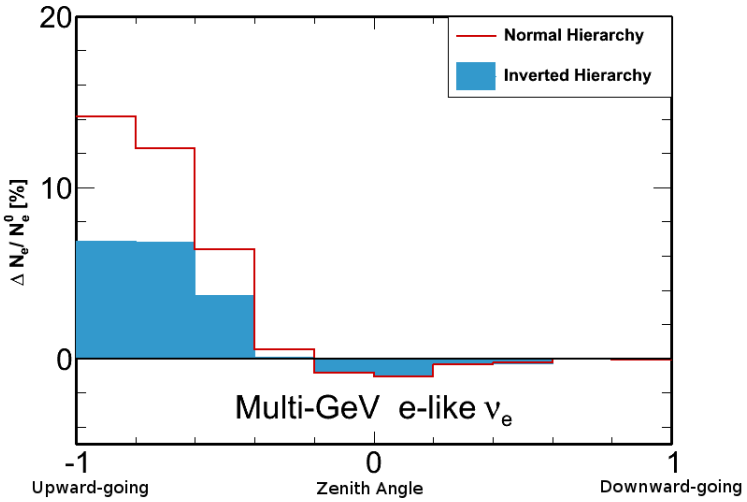

Figure 1.5: Normalised expected number of events for the possible mass hierarchies as a function of the zenith angle. The blue solid bars refer to the inverted hierarchy, whereas the red lines represent the normal one. The values are normalised by the number of events that would be observed if no oscillation occurred, which would mean that the mass hierarchy problem would not matter.
[25]

Assuming a given hierarchy, the elements of the PMNS matrix can be determined experimentally. The latest results in the normal mass hierarchy, considering the 3σ range of each element, are

[21]:

$$U = \begin{pmatrix} 0.821^{+0.021}_{-0.024} & 0.550^{+0.035}_{-0.032} & 0.150^{+0.006}_{-0.007} \\ 0.308^{+0.188}_{-0.064} & 0.600^{+0.078}_{-0.133} & 0.738^{+0.034}_{-0.092} \\ 0.480^{+0.045}_{-0.193} & 0.580^{+0.113}_{-0.092} & 0.658^{+0.091}_{-0.040} \end{pmatrix}$$

For the inverted mass hierarchy, one has:

$$U = \begin{pmatrix} 0.821^{+0.021}_{-0.020} & 0.550^{+0.029}_{-0.032} & 0.150^{+0.005}_{-0.007} \\ 0.403^{+0.114}_{-0.166} & 0.537^{+0.158}_{-0.082} & 0.742^{+0.021}_{-0.093} \\ 0.404^{+0.125}_{-0.147} & 0.640^{+0.065}_{-0.173} & 0.654^{+0.093}_{-0.025} \end{pmatrix}$$

The data that were used to obtain these results come from various sources. The one that had the biggest contribution were Super-Kamiokande and Borexino for the solar experiments, Super-Kamiokande for the atmospheric ones, and KamLAND, Double Chooz, MINOS, T2K and NOνA for the reactor and accelerator experiments. More details can be found in [27].

To observe neutrinos, they must interact with the detector. They can do so through the weak interaction. Before reviewing the possible means to do so, let us mention that the explanations up to now are in the realm of Standard Model physics. Currently unknown non-standard physics interactions may play an important role in the final neutrino, greatly straying from the expected fluxes given by the PMNS matrix. This will be discussed in more details further in this work.

1.5 Neutrino interactions

As was explained before, neutrinos only interact through the weak interaction. Their possible interactions can be represented by two Feynman diagrams. They correspond to the neutral and charged current interactions:

Figure 1.6: Feynman diagram of the Charged Current, or CC (left) and Neutral Current, or NC (right). l can be any leptonic flavour. The wavy line represents a boson.

In the diagram for the charged current interaction, l may be any leptonic flavour, *i.e.* e, μ or τ. The boson is the charged W. Depending on its charge, the neutrino and lepton are particles or antiparticles, as the total charge must be conserved. For the neutral current diagram, the boson is a Z^0, so the total charge is 0. One speaks of charged (neutral) current if the interaction boson is a charged $W^{\pm}$ (neutral Z^0).

A diagram that represents an interaction is called a vertex. Details about their mathematical expression can be found in Appendix A. The charged current vertex will be used when studying the Glashow Resonance process further in this work.

1.5.1 Neutrino-electron elastic scattering

Neutrinos and antineutrinos can interact with electrons through elastic scattering:

$$\overset{(-)}{\nu_l} + e^- \rightarrow \overset{(-)}{\nu_l} + e^-$$

where $l = e, \mu, \tau$ is the neutrino flavour. The term "elastic" comes from the fact that the incoming and outgoing particles are of the same type, which implies that there is no energy threshold for the process. It only redistributes the energy and momentum. An important feature to mention is that the produced electron moves in a direction close to the one of the incoming neutrino. The detectors mentioned above such as SNO use this elastic scattering to detect neutrinos, as the final electron will emit Cherenkov radiation. Let us note however that depending on the fact that the incoming particle is a neutrino or antineutrino, the Feynman diagrams will not be the same. In the case of a neutrino, the diagram of the elastic scattering is the one on Fig.1.7a. If it is an antineutrino, the neutral current interaction will be the same, but the charged current one will be different. The CC t-channel is replaced by a CC s-channel, as can be seen on Fig.1.7b. Let us note that the following diagram are represented for electron (anti)neutrino. If one considers an incoming $\overset{(-)}{\nu}_{\mu,\tau}$, only the Z^0 t-channel diagram would contribute since there are no vertices containing a $\bar{\nu}_{\mu,\tau}$ and and e.

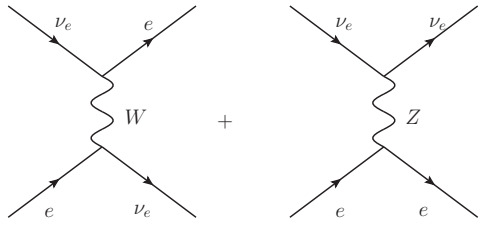

(a) Feynman diagram of an electron neutrino-electron elastic scattering. The process is written $\nu_e + e \rightarrow \nu_e + e$, but it is actually the sum of two diagrams, as the interaction boson can be a charged W or a neutral Z^0.

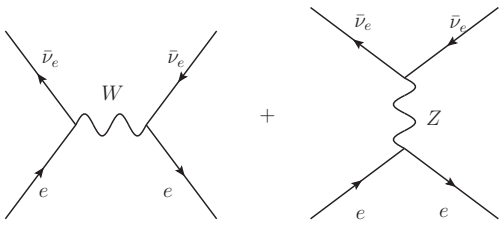

(b) Feynman diagram of an antineutrino-electron elastic scattering.

Figure 1.7

One can note that there will be no neutrino-tau or neutrino-muon scattering, since these two particles are unstable and thus not found in the detector.

1.5.2 Neutrino quasi-elastic scattering

Here, quasi-elastic scattering refers to the charged-current processes in which a neutrino scatters off a nucleon, converting a neutron into a proton or vice-versa depending on whether the incoming neutrino is a particle or an antiparticle. For such a process to happen, the incoming neutrino must have an energy above a certain threshold, which vary from one reaction to another. The general form of an inelastic scattering is:

$$\overset{(-)}{\nu_l} + A \rightarrow \sum_X X$$

The reactions as well as their threshold are summarised in Table 1.2. The term "quasi-elastic" comes from the fact that although the nucleon which the neutrino interacts with remains a single nucleon, the charge changes through the charged current interaction [28].

Let us show some examples of these type of processes:

$$\nu_l + n \to p + l^-, \qquad \bar{\nu}_l + p \to n + l^+$$

The second process where $l = e$ is called the inverse neutron decay.

Another process that can fall into this category is the inverse muon decay. This could be seen as a "flavour exchange" between a muon neutrino and an electron:

$$\nu_\mu + e^- \to \nu_e + \mu^-$$

Process	**Threshold** E_ν^{th}
$\nu_e + {}^{71}Ga \to {}^{71}Ge + e^-$	0.23 MeV
$\nu_e + {}^{37}Cl \to {}^{37}Ar + e^-$	0.82 MeV
$\bar{\nu}_e + p \to n + e^+$	1.81 MeV
$\nu_\mu + n \to p + \mu^-$	110.16 MeV
$\nu_\tau + n \to p + \tau^-$	3.45 GeV
$\nu_\mu + e^- \to \mu^- + \nu_e$	10.92 GeV

Table 1.2: Different process of quasielastic scattering. The first 2 were used respectively in the GALLEX and the Homestake experiment [4].

1.5.3 Elastic neutral-current interactions

Scattering can also occur through the neutral Z^0 boson. The process has the form

$$\overset{(-)}{\nu_l} + N \to \overset{(-)}{\nu_l} + N \qquad N = n, p$$

1.5.4 Deep(ly) inelastic scattering

This section will be especially important for this work. Deep inelastic scattering (DIS) occurs at high energies, which is the domain considered for the Glashow Resonance, or even IceCube in general. The word "inelastic" is there to translate the fact that, at these energies, the nucleons with which the neutrino will interact will not remain intact after scattering. More specifically, the interaction will result in a hadronic shower. The word "deep" on the other hand characterises the fact that the neutrino can probe the inner structure of the nucleon, as can be seen on the figures below [28].
First, let ut consider the charged current DIS interactions. The general form of the processes are:

$$\overset{(-)}{\nu_l} + N \to l^\pm + X$$

where, X represents any set of hadrons.

There can also be neutral current DIS interactions, where the general form is:

$$\overset{(-)}{\nu_l} + N \to \overset{(-)}{\nu_l} + X$$

The corresponding diagrams are the following:

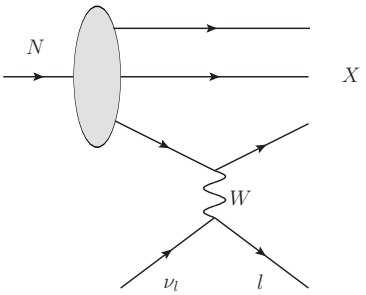

(a) Feynman diagram of a charged current DIS interaction. ν_l and l can refer both to particle or antiparticle.

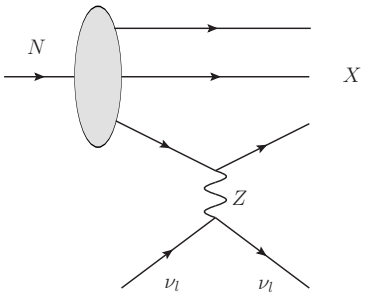

(b) Feynman diagram of a neutral current DIS interaction.

Figure 1.8

Depending on the leptonic flavour l, the processes exhibit some properties, such as a specific topology, which will be discussed in details in Chapter 2, where IceCube events are described.

1.5.5 Neutrino production

All the processes above can be used to detect neutrinos that come from extraterrestrial or even extragalactic sources. Hadron decays, on the other hand, can explain through which processes those incoming neutrinos are produced. It can happen on Earth, more specifically in the atmosphere, or in extragalactic locations, as was explained in Section 1.2. One of those processes is charged pion decay:

$$\pi^{\pm} \rightarrow l^{\pm} + \overset{(-)}{\nu_l} \qquad (l = e, \mu)$$

The pion can be created in beam dumps, *i.e.* regions in which the cosmic ray flux meets a dense medium, resulting in the production of pions. There can also be kaons produced in the same place. They will decay according to the same process as pions.

Another possible hadron decay process is neutron decay, known as β^- decay:

$$n \rightarrow p + e^- + \bar{\nu}_e$$

Chapter 2

Sources of ultrahigh-energy ν and detection

2.1 Flux of ultrahigh-energy neutrinos

A part of the possible neutrino sources were briefly introduced in the first chapter. The most essential type of neutrinos for this work are the (ultra)high-energy ones ((U)HE). Thus, let us continue the analysis of Fig.1.2. As a reminder, the different fluxes on the graph are a combination of observations and theoretical predictions. The true shape of the plot may be different.

2.1.1 Atmospheric neutrinos

From this point on, the different fluxes are all at high energies.

From a few hundreds of MeV to tens of TeV, the dominant flux is that of atmospheric neutrinos. When a high-energy cosmic ray, often a proton, hits a nucleus of the atmosphere, it creates a shower of hadrons, mainly pions. These decay into a muon and a muon neutrino. The muon can also decay into an electron, a muon neutrino and an electron neutrino[1]. The end product, from a flavour ratio perspective, is therefore $\nu_e : \nu_\mu : \nu_\tau = 1 : 2 : 0$.

$$N_{CR} + N_{atm} \rightarrow X + mesons : \begin{cases} \pi^0 \rightarrow \gamma + \gamma \\ \pi^\pm \rightarrow \mu^\pm + \overset{(-)}{\nu}_\mu, \quad \mu^\pm \rightarrow e^\pm \overset{(-)}{\nu}_e \overset{(-)}{\nu}_\mu \end{cases}$$

where N_{CR} represents a nucleus of a cosmic ray, typically a proton, and N_{atm} one of the atmosphere.

[1]Here, neutrinos can mean neutrinos or antineutrinos. More details of the processes can be seen on Fig. 2.1

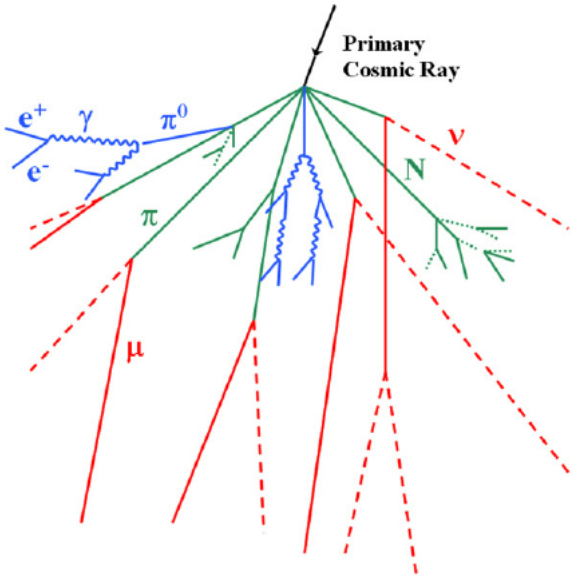

Figure 2.1: Different processes that result from the interaction of an incident high energy particle, a cosmic ray, with a nucleus of the atmosphere, from [29].

The spectrum of atmospheric neutrinos behaves as a power law, which can be approximated as $\sim E_\nu^{-2.7}$. Such a power law can be obtained via the Fermi mechanism, or diffuse shock acceleration. For more information, one can refer to [30].

Let us review what particle(s) originating from the cosmic-ray-atmosphere interaction can be observed on the ground. The γ rays produced by the decay of the π^0 will not reach us as the atmosphere will shield us from them. The muon neutrinos will always travel to the ground. Finally, the muons are in a situation in-between. Considering that they travel at relativistic speed, their path length before decaying is given by $\gamma_\mu \tau_\mu c = (E_\mu/m_\mu) \times 0.6$ km. If their energy is above 10 GeV, it will be enough to reach the ground before decaying. In this situation, the only observed neutrinos will be the muon (anti)neutrinos from the pion decay, since the muons will not have decayed before entering the detector.

As stated before, the spectrum of atmospheric neutrinos mimics the cosmic ray spectrum, *i.e.* a power law of $\sim E_\nu^{-2.7}$. However, when the energy of the charged pions reaches a few GeV, the chance that they decay before losing a significant fraction of their energy becomes smaller. From that point on, the power law of the spectrum is steeper, and can be consider to be $\sim E_\nu^{-3.7}$ for this reason [31].

The atmospheric neutrinos are detected by IceCube and are a background in which we are not interested, as our goal is to study neutrinos that come from extragalactic sources.

The energy spectrum of the incoming cosmic rays can also be used to determine a threshold that can help to distinguish the background atmospheric neutrinos from the extragalactic ones. As the Lorentz factor is large at high energy, *i.e.* when the speed is important, one can consider that the pions carries $\sim 1/5$ of the energy of the primary cosmic ray. The product of pion decay at high Lorentz factor will have roughly the same energy. Whereas the π^0 decays into two particles, two γ, the charged pions decay in 4 particles each. As it is considered that each product particle carries the same fraction of energy, each photon bears $\frac{1}{5} \times \frac{1}{2} = \frac{1}{10}$ of the energy, whereas a neutrino carries $\frac{1}{5} \times \frac{1}{4} = \frac{1}{20}$ of the energy. As can be seen on Fig. 2.2, the flux of cosmic ray can be considered to decrease drastically after the knee, which happens at an energy of roughly $E_{knee} = 2 \times 10^3$ TeV, or in other words a few PeV. Therefore we expect the

atmospheric neutrino flux to have a similar decrease at $E_{knee} \times \frac{1}{20} \sim 100$ TeV. This means that if a neutrino with an energy higher than 100TeV is detected by IceCube, one can consider its origin to be extragalactic.

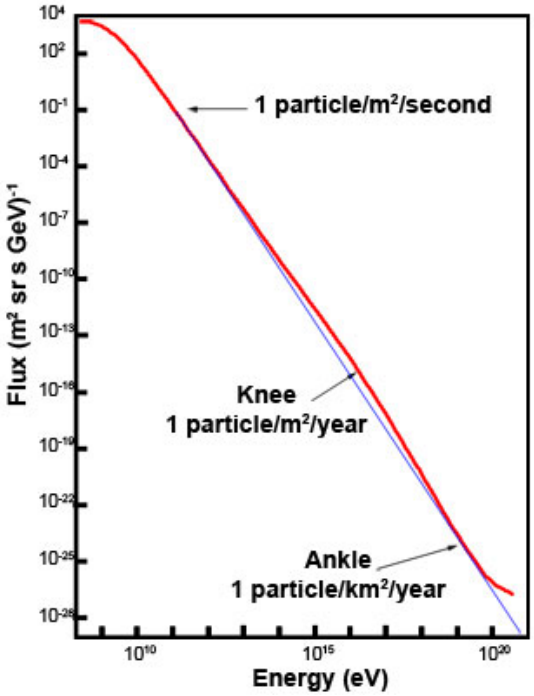

Figure 2.2: Energy spectrum of the incoming cosmic rays. The red lines correspond to what has been detected, whereas the blue line is an exponential decay. The two lines are very similar, but two important features make the cosmic ray flux different from a simple exponential decay: a knee, *i.e.* a slight bump of the flux, at around 10^{16} eV, and and ankle, at around 10^{20} eV. Taken from [32].

Another way that can be used to determine the atmospheric background from the extragalactic sources is the following: if the produced muon hasn't decayed yet when entering the detector, which happens if the energy of the muon is above 10 GeV as mentioned above, the detected neutrino will be accompanied by a muon track. It is a signature of an atmospheric neutrino.

2.1.2 Neutrinos from extragalactic sources

The next source in Fig. 1.2 is the Active Galactic Nuclei, orAGN. This is the first example of an "extragalactic sources". These are cores of galaxies that outshine all the other stars present in it. More specifically, they are supermassive black holes that accrete matter from their galaxy. The matter that falls onto the black hole will form an accretion disk, which will heat up because of gravitational and frictional forces [33]. The flux of neutrinos from AGN expands from a few GeV to the EeV scale.

The neutrinos that come from extragalactic sources have a flux ratio of $\nu_e : \nu_\mu : \nu_\tau = 1 : 2 : 0$ at the source, meaning that no tau neutrino is produced, and there are twice as many muon neutrinos as there are electron neutrinos. This can be explained. In the Universe, the sources of neutrinos are cosmic-ray accelerators. They are "beam dumps". As the name implied, it means that the cosmic-ray beam will be dumped in a dense medium where pions and kaons are produced. The pions are the dominant contribution [34]. They will decay as before to $e^{\pm}$, $\overset{(-)}{\nu_e}$

and $\overset{(-)}{\nu}_\mu$, leading which leads to the previously specified flux composition: no ν_τ, and two times more $\overset{(-)}{\nu}_\mu$ than $\overset{(-)}{\nu}_e$ [35].

Of course, as already mentioned, the origins of the different neutrino fluxes are not known. The same can be said about the mechanism through which neutrinos form. One of the most likely cases is the $p\gamma$ mechanism. A cosmic ray reacts with a photon. A neutron and a π^+ are created. The pion decays into a muon and a muon neutrino, and the former will further decay as follows:

$$p\gamma \to n\pi^+, \quad \pi^+ \to \mu^+\nu_\mu, \quad \mu^+ \to \bar{\nu}_\mu\nu_e e^+$$

The final flux ratio will be $1:1:0$ for the neutrinos, and $0:1:0$ for the antineutrinos.

Another source of extragalactic neutrinos is a Gamma Ray Burst, or GRB. GRBs are assumed to be the result of a cataclysmic event at the end of the life of massive stars, such as the merger of two neutron stars or the collapse of a fast-rotating central core. To describe this phenomenon, let's split it into three parts. Firstly, there is a source of energy, such as the collapse mentioned just above. Secondly, this will result in a huge liberation of gravitational energy in a very short time. It will lead to a fireball of photons, magnetic fields, baryons and electron-positron pairs. This fireball will relativistically expand along the rotational axis due to radiation pressure. Thirdly, there will be a relativistic shock with the interstellar medium which will expand the fireball by a factor 10^6 over 1 second. This will lead to the acceleration of particles and synchrotron radiation. Finally, the photons can interact with nucleons and through $p\gamma$ processes, neutrinos are created [36][37].

2.1.3 Cosmogenic neutrinos

Cosmogenic neutrinos are neutrinos produced by the resonant reaction of high energy cosmic rays (mainly proton p) scattering against cosmic microwave background photons (γ_{cmb}). The process is the following:

$$p\gamma_{CMB} \to \Delta^+ \to \pi^+ n$$

with a proton with an energy of $E_p \simeq 500\ EeV$ [38]. This is not a regular $p\gamma$ process because there is the creation of an on-shell Δ^+, which will decay. The produced pion can then decay in ν_μ and μ, and the neutron can give a ν_e.

These are the known sources of neutrinos. However, not all are detected by IceCube. As the detector has an energy threshold around 0.1 TeV, only part of the atmospheric neutrinos as well as extragalactic[2] ones will be detected. However, only events with an energy higher than 100 TeV are considered, because it is above this threshold that the event rate is clearly higher than the atmospheric neutrino event rate derived from the well-known cosmic ray flux. This excess characterises the presence of extraterrestrial neutrinos [39].

Before going any further, let us compare the behaviour of the neutrino flux with the cross section. On the one hand, the higher the energy, the lower the flux. On the other hand, the higher the energy, the bigger the neutrino interaction cross section. However, the two do not compensate: fewer events are expected at higher energies. It is still nonetheless important to mention this behaviour as both quantities have a role to play in the expected event rates. Details about the analytical expression of the cross sections will be given later.

Even though there are predictions of the extragalactic neutrino flux, it is mostly unknown. Thus,

[2] *i.e.* neutrinos from AGN and cosmogenic neutrinos, as they both come from outside our galaxy

one can try to constrain it using data we have access to. A candidate is the cosmic ray flux, which is a well-known quantity. Waxman and Bahcall tried to link it with the neutrino flux in order to constrain it in some way. They were successful, and they found what is now called the Waxman-Bahcall bound.

2.2 The Waxman-Bahcall bound: an upper limit to the astrophysical neutrino flux

The Waxman-Bahcall upper bound is a theoretical limit that should constrain the neutrino flux, giving it a maximum value. It is obtained from a known cosmic ray flux. In this section, we will explain how such a limit was derived. The cosmic-ray flux above $3 \times 10^{18} eV$ is dominated by protons of extragalactic origins. At lower energy, heavy ions from our galaxy dominate. The flux that one expects from a Fermi acceleration if the extragalactic sources are cosmologically distributed is consistent with what is observed. The flux is then such that $dN_{CR}/dE_{CR} \propto E_{CR}^{-2}$. In the energy range $[10^{19} eV,\ 10^{21} eV]$, the energy production rate of protons is $\dot{\epsilon}_{CR} \approx 5 \times 10^{44}\ erg\ Mpc^{-3}\ y^{-1}$. The energy-dependent cosmic rays generation rate is

$$E_{CR}^2 \frac{d\dot{N}}{dE_{CR}} = \frac{\dot{\epsilon}_{CR}}{log(10^{21}/10^{19})} \approx 10^{44}\ \text{erg Mpc}^{-3}\ \text{yr}^{-1}$$

From this quantity, the present muon neutrino energy density can be obtained:

$$E_\nu^2 \frac{dN}{dE_\nu} \approx 0.25\ \epsilon\ t_H E_{CR}^2 \frac{d\dot{N}}{dE_{CR}}$$

Let us analyse the different added factors. $t_H \approx 10^{10} yr$ is the Hubble time, which accounts for the time that has passed since the "beginning" of the Universe. ϵ is the fraction of energy of proton lost through photo-meson productions[3], mainly of pions, before escaping the source, as a lot of radiation is present there. If ϵ is energy independent, and it is supposed to be equal to 0.05, the neutrino flux and the proton flux will have the same energy dependence. The 0.25 accounts for the fact that pions are created with equal probability with charged ones, and that a charged pion decays into 4 particles, among which half of them are muon (anti)neutrinos. Thus, half of the energy the initial cosmic ray is carried by charged pions $\pi^\pm$, and half of the energy of charged pions is carried by muon neutrinos, hence the $0.5 \times 0.5 = 0.25$. An upper bound for the muon neutrino intensity I_{max} can then be obtained, for $\epsilon = 1$:

$$\begin{aligned} I_{max} &\approx 0.25 \xi_Z t_H \frac{c}{4\pi} E_{CR}^2 \frac{d\dot{N}}{dE_{CR}} \\ &\approx 1.5 \times 10^{-8}\ \xi_Z\ GeV cm^{-2} s^{-1} sr^{-1} \end{aligned}$$

ξ_Z denote the potential contribution of high redshift sources. It is close to one, and so far no such source has been observed. Finally, the expected neutrino intensities can be obtained by expressing the cosmic ray energy in terms of the neutrino flux. For the muon neutrino — not the antineutrino — one has to take half the maximum intensity, as the latter is for $\nu_\mu + \bar{\nu}_\mu$. One can then write:

$$\begin{aligned} E_\nu^2 \Phi_{\nu_\mu} &= \frac{c}{4\pi}\ E_\nu^2\ \frac{dN_{\nu_\mu}}{dE_\nu} \\ &= \frac{1}{2} \epsilon I_{max} \end{aligned}$$

with $\Phi_{\nu_e} \approx \Phi_{\nu_\mu} \approx \Phi_{\bar{\nu}_\mu}$, as is expected from the initial flux ratio.

[3] A photo-meson production is the production of meson by the interaction of nucleons with photons [40].

By using this bound as the neutrino flux, one should expect a maximum of 100 events per year in a 1 km^3 detector like IceCube. Details about how the expected number of events is computed will be shown later.

Let us discuss this upper bound. It must not be understood as an absolute limit that cannot be exceeded. The Waxman-Bahcall bound is an upper bound for high-energy neutrinos that are produced through photo-meson interactions in sources that have a size equal to the proton - photo-meson mean free path. There can be neutrinos fluxes higher than their cosmic ray counterpart, for instance from optically thick sources. From such celestial objects, only neutrinos would escape, thus the ratio of emitted neutrinos over cosmic-rays would be higher than in optically thin sources. It does not mean the bound is violated, only that we do not see the cosmic rays. It is also possible to exceed the bound if the neutrinos are produced through processes that do not yield cosmic rays, for instance by dark matter decay. However, this bound is currently consistent and not violated, which further reinforce the link between neutrinos and cosmic rays [41]. One could also raise the question of energy dilution due to the redshift. For proton produced at $t < t_H$, there is a loss of energy due to the redshift. The cosmic-ray generation rate per (comoving) volume may be independent of time, even on the scale of cosmic time. If there were a dependence, and the dependence was such that the rate was lower before, then it doesn't affect the current bound. Let us consider the situation in which it is higher at high redshift. The possible interaction with the cosmic microwave background means that the farther a cosmic ray is coming from, the more energy it is likely to have lost through photo-meson production. If a cosmic ray with an energy higher than 10^{18}eV is created at a redshift higher than $z = 1$, it will lose energy and its final energy will be under this value. Cosmic rays with an energy under that value originating from $z > 1$ will be "hidden" in the contribution from Galactic sources, which are dominant at these energies. To have higher energy cosmic ray, the sources must be at low redshift, *i.e.* $z < 1$, so the redshift dependance is not very significant [42].

The final aspect that one could discuss is the validity of this bound when it comes to a detector such as IceCube. The range of energy that is studied is from about 10^{13} eV to 10^{15} eV. The bound, on the other hand, is valid for an energy larger than 10^{19} eV. Thus, to obtain the corresponding one for lower energy, the bound is simply extrapolated by assuming a $\propto E^{-2}$ energy spectrum from the source. The result will not be as rigorous as for higher energies, but is still plausible [41].

This upper bound will give a limit to the event rate. This limit allows to compute the maximum number of events that can occur in a year for a given volume, and to choose a suitable one. The short answer is to build a detector as big as possible to detected as many events as one can, since that number will never be tremendous. However, there are of course technical limits to the detector size. The result of this question was to build a kilometre-cube detector in a medium as default-free as possible. This would mean that according to the Waxman-Bahcall bound, around a hundred events could be detected in a year. The most obvious choice was the South Pole ice, for the frozen water is very pure there. That detector is called IceCube.

2.3 IceCube: a detector for astrophysical neutrinos

IceCube is one of detectors used to observe high-energy neutrinos. It consists roughly in a cubic kilometre of very pure "instrumented" ice at the South Pole. In this section, the design of the detector will be explained.

IceCube contains 5160 digital optical modules (DOMs). A DOM is made of a ten-inch photomultiplier tube coupled with electronics. Each of these DOMs is attached to a vertical string

that was put into the Antarctic ice after having drilled a hole. The modules are placed at a depth that ranges from 1450 to 2450m, and expand over roughly a square kilometre, hence the name "IceCube", because the detector is about one cubic kilometre of ice. The strings are placed in a hexagonal network with a spacing of 125 meters. One string contains 60 modules, with a vertical separation of 17m. However, not all the DOMs are equally spaced. There is also a "surface array", called IceTop. Its purpose is mainly the calibration of IceCube, as well as a "veto detector". If events are generated by an air shower, they are background events and thus are not of interest here. If IceTop detects a shower at a time that coincides with an event with an energy above 10^{15} eV, this event can be vetoed. There is a denser sub-array, DeepCore, in which the horizontal separation is 70m, with a vertical one of 7m. The threshold for the neutrino energy is lower than for the other strings. It goes down to around 10 GeV, therefore allowing the study of neutrino oscillations [43].

Having a cubic kilometre detector is not an exaggeration. Indeed, when it comes to regular photon telescope, the biggest are only of a few meters, nowhere near the size of Icecube. The reason for which such a size is used is because to the aforementioned low interaction of neutrinos with matter, as well as the low flux. One can note that the higher the energy, the higher the cross section for neutrino interactions. However, at high energy, the neutrino flux almost vanishes, which implies that all in all, fewer events are detected at higher energies. Thus, having a huge detector can counterbalance that faint flux, faint flux that is predicted by the Waxman-Bahcall bound. By knowing this limit, one can tell that a cubic kilometre detector can ensure that even events at the Glashow Resonance energy will be detected. Moreover, a neutrino event can be quite big at these energies. Thus, to contain it, the size must be chosen accordingly. Finally, one might simply ask why we want to go to such high energies. The reason, as it was explained above, is that the neutrino at high energies are from (extra)galactic sources, which means they allow us to study the Universe, more specifically in region of the Universe previously inaccessible via photons at these energies. Now that the detector has been described, one can wonder how everything will work together, or in other words, how a neutrino is detected.

2.4 Neutrino detection at IceCube

IceCube was built to detect neutrinos through the light emitted as a consequence of their interaction. They will interact within the detector, *i.e.* with the ice, produce a secondary and electrically charged particle which will emit light. This radiation can be Cherenkov light, or simply bremsstrahlung.

The Cherenkov light is the radiation emitted by a charged particle that travels in a dielectric medium, in which the refraction index n is larger than 1, at a velocity larger than the local speed of light, given by $\frac{c}{n}$. In the process, part of the energy of the particle is converted into light, and a coherent wavefront is created.

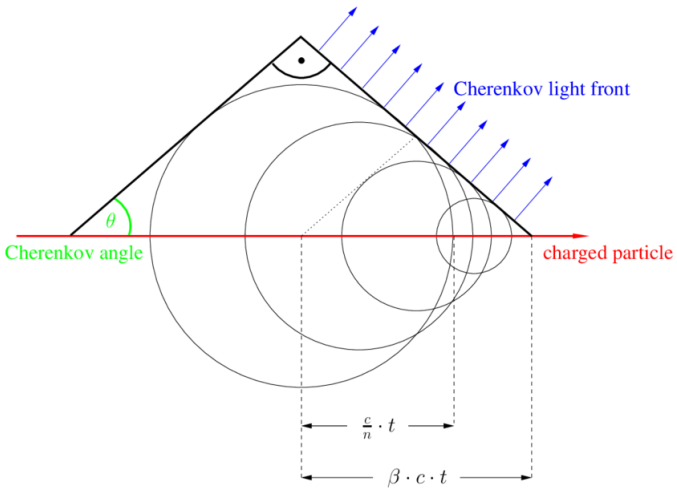

Figure 2.3: Sketch of the wavefront of Cherenkov radiation. The red line represents the path of a charged particle moving at a speed greater than the local speed of light. The blue lines correspond to the Cherenkov radiation. n is the refractive index of the medium, t the time that has passed between when the charged particle was at the center of the biggest circle and its current position (the rightmost tip of the triangle). The charged particle travels a distance of $\beta \cdot c \cdot t$, whereas the light travels a distance $\frac{c}{n} \cdot t$ during that time. $\beta = v/c$ is the relative velocity of the particle in the medium. c/n is the local speed of light. Taken from [44]

IceCube can detect all neutrino flavours. The detected muons can have an energy that ranges from 10^{11}eV to 10^{18}eV, and even further [45]. The DOMs in IceCube will detect the light. The information will be digitised, then assigned a timestamp with a precision under 5ns. The final information will then be sent to the surface. By combining what every DOM found, a picture representing the array of IceCube as well as the amount of light and the time of detection of each module can be created, as can be seen in Fig. 2.4. Once the data of the event has been built at the surface, it will be filtered and then sent for further processing to the Northern hemisphere thanks to a 24-hour satellite connection [45].

A reconstructed event is shown in Fig. 2.4. There can be several topologies from track-like to cascade events, and combinations of these two categories can exist. As it will be seen, these topologies give information on the types of neutrinos that were detected, and even on their energies.

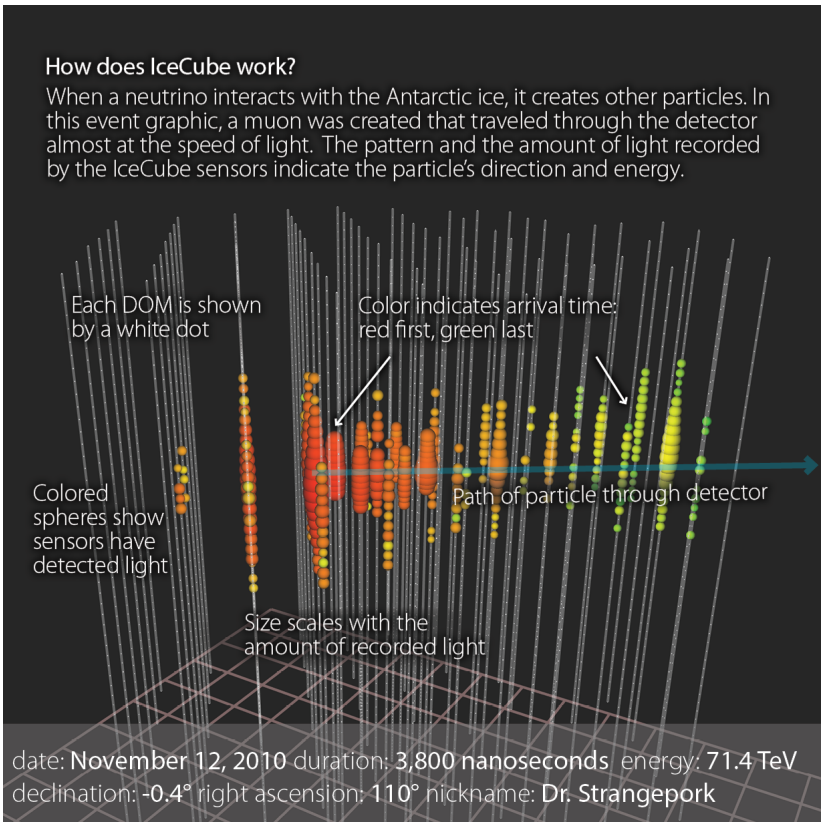

Figure 2.4: Reconstructed image of the DOMs array of IceCube. The vertical lines correspond to the strings to which the DOMs (little white dots) are attached. The colours represent the time of arrival (the redder, the earlier), whereas the size of the dots represents the amount of light that the digital optical module detected (the bigger, the more light). From [43]

2.5 Types of neutrino-induced events

2.5.1 Neutral current

The first category of interaction is called Neutral Current, or NC. It comes from the fact that the boson involved in the process is a neutral Z^0. The general form of the said process is

$$\nu N \xrightarrow[\mathrm{Zo}]{\mathrm{NC}} \nu X$$

where N is a nucleon (proton p or neutron n) at rest, the incoming and outgoing neutrinos have the same flavour, and X is so far unspecified and can be different things. It will have a high mass and lead to a cascade of radiation, *i.e.* a loss of energy through radiation that is so fast that all the energy of X is radiated instantly, hence the roughly spherical shape. As neutrinos do not emit radiation when passing through the medium, there will only be a cascade of photons coming from the X.

2.5.2 Charged current

The second category is the Charged Current, or CC, events. The process can be written

$$\nu_l N \xrightarrow[\mathrm{W+,-}]{\mathrm{CC}} l^- X$$

where ν_l is a neutrino of a given flavour (μ, e or τ), and l^- is a charged lepton. The name of the CC interaction comes from the fact that the boson involved is a charged W^+ or a W^-. The total charge is conserved. One can note that the lepton is linked to the flavour of the neutrino. Therefore, if the process involves a ν_τ, the lepton l^- will be a τ^-. The same goes for the other flavours. Under 10 GeV, the outgoing lepton will carry on average 50% of the incoming energy, and about 80% at higher energies. One can wonder if the different possible cases are distinguishable. Fortunately, given the right conditions, this can be the case. As stated before, the detection of a neutrino event by IceCube will be done thanks to the created particles, which will emit photons. However, a charged lepton will have different signature depending on its nature. The first possibility is to have $l^- = e$. As the radiated energy is proportional to the inverse of the squared mass, the electron being very light ($m_e = 0.511\ MeV$ in natural unit [46]) implies a very quick loss of energy, as for the X particle. One would therefore have a mixture of two cascades, one that comes from the X, one from the e, which is shown on Fig. 2.5.

The second case is $l^- = \mu^-$. A muon has a mass of 100 MeV [46]. It is much higher than that of the electron.

Furthermore, because of its mass dependance, bremsstrahlung will be less powerful. It results in a slower loss of energy, which is characterised in the detector by a track, rather than a cascade, which can be seen in Fig. 2.6a. One can note that there can still be a cascade due to the X. The advantage of a track is that it has a directionality that allows to deduce with accuracy the origin of the incident neutrino. The downside is that only a fraction of the energy of the produced particle, the muon, is deposited in the detector, which decreases the accuracy on the energy. With the cascade, the opposite holds: there is almost no directionality, but all the energy is deposited in the detector.

Finally, the last possibility is $l^- = \tau^-$. Its mass is 1.777 GeV [46]. Being much heavier, one would expect a behaviour similar to that of the muon, *i.e.* a cascade and a track. However, a τ has a lifetime of 2.96 $10^{-13}s$ [46]. It has many decay channel. Since it has a sufficient mass, it can and will decay quickly into several particles, such as hadrons and leptons, which can have very different masses [47][48]. As this is roughly as light as the electron, it means the particles that result from the decay of the τ lepton will produce a cascade. If it is the case, then one would see a mixing of different cascade. However, if the energy of the incident neutrino is high enough, typically above 100 TeV, the τ lepton will travel enough so that the cascade due to the X and the one due to the particles created after the decay of the τ will be separated by a microtrack, as can be seen on Fig.2.6b. However, to be able to distinguish that track and resolve the two cascades, the energy of the incoming ν_τ must be of the order of the PeV.

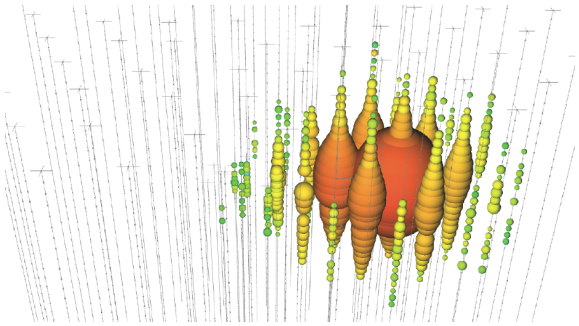

Figure 2.5: Simulation of a cascade-like event. The colours represent the time of arrival (the redder, the earlier), whereas the size of the dots represents the amount of light that the digital optical module detected (the bigger, the more light). From [49].

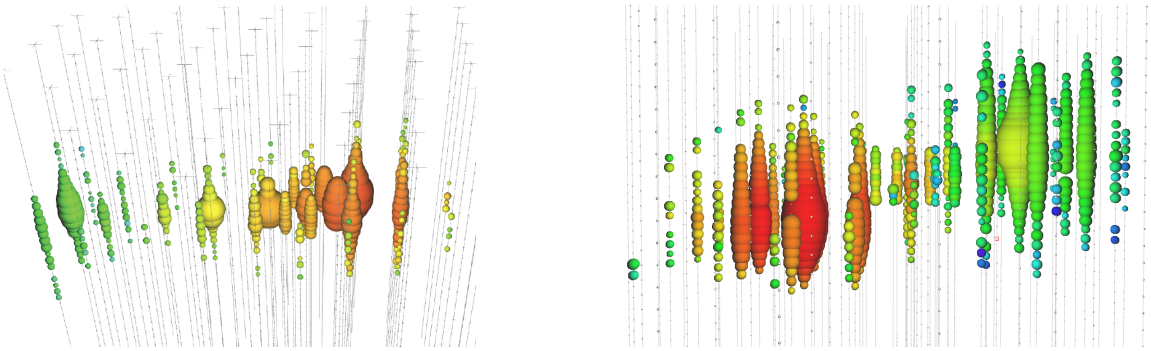

(a) (b)

Figure 2.6: On the left: Simulation of a track-like event [49].
On the right: Simulation of a double bang event at an energy above PeV [50].
The colours represent the time of arrival (the redder, the earlier), whereas the size of the dots represents the amount of light that the digital optical module detected (the bigger, the more light).

The different situations above are for neutrinos. However, the same holds with antineutrinos, the only difference being that the charge is the opposite.

One can note that it is not possible to distinguish the NC interactions from the CC ones in general.A muon neutrino is the only flavour leading to a track-like event, and a high energy tau neutrino will give birth to two cascades. These are unique topologies. However, a "low energy" tau-neutrino and an electron-neutrino induced event will have the shape of a single cascade, thus leaving us unable to determine the initial flavour. As the final mixing ratio is $\approx 1:1:1$, one should expect roughly two times more cascade than track-like events, because ν_e and ν_τ yield a cascade, whereas only a ν_μ will result in a track.

While these were the outlines of the possible types of events involving a neutrino and a nucleon that can occur within IceCube, there also exist interactions between neutrinos and leptons. One particular case is of interest and will be discussed in more depth in the next chapter. That process is called the Glashow Resonance. In the meanwhile, let us just present its general aspects.

Glashow resonance

The Glashow Resonance (GR) is a resonant process that occurs at the energy of 6.3 PeV, involving an electron antineutrino and an electron, producing an on-shell W^-. The process can be written:

$$\bar{\nu}_e e \xrightarrow[\text{W-}]{} ab$$

where a and b are not specified yet.

The cross section for this interaction is orders of magnitude lower than the two other cases mentioned above, charged- and neutral- current events between a neutrino and a nucleon. However, at the energy of the Glashow Resonance, there is a spike [51], as can be seen on Fig. 2.7. This means that, in general, the antineutrino-electron interaction can be neglected as the cross section is very low, but must be taken into account if the energy is near that of the resonance, as the cross section is of the same order as the others.

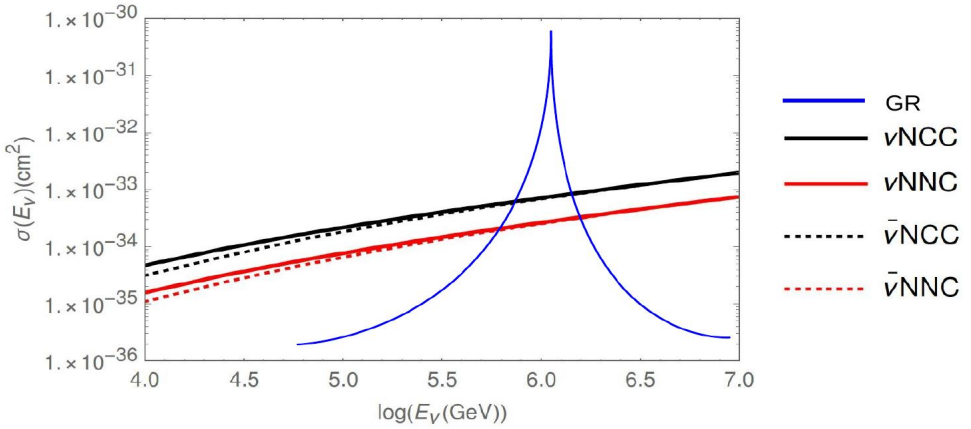

Figure 2.7: Cross section of the Glashow Resonance (blue), Charged Current and Neutral Current events for neutrinos (solid dark and red lines) and antineutrinos (dashed black and red lines) as a function of the neutrino energy, around the Glashow Resonance energy (6.3 PeV), from [10]

As already explained, the Glashow Resonance is the reaction of an electron antineutrino $\bar{\nu}_e$ and and electron e which produces an on-shell W^-. That W^- boson will then decay, either hadronically of leptonically. If it decays leptonically, there can be several cases, which are summed up in the following table:

Incident particles	**Products**
$\overline{\nu_e} + e$	$\mu^- + \overline{\nu_\mu}$
	$\tau^- + \overline{\nu_\tau}$
	$e^- + \overline{\nu_e}$

In the first case, where a muon is produced, only a track will be visible. In a muon neutrino event, there is a cascade due to the X in the product in addition to the track left by the muon. Here only the track is present, for in this case the X product is an antineutrino, which is "invisible"[4] for IceCube. The same goes for the case where a tau is produced. The first cascade, due to the X, is missing, so only the second bang of the Double Bang is present. Finally, if an electron is produced, a cascade will be observed, which is not distinguishable from the previous situation (NC or CC). However, since the GR event rate is much higher than the electron neutrino event rate, a single cascade event at 6.3 PeV with an incident $\bar{\nu}_\tau$ that would react with a τ^-, or a $\bar{\nu}_\mu$ with a μ^-, but there are no τ nor μ inside the detector. One could say that there are still the few created by neutrino events, but these are negligible. Moreover, muons and taus are not stable particles, so this event is not likely to happen elsewhere either.

When detecting an event, two observables are important: the neutrino energy and its direction. Once the reconstitution has been done, the next step is to try to determine these two unknowns.

2.6 Reconstruction of the neutrino energy

The main topic of this thesis is the Glashow Resonance. As its name implies, it is a resonant phenomenon. It occurs at a certain energy, thus it is mandatory to be able to reconstruct as accurately as possible the energy of the initial neutrino with the data given by IceCube. As it

[4]It is actually visible, but only if it interacts with the matter within the detector, which is rarely the case, as opposed to muons that will always leave a track, for instance.

was stated before, the main data one has access to is the light emitted by the produced particles. This light can give us information on the energy and direction of the neutrino that was detected. Depending on the event topology, the accuracy to which we have access varies.

2.6.1 Muon tracks

As the track events are much more directional than cascades, they allow a good reconstitution of the origin of the neutrino. These type of events are also central in the creation of a map of the Universe from neutrinos. Such a map will be shown at the end of this section. When studying muon tracks, only the up-going ones are considered. Doing this ensures that the track originates from a neutrino event. Indeed, down-going muons could come from the interaction between a cosmic ray and the atmosphere. However, if such a muon was coming from the other side of the Earth, it would have decayed before being observed as an up-going track. Thus, up-going muons are necessarily created not too far from the detector. This happens through ν_μ events.

The energy loss of the muon comes mainly from ionisation, bremsstrahlung, pair production and photo-nuclear processes. It can be parameterised as follows:

$$-\frac{dE_\mu}{dx} = a + b\ E_\mu$$

where a and b characterise the different energy loss channels, and x is the variable that represents the path length in a non-vacuum medium, here the detector. a characterises the energy loss through ionisation, and is approximatively equal to ≈ 2 MeV/cm in water. b characterises the other energy losses. It is linear in the energy, and can be decomposed as $b = b_{brem} + b_{pair} + b_{photonucl}$. In water, at an energy $E_\mu = 100$ TeV, one has $b \approx (1.7 + 1.2 + 0.6) \times 10^{-6}$ g/cm^2 $= 3.5 \times 10^{-6}$ g/cm^2. One can also note that the energy losses described by b become dominant over a above 1 TeV. Mechanisms that create particles, such as pair production, will create relativistic particles that will induce more Cherenkov light. The measurements allow us to quantify the left-hand side, dE_μ/dx. By constraining a and b, one can deduce the energy of the muon when it entered the detector.

Instruments such as IceCube are well suited for the detection of muon tracks at high energies, typically above one TeV, for several reasons. First, since the atmospheric neutrino flux is expected to decrease more quickly than the astrophysical one ($\propto E_{atm}^{-3.7}$ vs $\propto E_{astroph}^{-2}$ at high energy), one expects a better signal-to-noise ratio as the energy gets larger. Also, it can be shown that the mean angle between the incident neutrino direction and the muon track decreases with energy[5], thus allowing for a better tracing of the neutrino origin. Finally, for an energy higher than 1 TeV, the amount of light emitted by the muon depends linearly on the energy. The accuracy of the energy reconstitution then becomes $\sigma(\log E_\mu) \approx 0.3$. The muon energy can then be translated into the incoming neutrino energy by using *unfolding procedures* [52]. For more details, one can see [53] and [54].

One can note that at a depth of 1 km, the down-going muons created by cosmic ray interactions with the atmosphere, in other words, the background muons, are much more numerous than the up-going muons that come from neutrino interactions. The factor is about 10^6.

2.6.2 Cascades

The other topology of events is the cascade. Whereas for a track-like event, only dE/dx was measurable, here the light deposited within IceCube is a proxy for the total energy of the incoming neutrino. For a charged current event, the deposited energy is close to the incoming

[5] $\sqrt{\langle\theta^2\rangle} \approx \frac{1.5^\circ}{\sqrt{E_\nu\,[\mathrm{TeV}]}}$ [52]

neutrino energy. However, for neutral-current processes, there is an invisible outgoing neutrino, which carries part of it. The deposited energy is then only a lower limit. As IceCube cannot distinguish CC from NC, energy reconstitution must be seen as a lower limit [55].

Whereas the background for track events was very high, it is smaller for cascade ones. The former topology was more suited for mapping the neutrino direction, and the latter is useful when it comes to studying the diffuse flux of neutrinos.

On average, IceCube achieves an energy resolution in all channels of $\approx 15\%$ for high-energy events [55]. The angular resolution is under 1° for muon tracks, and about 10° for cascade events [56].

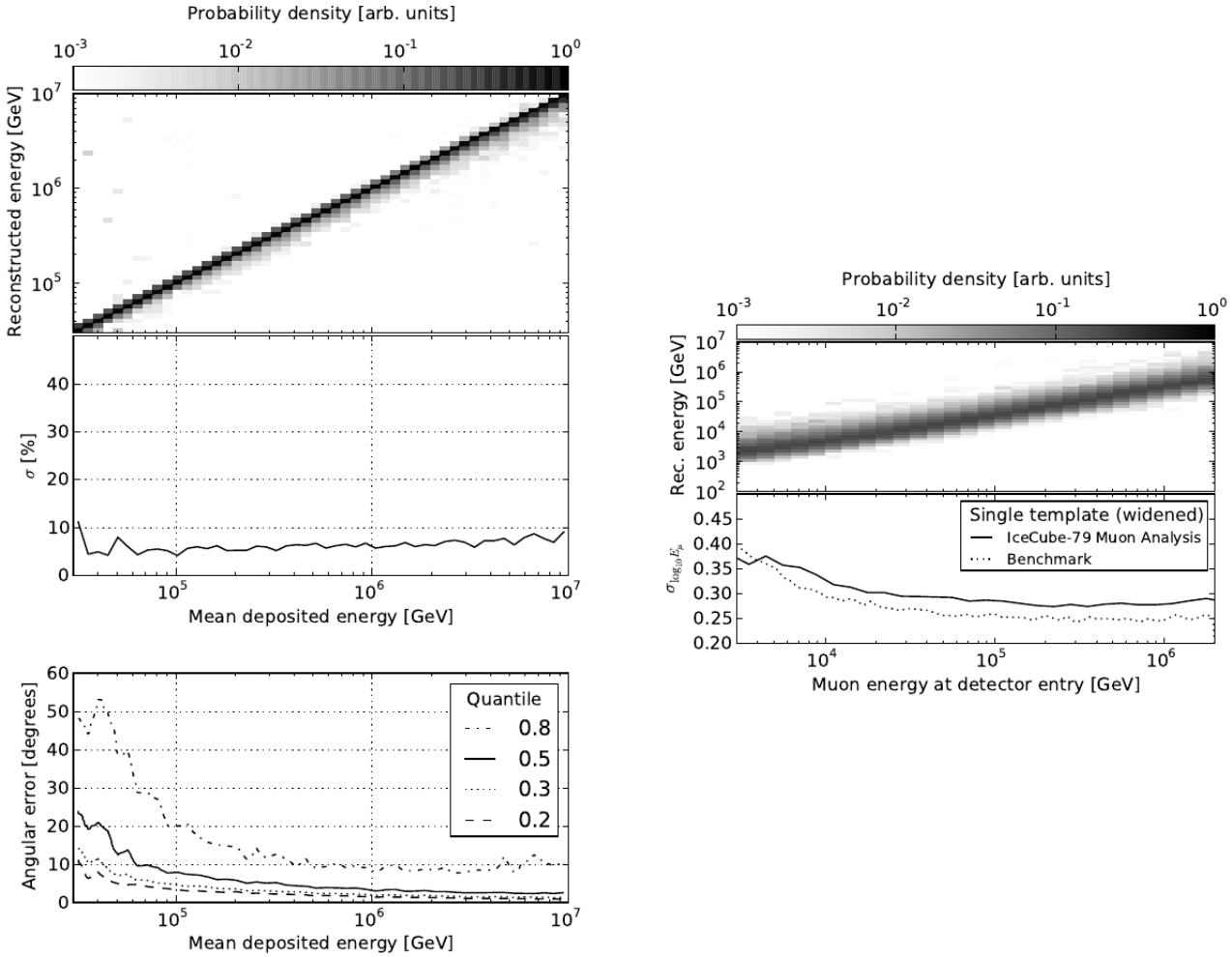

Figure 2.8: On the left: Reconstructed energy for a ν_e induced cascade event as a function of the deposited energy by the incoming ν_e. On the bottom is shown the energy resolution as well as the quantile of the angular one.
On the right: Reconstructed energy for track-like event as a function of the muon energy at the entry of IceCube. On the bottom is shown the error on (the logarithm of) the incoming muon energy [55].

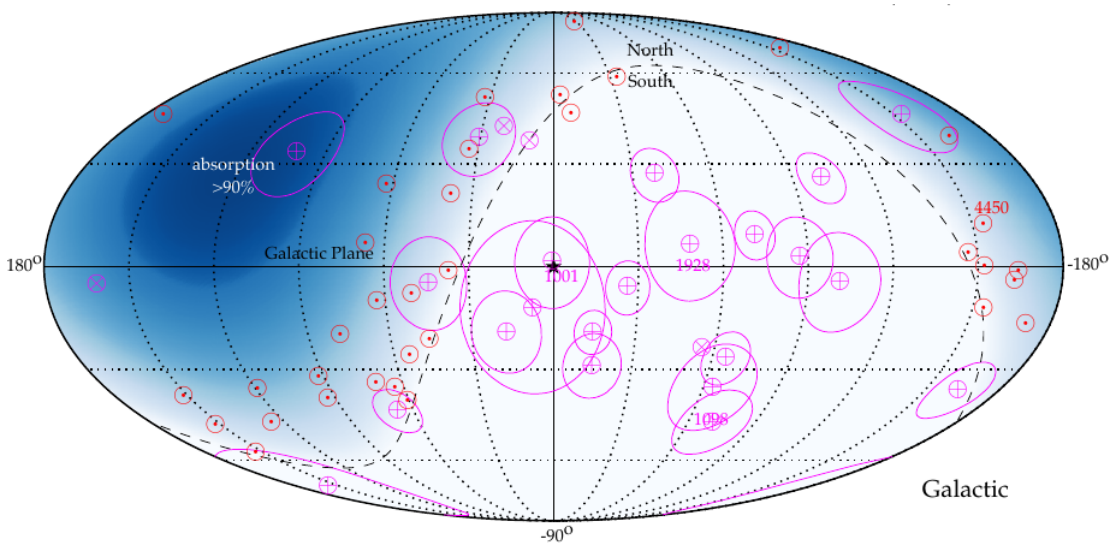

Figure 2.9: Arrival direction of neutrino events for the 8 year up-going track analysis (red) with a reconstructed muon energy >200 TeV and for the 6 year HESE analysis (pink, cascades ⊕, tracks ⊗).The circles around the event represents the angular resolution of cascade events. The blue region on the left represents the region where absorption of 100 TeV neutrinos by the Earth is important. Taken from [57].

Fig. 2.9 shows the origin of neutrino events over 8 years, considering HESE and Through-going muon events. As it can be noticed, one can count their numbers just by looking at them, which would not be possible for a photon map. This is, of course, to be expected considering the almost non-existent interaction of neutrinos with matter. Still, one can wonder if so few is normal. To answer this question, one has to compute the expected number of events.

2.7 Expected number of events

Neutrinos are particles that interact very feebly with matter. Despite their abundance, the number of events that one can expect is low, even with a detector as big as IceCube. It is then useful to compute this number either from a fully theoretical point of view, using the neutrino interactions cross sections, or from a more experimental one, using simulations of IceCube. The latter will be lower than the former, since it takes into account more sources of non-optimal behaviour, but closer to what could be expected in reality.

2.7.1 Cross section: a fully theoretical framework

Let us assume for the moment that the different cross sections of neutrino interactions are known. The expected rate of event for a given process is:

$$Rate = 4\pi N_A V_{eff} \int dE_\nu \ \sigma_i(E_\nu) \ \phi_{\nu_i}(E_\nu) \ [58]$$

where $N_A = 6.022 \times 10^{23}\text{cm}^{-3}$, $V_{eff} \approx 2\text{km}^3$, σ_i is the cross section of the process i (*e.g.* $\nu_\mu N \rightarrow \mu + anything$), and ϕ_{ν_i} the corresponding flux of incident neutrinos. Let us note that the expression is slightly different for the Glashow-resonance events since the reaction sites are electrons and not nucleons. In that case, one has

$$Rate = 2\pi \frac{10}{18} N_A V_{eff} \int dE_\nu \ \sigma_{\bar{\nu}_e e}(E_\nu) \ \phi_{\bar{\nu}_e}(E_\nu)$$

The $\frac{1}{2}$ comes from the fact that one considers only the upper-half sphere. As the Glashow Resonance cross section is high when compared to others, up-going $\bar{\nu}_e$ are more likely to already have undergone a resonant event since they travelled within the Earth, hence the 2π instead of the 4π. $N_A V_{eff}$ is an approximation of the number of nuclei in IceCube, which are H_2O. One nucleus contains 18 nucleons, and 10 electrons. Thus, for one nucleus (18 neutrino interaction sites), there are 10 electrons (GR reaction sites), hence the fraction. The expression of the different cross sections will be given later in this work, in 3.2.3.

2.7.2 Effective area: a more realistic approach

Another way to compute the expected number of events is by using directly the characteristics of IceCube. By doing so, one obtains a more realistic number, as we are not working in an ideal theoretical framework that would not consider some experimental aspects. An important factor in the number of detected neutrinos is the sensitivity of the detector. The more sensitive, the more events are detected. There exists different ways to express this sensitivity. The one that will be used here to compute the number of expected neutrino events is the effective area A_{eff}. It can be defined by

$$A_{eff}(E,\theta) = \frac{N_{detected}(E,\theta)}{N_{generated}(E,\theta)}$$

where $N_{generated}$ and $N_{detected}$ respectively the number of generated and detected muons in the test sample with an energy E, and a zenith angle θ [45]. Once the effective area is known, one can compute the number of expected events with the following:

$$N_{events} = \int_0^t \int_\Omega \int_{E_{min}}^{E_{max}} A_{eff}(E',\theta') \frac{d^3\phi}{d\Omega'\ dE'\ dt'} dE' d\Omega' dt'$$

where ϕ is the flux, Ω is the solid angle, and t the time [59].

The following graph shows the effective areas for the three flavours of neutrinos for the IceCube detectors [60].

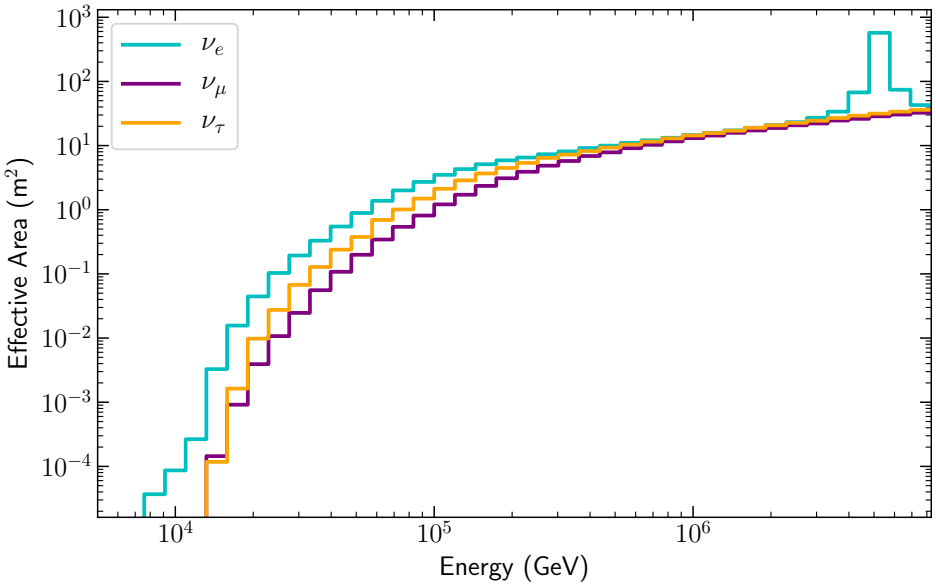

Figure 2.10: Effective area of IceCube for the different energy bins as a function of the incoming neutrino energy for an electron neutrino (blue), a muon neutrino (purple), and a tau neutrino (orange). One can note the spike related to the Glashow resonance in the 10^6 GeV (PeV) range. The effective areas data can be found on [60].

One can note the spike related to the Glashow resonance at 6.3 PeV, exclusive to the electron antineutrino effective area. Since IceCube doesn't distinguish between particles and antiparticles, this spike is in the electron neutrino effective area, which must be understood as "$\nu_e + \bar{\nu}_e$ effective area". The lines are not smooth because they are the result of simulations with a given energy binning. Let us mention that this binning is not frozen in time, as we will show later.

2.7.3 Model of flux

As was stated above, the sources of neutrinos are not well known, which implies that the flux is also surrounded by uncertainties. Several models of fluxes exist. In this work, a power law will be used. This choice is not random. The neutrino diffuse flux was fitted with different functions, such as a single power law, or a double power law (the sum of two power laws with different normalisations and spectral indices), and it appears that the single power law model is preferred with respect to the others [61]. One can note that this flux will be lower than the Waxman-Bahcall bound that was explained before. This power law depends on several variables that we don't know with precision. For instance, the power index remains uncertain, as it will be explained.
The power-law model has the following form:

$$\frac{d\phi}{dE_\nu} = \phi_0 \left(\frac{E_\nu}{100 \text{ TeV}} \right)^\gamma$$

with $\phi_0 = 1.1 \times 10^{-18}$ GeV^{-1}s^{-1}sr^{-1}cm^{-2} and $\gamma \in [-2.9, -2.1]$ [62]. The value of the power index actually depends on how the flux was fitted. If one uses the High-Energy Starting Events (HESE), *i.e.* high-energy events that start within the detector, the index will be the lower boundary. If one decides to do it with the through-going muons (Thμ), in other words, infer the

flux from the up-going muons, the upper value is obtained. The fact that different power indices are obtained using different methods is a problem, since in both cases, we are observing the same thing: neutrinos. It is a hint that we are missing something. That discrepancy can lead to big differences in the prediction, as will be discussed later in Chapter 3.

2.7.4 Event rates and expected number of events

When computing the expected rate of events for the different flavours using a power index $\gamma = -2.5$ [62] and the above normalisation, one obtains the following:

Flavours	**Event rate (s^{-1})**	**Number of event in 1 year**
$\nu_e + \bar{\nu}_e$	$8.17\ 10^{-8}$	2.58
$\nu_\mu + \bar{\nu}_\mu$	$3.94\ 10^{-8}$	1.24
$\nu_\tau + \bar{\nu}_\tau$	$5.59\ 10^{-8}$	1.76

For these computations, a threshold of 60 TeV was imposed, because neutrinos with an energy lower than this are considered to be of atmospheric origins, *i.e* they are the background we are not interested in [63]. Hence one expects to a total of 5.58 events per year. Here, one can associate a quantitative meaning to the qualitative assertion "neutrinos do not interact a lot with matter". Why a $1 - \text{km}^3$ detector must be built appears obvious when such number are computed. Such a tremendous volume does not feel as an exaggeration anymore.

2.7.5 Neutrino flavour ratio

When neutrino mixing was presented before, it was said that in some cases, differentiating neutrinos from antineutrinos is mandatory. The main example is at the heart of this thesis, the Glashow Resonance, for which only $\bar{\nu}_e$ matters. Thus, it is necessary to compute what are the final flavour ratios if neutrinos and antineutrinos are considered separately.

It can be shown[6] that from an initial flux $F^0 = (F^0(\nu_e), F^0(\nu_\mu), F^0(\nu_\tau))^T$, the flux after mixing $F = (F(\nu_e), F(\nu_\mu), F(\nu_\tau))^T$ is given by

$$F = AA^T\ F^0 \qquad \text{with } A = \begin{pmatrix} |U_{e1}|^2 & |U_{e2}|^2 & |U_{e3}|^2 \\ |U_{\mu 1}|^2 & |U_{\mu 2}|^2 & |U_{\mu 3}|^2 \\ |U_{\tau 1}|^2 & |U_{\tau 2}|^2 & |U_{\tau 3}|^2 \end{pmatrix}$$

Let us compute what would be the final flavour ratio in the case where the mechanism through which neutrinos are produced is the $p\gamma$. The initial flux ratio for all the neutrinos is $1:2:0$, with a contribution of $1:1:0$ from the ν and $0:1:0$ from the $\bar{\nu}$. The final ratios are given with their "3σ"[7] range. As expected, they are different from the simple $1:1:1$.
All mathematical details are given in Appendix B.

Initial flavour ratio	**Final flux ratio**($\pm 3\sigma$)
$\nu = 1:1:0$	$0.73^{+0.11}_{-0.03} : 0.62^{+0.03}_{-0.01} : 0.65^{+0.01}_{-0.11}$
$\bar{\nu} = 0:1:0$	$0.19^{+0.10}_{-0.04} : 0.44^{+0.03}_{-0.10} : 0.38^{0.01}_{-0.03}$
$\nu + \bar{\nu} = 1:2:0$	$0.92^{+0.19}_{-0.04} : 1.06^{+0.05}_{-0.09} : 1.03^{+0}_{-0.11}$

[6] cf Appendix B

[7] It is not really the 3σ range. As it will be explained right after, it is actually the maximum and minimum values one can expect.

To obtain these values, the error propagation was done as follows. The PMNS matrix is parameterised by three mixing angles and a CP violation phase. It can be written as:

$$U = \begin{pmatrix} c_{12}c_{13} & s_{12}c_{13} & s_{13}e^{-i\delta} \\ -s_{12}c_{23} - c_{12}s_{23}s_{13}e^{i\delta} & c_{12}c_{23} - s_{12}s_{23}s_{13}e^{i\delta} & s_{23}c_{13} \\ s_{12}s_{23} - c_{12}c_{23}s_{13}e^{i\delta} & -c_{12}s_{23} - s_{12}c_{23}s_{13}e^{i\delta} & c_{23}c_{13} \end{pmatrix} \text{[22]}$$

with $c_{ij} = \cos(\theta_{ij}),\ s_{ij} = \sin(\theta_{ij})$.
The values of the different mixing angles θ_{ij} and the phase δ with their 1σ error are given in [21] and are the following:

	Best fit value $\pm$ 1σ variation on parameters
θ_{12} (°)	$33.82^{+0.78}_{-0.76}$
θ_{23} (°)	$48.3^{+1.1}_{-1.9}$
θ_{13} (°)	$8.61^{+0.13}_{-0.13}$
δ (°)	222^{+38}_{-28}

Table 2.1: Best fit value of the PMNS matrix parameters: the 3 mixing angles θ_{12}, θ_{23}, θ_{13} and the CP violating phase δ, with their corresponding 1σ variation. Values given by [21].

These are for the normal ordering mass hierarchy. However, the values are not that different for the inverted one. What was done is consider every combination of angles within their respective 3σ range to obtain the interval in which the prediction of mixing ratio can vary. However, it is not the regular 3σ interval, rather the maximum and minimum values that can be expected. The PMNS matrix must be unitary, thus by working with sine and cosine function, that condition is always fulfilled. This method allows to consider the asymmetric error and no symmetrisation is required.

Chapter 3

The Glashow Resonance: the long sought process

The Glashow resonance is a resonant process involving an electron antineutrino and an electron that interact through an on-shell W^-. It was first presented by Sheldon L. Glashow in 1959 [64]. This process will prove to be of utmost importance in the following part of this work, hence this dedicated chapter. In a few words, this event became important because the expected rate of events should be higher than for other neutrino events, due to its resonant nature, but it wasn't observed in 6 years of observation. Only one candidate event was detected during another observation run of 4.6 years.
An introduction to resonant processes will be made before the actual Glashow Resonance is analysed.

3.1 Cross section

3.1.1 An introduction to resonance

Before considering the true computation of the Glashow resonance cross section, it is instructive to consider a similar process in the realm of quantum electrodynamics, *i.e.* without involving the Weak Interaction. This will allow us to observe where the resonance comes from. The process, which we'll call "Pseudo Glashow Resonance", is as follows:

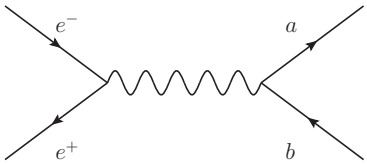

Figure 3.1: Pseudo Glashow resonance, without involving the Weak Interaction. More specifically, the process involves a fermion and an antifermion (*e.g.* an electron and a positron here), x and y may represent any particle-antiparticle pair, e.g. muon and antimuon. The propagator represents a massive photon, similar to a Z^0.

To compute the cross section of this process, the Proca propagator is used, because it describes a massive vector boson. It is obtained by solving the inhomogeneous field equation for a point-like

source obtained from the Lagrangian of a free massive vector boson [65].
Without going over all the details[1], one can obtain:

$$\sigma = \frac{e^4}{12\pi^2} \frac{s}{(s-M^2)^2 + M^2\Gamma^2}$$

The details are not shown here, but when the actual Glashow Resonance will be studied, they will be. This expression can be simplified by using the Narrow-Width approximation, which is

$$\frac{1}{(s-M^2)^2 + M^2\Gamma^2} \to \frac{\pi}{M\Gamma}\delta(s-M^2)$$

as Γ tends to zero[2]. While being useful mathematically, this approximation actually has a physical meaning. The decay width is proportional to the inverse of the lifetime of a particle [66]. The bigger the width, the smaller the lifetime, and vice-versa. In other words, considering as a first approximation that the width tends to zero means that we consider that the lifetime tends to infinity. Even though it has a physical meaning, one can wonder if the approximation holds, and where it comes from. If one computed the exact expression of the cross section and plotted it, one would obtain something similar the blue curve on Fig. 2.7. Considering the Narrow-Width Approximation is equivalent to replacing the spike in the curve by a Dirac delta distribution at the center of the said spike. Numerically, if one computed the area under the curve using rectangles, there would be one dominant one right under the spike, which can be approximated as a delta. If there wasn't such a dominant spike, in other words, if the area of the spike wasn't several orders of magnitude bigger than that under other parts of the curve, the approximation would not hold. However, it does, because any unstable particle[3] implies that a scattering process that induces the creation and then the decay of such a particle will be enhanced when the energy of the center-of-mass, s, is near the square mass M^2, as can be seen in the expression of the cross section and in Fig. 2.7. Therefore, considering the Narrow-Width approximation means that we consider the process to occur precisely at that resonant energy, hence the delta. A consequence of this Narrow-Width Approximation is that the process can be considered not as a single one, but rather as a 2-step phenomenon. From the point of view of Feynman diagrams, it would be equivalent to write:

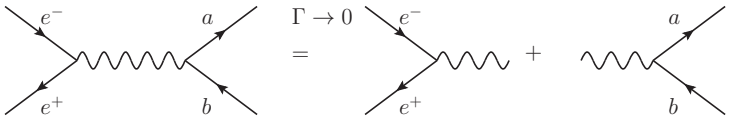

Figure 3.2: Pseudo Glashow Resonance shown in two steps, *i.e* on 2 separate processes. This holds while the decay width Γ tends to zero, so that one can consider a first step that creates a massive on-shell boson, and another one in which the boson decays.

When considering the two processes individually, one computes the cross section of the first step, then the branching function[4] of the second. The cross section of the 1-step process is equivalent

[1]The full details of the computation will be shown for the actual Glashow Resonance process. The current computation follows along similar lines.

[2]See Appendix C for the proof.

[3]The propagator of an unstable massive particle is not $-i\frac{g^{\mu\nu} - \frac{q^\mu q^\nu}{M^2}}{q^2 - M^2}$ but $-i\frac{g^{\mu\nu} - \frac{q^\mu q^\nu}{M^2}}{q^2 - M^2 + iM\Gamma}$. There is an additional term in the denominator which contains the decay width. A stable particle has an infinite lifetime, *i.e.* $\Gamma = 0$.

[4]The branching function of the decay channel i, B_i, is given by $B_i = \Gamma_i/\Gamma$, where Γ is the decay width of the boson, and Γ_i the decay width relative to the channel i.

to the product of both.

Now that the resonant phenomenon in the realm of quantum electrodynamics has been introduced, let us dive into the electroweak one, in which the Glashow Resonance lives.

3.1.2 The Glashow Resonance

The Glashow Resonance is an s-channel process through which an electron antineutrino interacts with an electron at rest[5] through an on-shell W^-. The resonance occurs when the antineutrino has an energy of 6.3 PeV in the lab-frame, as it will be shown right after.

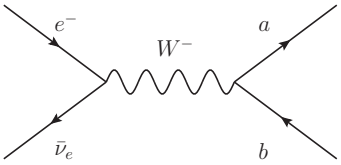

Figure 3.3: Glashow Resonance diagram. The process involves the interaction of an electron and an electron antineutrino through a negatively charged weak boson. x and y are unspecified particles.

The total cross section of the phenomenon can be computed and is given by

$$\sigma_{GR}(E_\nu) = \frac{4}{3}\frac{G_F^2 m E_\nu}{2\pi}\frac{1}{\left(1-\frac{2mE_\nu}{M_W^2}\right)^2+\frac{\Gamma_W^2}{M_W^2}}$$

with G_F the Fermi coupling constant, m the mass of the electron, E_ν the energy of the neutrino, Γ_W the decay width of the W boson, and M_W its mass.

The resonance occurs when the denominator is minimal, which happens when

$$\frac{2mE_\nu}{M_W^2} = 1 \qquad \Longrightarrow \qquad E_\nu = \frac{M_W^2}{2m} \approx 6.3\ PeV$$

The detailed computation can be found Appendix D.

3.2 High Energy Starting Events

The number of expected Glashow Resonance events can be computed in different ways. As explained above, one can use the effective areas, or the analytical cross section. In addition, several spectral indices are available. In this section, all of this will be analysed.

Let us first consider a High Energy Starting Event, or HESE. When a neutrino travels in the Universe, it can interact as long as there is matter, even though the probability is very low. If this event occurs very far from the detector, for instance on the Moon, it would be useless for IceCube. If the event begins in the detector, *i.e.* the interaction vertex is inside the cubic kilometre of instrumented ice, one speaks of starting events. From an energy of the order of the MeV, one speaks of high-energy starting events. However, IceCube has an energy threshold under which it is not sensitive, which stands at roughly 10 GeV, thus only these energies onward will be detected.

[5]The electron being at rest means it is part of the detector material, which is by definition at rest in the lab-frame.

3.2.1 Cross section and effective area

First, let us try to understand what would be the number of resonant events compared to the total number of electron (anti)neutrino events. The muon and tau events are not considered, since the Glashow Resonance does not involve any of them, and IceCube is able to distinguish between the three flavours around the GR energy, *i.e.* in the PeV range. A resonant event is defined here as an electron antineutrino event that occurs in the resonant energy bin defined by [4.75 PeV, 8 PeV]. Let us note that it is only possible to distinguish antineutrino from neutrino events while working with the analytical cross section. When working with effective areas, a resonant event would be any electron (anti)neutrino event in this bin.

Before going further, please note that using cross sections or effective areas do not mean working with different or competing methods. Rather, effective areas also include specific detector effects that are missed when working in a purely theoretical framework. In that sense, effective areas are more complete since they already take neutrino cross sections into account, and thus constitute a more accurate estimation of the rate of events. The disadvantage is that since neutrino flavours cannot be distinguished by IceCube, they cannot either be distinguished with effective areas.

Let us first consider why this resonant bin has been defined as above. The IceCube data are given in three columns: the left and right border of the energy bin, and its effective area. The spike corresponding to the Glashow Resonance, given by the theoretical cross section, is in the [5.75 PeV, 6.92 PeV] bin. However, choosing only this bin leads to wrong predictions as it is too narrow and does not contain the whole spike. Thus, the previous and following bins were included, hence the chosen energy range.

Computing the expected number of events using the effective areas will give a lower value than with the theoretical cross section. This might come as a discrepancy, since the resonant events are only due to $\bar{\nu}_e$, which are only a fraction of the total ν_e flux. It can be explained by the fact that the detection is not perfect. These additional detector effects are considered in the effective areas, but are absent when working in a purely theoretical framework, as it is done when using the analytical cross section.

3.2.2 Fraction of $\bar{\nu}_e$ at the Earth

If we study the Glashow Resonance, it is important to distinguish particles and antiparticles in the incoming flux of neutrinos as only the $\bar{\nu_e}$ matter. Different mechanisms will lead to different initial neutrino flavour ratios, which will then mix and provide different final ratios. As how the neutrinos are produced remains unknown, one must consider different initial ratios, and how they will end up after mixing.

One production mechanism is the $p\gamma$. It leads to a $1:1:0$ and $0:1:0$[6] at source. Another is β^- decay, where a neutron decays into a proton, an electron and a neutrino: $n \to pe\bar{\nu}_e$. Here, one has $0:0:0$ and $1:0:0$. These two situations may be seen as two extremes, in the sense that the former mechanism leads to no $\bar{\nu}_e$, whereas the latter gives a flux entirely made of them. One can plot the $\bar{\nu}_e$ ratio after mixing as a function of the initial one. Only the anti-neutrinos matter here, as neutrinos will only oscillate in neutrinos, not antineutrinos. The results are shown on Fig. 3.4 with the associated "3σ error range"[7].
The procedure was the following: the final ratio was computed for a ratio of $\alpha : 1-\alpha : 0$, α ranging from 0 to 1. When it is equal to 0 (extreme left), we are considering the β^- decay

[6] This writing means that the ν flux ratio is $1:1:0$, while the $\bar{\nu}$ one is $0:1:0$.

[7] Once again, it is not the 3σ error, but rather the minimum and maximum values one could expect, obtained by considering the 3σ range of the PMNS matrix parameters.

mechanism. When it is equal to 1, we are considering the $p\gamma$ one. As a reminder, we are only talking about antineutrinos. For each value of α, the 3σ range was computed in a similar way to the PMNS matrix error range.

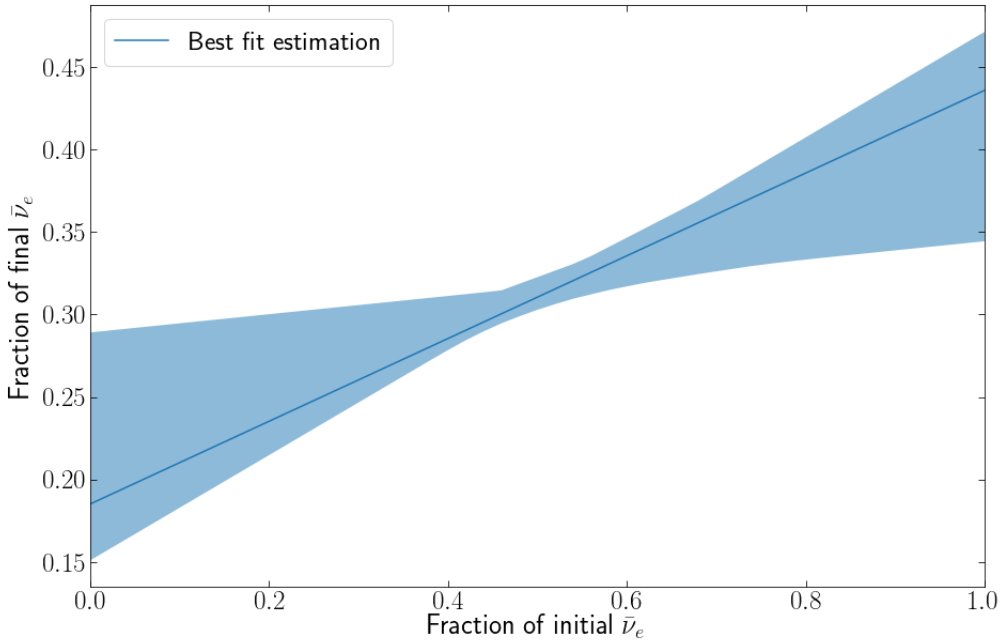

Figure 3.4: Final number of $\bar{\nu}_e$ after standard oscillation mixing as a function of the initial number of $\bar{\nu}_e$. The solid line corresponds to the result considering the best fit values of the PMNS matrix, and shaded areas correspond to the "3σ error range".

3.2.3 Event rates as a function of $\bar{\nu}_e$

Using the cross section derived above, let us compute the number of Glashow Resonance events one should expect in the [4.76 PeV, 8 PeV] energy bin. Moreover, let us plot the number of expected non-resonant events in the same bin as well. These events are the Neutral and Charged Current events. To do so, the cross sections are taken from [51] and are modeled as power laws as follows:

$$\sigma_{CC}(\nu N) = 2.69 \times 10^{-36} (\frac{E_\nu}{1GeV})^{0.402}\ cm^2 \qquad \sigma_{NC}(\nu N) = 1.06 \times 10^{-36} (\frac{E_\nu}{1GeV})^{0.408}\ cm^2$$
$$\sigma_{CC}(\bar{\nu} N) = 2.53 \times 10^{-36} (\frac{E_\nu}{1GeV})^{0.404}\ cm^2 \qquad \sigma_{NC}(\bar{\nu} N) = 0.98 \times 10^{-36} (\frac{E_\nu}{1GeV})^{0.410}\ cm^2$$

One obtains the following plot:

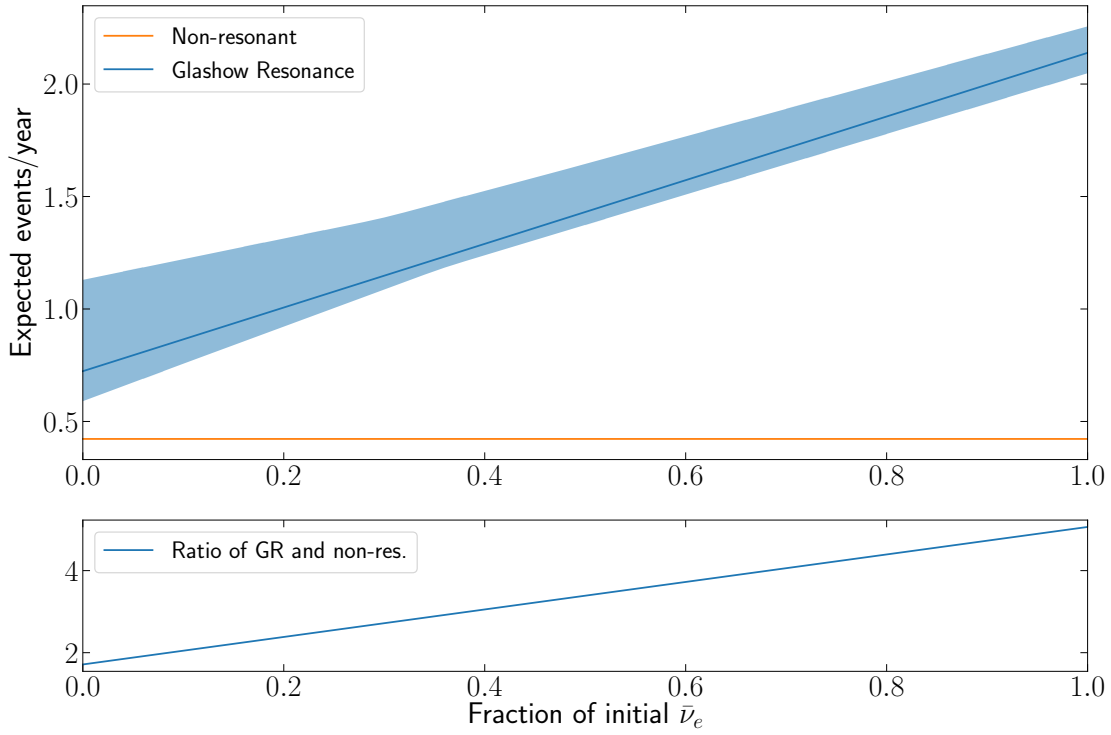

Figure 3.5: Top: Expected number of resonant (*i.e.* Glashow Resonance) and non-resonant events (all the other possible neutrino interactions within the detector) in the [4.76 PeV, 8 PeV] energy bin during a year as a function of the fraction of initial $\bar{\nu}_e$.
Bottom: Ratio of resonant over non-resonant expected event rate as a function of the fraction of initial $\bar{\nu}_e$.

First, it can be seen that the number of non-resonant events does not vary with the fraction of $\bar{\nu}_e$. These events are computed using the above cross sections. Their number only depend on whether the interaction is through a charged $W^{\pm}$ or a neutral Z^0, and if the particle that interacts with the nucleon is a neutrino or an antineutrino. It does not depend on the flavour. What matters is the number of total (anti)neutrinos, so it does not matter how they are distributed among the flavours. In our situation, the number of $\bar{\nu}$ is 1, no matter whether the flavour ratio is $0:1:0$, $1:0:0$ or something in-between.

The number of expected resonant events varies a lot depending on the initial fraction of $\bar{\nu}_e$. It ranges from less than 1 to more than 2 in a year. One can note that no $\bar{\nu}_e$ at the source does not mean that no resonant event occurs, since there is always a non-zero $\bar{\nu}_e$ component in the final neutrino flux. However, the intuition that more $\bar{\nu}_e$ at the source implies more $\bar{\nu}_e$ at the end, and thus more resonant events, is right.

3.2.4 Event rates as a function of the spectral index γ

The mechanism(s) through which neutrinos are produced is unknown. The same goes for the flux. It can be fitted by a power law of the form $\frac{d\phi}{dE_\nu} = \phi_0 \left(\frac{E_\nu}{100\ TeV}\right)^{\gamma}$. Depending on the source, different spectral indices are to be expected. Without concerning ourselves with the

normalisation, the index can vary from -2.9 using HESE to obtain the fitting, to -2.2 using through-going muons. One can plot the expected number of events, fixing the initial flux ratio of $\bar{\nu}$ at $0:1:0$[8].

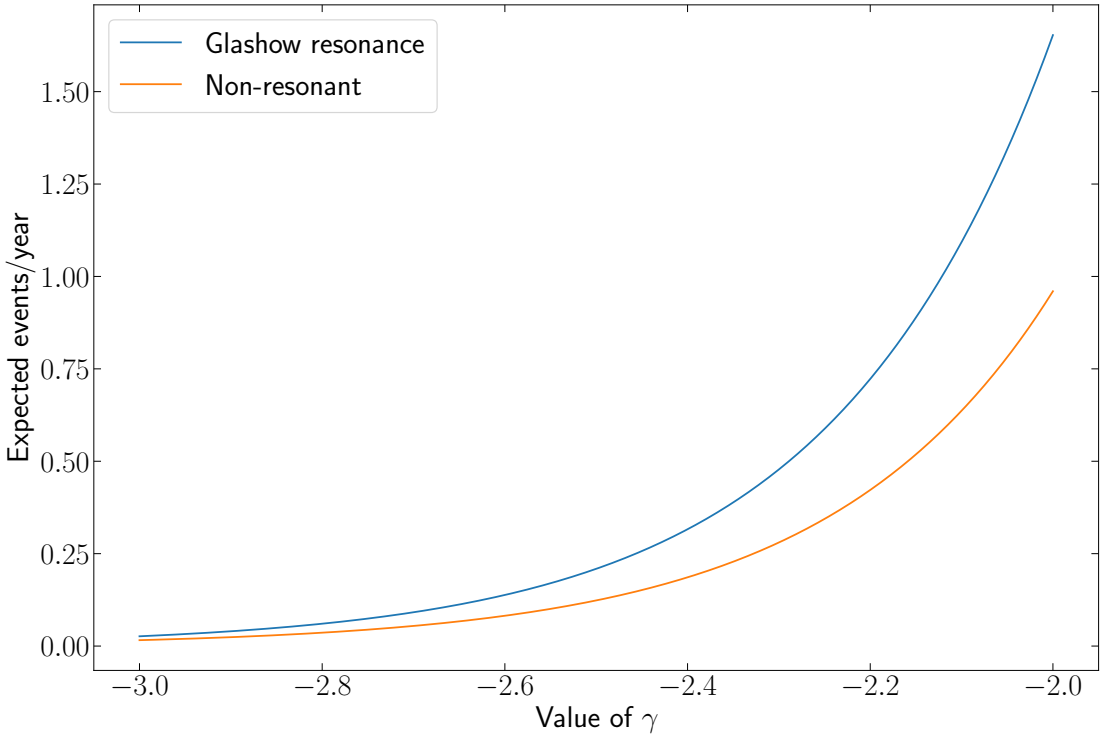

Figure 3.6: Number of expected resonant (Glashow Resonance) and non-resonant events (all the other possible neutrino interactions within the detector) per year as a function of the power index γ in the resonant energy bin ([4.76 PeV, 8 PeV]).

The softer the spectrum, *i.e.* the more negative the value of γ, the fewer expected events. Depending on the index, although the difference is only 0.8, since it is a power law, it gives widely different predictions, as can be seen on on Fig. 3.6. There are 2 important value of the spectral index gamma, given by the fitting of the diffuse neutrino flux using either starting events or through-going muons originating from neutrino events. The best-fit spectral index obtain using starting events is $\gamma = -2.91$ and one predicts 0.061 event per year (0.038 resonant and 0.023 non resonant event). The best-fit index using through-going muons is $\gamma = -2.19$, and one predicts 1.193 events per year in the resonant bin (0.753 resonant and 0.440 non-resonant event) events per year. As will be explained later, the normalisation is different depending on the spectral index, but since the aim of this section is to only assess the importance of the spectral index, we assumed the same normalisation for both computation, which is $\phi_0 = 1.1 \times 10^{-18}$ GeV^{-1}s^{-1}sr^{-1}cm^{-2}. On can see that the different best-fit fluxes gives very different event rates. The one obtained by through-going muons means that around one observation per year in the resonant bin is expected, whereas the one obtained with starting event is so low that many years would have to pass before an event is detected.

[8]In this work, the $p\gamma$ mechanism at source will often be assumed.

3.3 PeV Energy Partially Contained Events

PeV Energy Partially-contained Events (PEPE) are cascade events centred outside the IceCube instrumented volume, but large enough to trigger a substantial number of DOMs inside the detector. PEPE will have greater uncertainties in their reconstructed energies, but the corresponding effective area is bigger, at least at high energy. In Fig. 3.7, one can see the IceCube detector from the top, with a clear distinction as to which part is used for which kind of events.

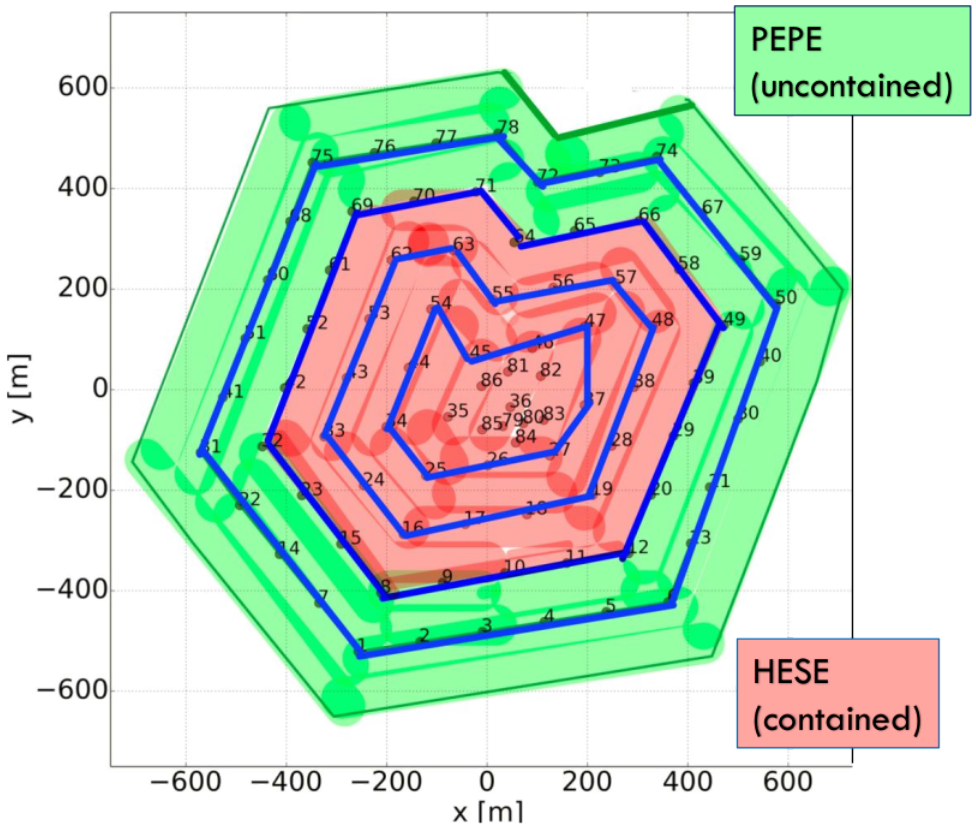

Figure 3.7: Horizontal cut view of the instrumented volume of IceCube. The red part detects the starting events, called HESE, whereas the green one detects the partially-contained events called PEPE. .

By considering the size of the cascade, one can compute new effective areas, this time for PEPE, via simulations. It is useful to compare them, as it is done in Fig.3.8 below, for the $\nu_e + \bar{\nu}_e$. At lower energy, the effective area for HESE is higher than for PEPE. When the energy reaches the PeV scale, the situation is reversed: the PEPE effective area is bigger than the HESE one. This can be understood as follows: the higher the energy, the bigger the cascade created by a neutrino event, thus the further from the detector this event can occur and still be detected. In other words, the higher the energy, the bigger the effective volume/area, for PEPE. The effective area of the lower-end of the energy spectrum is lower for PEPE because fewer DOMs than for HESE activate as the cascades are not big enough to be detected outside the PEPE region.

In Fig.3.8, the green curve seems smoother than the red one. This comes from the fact that the energy binning for the HESE simulations is older and less fine-tuned than for the PEPE. For instance, in the spike related to the Glashow Resonance, the red curve should constantly be under the green one. This is what would happen if smaller energy bins were used for HESE. No matter the binning, the area under the curve for a given type of event is constant. In our

case, the consequence is that the spike related to Glashow Resonance for HESE is wider than it would have been with a finer binning, for instance the one used for PEPE. This "inconsistency" will induce the spikes of the ratio in the high energy part plotted under. There should not be any. Nonetheless, one can still confirm that the general tendency of the PEPE effective area is to increase faster than the HESE one with respect to energy.

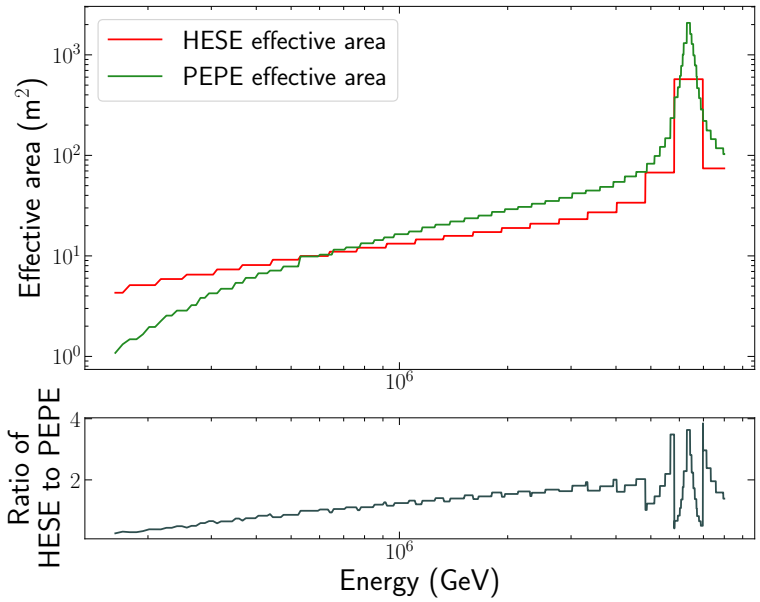

Figure 3.8: Top: Effective area of starting events (*i.e.* HESE, in blue) and partially-contained events (*i.e.* PEPE, in orange). Note the different binning. Bottom: Ratio of the effective area of PEPE over the one of HESE. The spikes are artefacts due to the different binnings between the two kinds of effective areas.

The partially contained events play an important role in the problem that is studied in this work. Using PEPE effective area, one ν_e event at roughly 6.3 PeV was detected during the 4.6 years of observation, which is likely to be a Glashow Resonant event [67]. However, during the 6 years of HESE inspection, no such event was detected. For the same observation period, one should expect around 2 times more PEPE than HESE in the resonant bin. Here, even though the observation window for the former was shorter, more partially contained event are still expected. The discrepancy between prediction and observation comes from the fact that these numbers are too low. Using the power-law flux presented in Section 2.7.3, with a spectral index of $\gamma = -2.5$ [62], 1.766 HESE and 2.904 PEPE are expected in the resonant bin per year of observation, using a spectral index $\gamma = -2.5$ and a normalisation $\phi_0 = 1.1 \times 10^{-18}$ GeV^{-1}s^{-1}sr^{-1}cm^{-2}. It is higher than what has been observed. However, please bear in mind that the spectral index is uncertain and has a big impact on the event rate. Thus, these must be considered as a mean of comparison rather than as absolute number of events.

3.3.1 Event rates as a function of ζ

When working with cross sections, it was easy to consider only the influence of the initial fraction of $\bar{\nu}_e$ because the GR cross section is only for this particle. The situation is different with the partially-contained events. We are working with effective areas, in other words, directly with

IceCube, which cannot distinguish between ν_e and $\bar{\nu}_e$. Therefore, it makes more sense to consider the fraction of electron neutrinos and antineutrinos in the neutrino flux at Earth rather than that of electron antineutrino only.

Let us define $\zeta = \frac{\nu_e + \bar{\nu}_e}{3}$ the fraction of $\nu_e + \bar{\nu}_e$ in the flux. The numerator represents the number of electron (anti)neutrino that arrive at the detector, and the denominator represents the total number of neutrino produced at source, here 3 if one assumes for instance a $p\gamma$ mechanism. The expected number of ν_e events per year of observation as a function of ζ is shown on Fig. 3.9.
Since we do not know the production mechanism nor the flux at Earth after mixing, we made that parameter ζ vary in order to account for a wide range of possibilities. We defined α and β as the numbers of $\bar{\nu}_e$ and ν_e in the flux at the Earth, respectively. The flux ratio is then given by $\bar{\nu} = \alpha : 1 - \alpha : 0$ and $\nu = \beta : 2 - \beta : 0$. α and β vary between 0 and 1, and 0 and 2 respectively. This ensured that the total number of neutrinos was always 3, while varying the flavour composition. For instance, α and $\beta = 0$ correspond to a flux without any $\overset{(-)}{\nu}_e$, while

As stated above, different analyses lead to different best-fit fluxes[9]. There is a flux fitting using the HESE, and another using the through-going muon events. The number of events was computed in the energy bin [$10^{6.6}$ GeV, $10^{6.98}$ GeV], which corresponds to the bins containing the Glashow Resonance spike in PEPE effective areas binning. The different best-fit fluxes and their corresponding errors are the following:

$$\frac{d\Phi_{HESE}}{dE_\nu} = 2.19^{+1.10}_{-0.55} \times 10^{-18} E_\nu^{-2.91^{+0.33}_{-0.22}} \text{ GeV}^{-1}\text{cm}^{-2}\text{s}^{-1}\text{sr}^{-1} \text{ [68]} \tag{3.1}$$

$$\frac{d\Phi_{Th\mu}}{dE_\nu} = 1.01^{1.10}_{0.23} \times 10^{-18} E_\nu^{-2.19\pm0.10} \text{ GeV}^{-1}\text{cm}^{-2}\text{s}^{-1}\text{sr}^{-1} \text{ [69]} \tag{3.2}$$

When the importance of the spectral index was discussed earlier, it was said that the differences between $\gamma = -2.9$ and -2.2 were important. In Fig. 3.9, in addition to the influence of γ, one can also realise the influence of the fraction of electron (anti)neutrinos. No matter the value of the fraction, the difference of prediction between the two fluxes can clearly be seen.

[9]For more details, see *Characterization of the Astrophysical Diffuse Neutrino Flux with IceCube High-Energy Starting Events*, and *Measurement of the Diffuse Muon Neutrino Flux using Starting Track Events in IceCube*, both by the IceCube Collaboration.

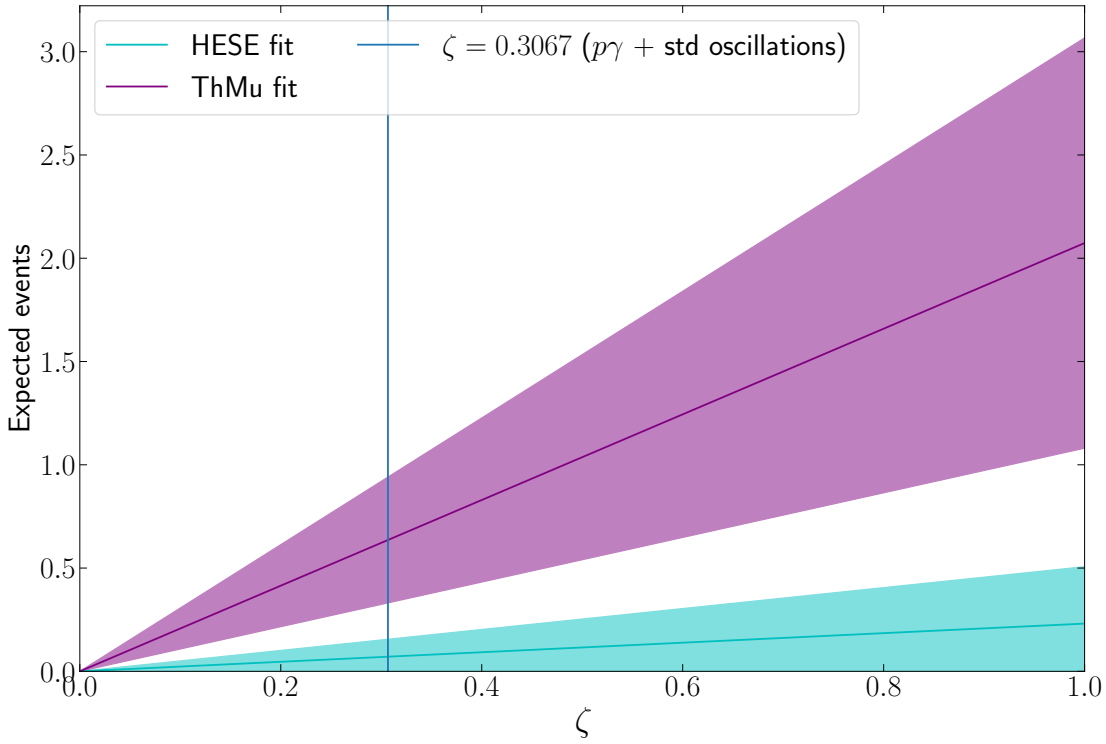

Figure 3.9: Expected number of ν_e events per year in the resonant energy bin as a function of the fraction of electron flavour in the total flux, *i.e.* as a function of $\zeta = \frac{\nu_e + \bar{\nu}_e}{3}$. Solid lines correspond to the best fit values, whereas the shaded areas represent the 1σ error range. The cyan elements refer to the HESE, and the purple ones are related to the Thμ. The vertical line corresponds to value of ζ given considering a $p\gamma$ mechanism at the source plus standard oscillation.

The propagation of error was done using the assumption of independent variables, which leads to the widely used variance formula

$$\sigma_f = \sqrt{\left(\frac{\partial f}{\partial x}\right)^2 \sigma_x^2 + \left(\frac{\partial f}{\partial y}\right)^2 \sigma_y^2 + \left(\frac{\partial f}{\partial z}\right)^2 \sigma_z^2 + ...}$$

with $\sigma_x,\ \sigma_y, \sigma_z, ...$ represents the errors (standard deviations) on the variables $x,\ y,\ z, ...,\ f$ is a function of the said variables, σ_f its error, and the ... symbolises all the other variables that f depends on and that have a non-zero error [70].

There is a clear discrepancy between the diffuse neutrino flux obtained using HESE (initiated by (ν_e and ν_τ) and using through-going muons (initiated by ν_μ), a discrepancy so large that there is no accord even within the error range. This is a problem since both these these fluxes fit the same thing, and thus should yield approximately the same power law and the same number of events.

To put figures on this problem,, Table 3.1 shows the number of ν_e PEPE in the resonant bin for a flavour ratio at Earth given by a $p\gamma$ mechanism at the source plus standard oscillations. There is around one order of magnitude in difference.

Model	ν_e PEPE/year
HESE fit ($\gamma = -2.91$)	0.062
Thμ fit ($\gamma = -2.19$)	0.562

Table 3.1: Number of ν_e PEPE per year in the resonant bin, considering a $p\gamma$ mechanism at the source and standard oscillation. For the HESE best-fit flux, $\gamma = -2.91$, and the normalisation is $\phi_0 = 2.19 \times 10^{-18}$ GeV^{-1}s^{-1}sr^{-1}cm^{-2}. For the Thμ best-fit flux, $\gamma = -2.19$, and the normalisation is $\phi_0 = 1.01 \times 10^{-18}$ GeV^{-1}s^{-1}sr^{-1}cm^{-2}

The only difference between HESE and Thμ lies in the families of neutrinos considered to do the fitting. It might be an indication that there exists a flavour selection mechanism that would deplete the ν_e and ν_τ flavours while leaving the ν_μ unaffected, or at least less affected, towards the higher energies. Since we are trying to reconcile a $\propto E^{-2.9}$ and a $\propto E^{-2.1}$ flux, the ν_e and ν_τ depletion with respect to ν_μ must be at least of around one order of magnitude in order. We will thus investigate flavour selection mechanisms that could result in such a difference between starting and track-like events.

Chapter 4

Non-standard physics in neutrino oscillations

So far, this thesis has focused on standard oscillations were considered. As a reminder, the problems we encounter are the following: firstly, one ν_e[1] resonant event was observed using IceCube PEPE effective areas during 4.6 years of observation, whereas none was observed using the HESE ones for a period of 6 years. In other words, standard oscillations alone fail to explain the decrease of Glashow Resonance such that only this one PEPE is observed. Secondly, the best-fit fluxes using through-going muon events or high-energy starting events are different to a point that they lead to drastically different predictions, the latter being much softer than the former. As stated, the main process that could modify the neutrino flux until now was neutrino oscillation in vacuum, which does not act as a flavour-selecting process. In other words, oscillation will not deplete one or several flavours with respect to others. However, a hint that flavour-dependent processes might play a role can be seen in the Thμ vs HESE problem. Indeed, considering different neutrino events (ν_μ event from outside the detector volume for Thμ, and event starting within the detector for HESE) leads to different fluxes. Thus, more exotic flavour-dependent non-standard interactions are good candidates as a solution to this problem. There are three places where these interactions, that could be interpreted as flavour selection, can take place: at the source, during the neutrino propagation, and at the Earth, for instance through the MSW resonance.

4.1 Flavour selection at the source: spectral averaging

Until now, the neutrino production mechanism that was considered was the $p\gamma$ one, which results in a $1:1:0+0:1:0=1:2:0$ flux. We have shown analytically[2] that through propagation, the ratio at Earth would be $1:1:1$. This was confirmed through computation in 2.7.5, where the final ratio after standard oscillations over long distances was roughly equal to $1:1:1$, at least within a factor 2. However, it may be possible for some non-standard physics to alter the ratios of the flavours at the source. These different spectra would propagate and result in different spectra at Earth as well.

Without examining what mechanism could lead to flavour-specific spectra, let us consider different arbitrary fluxes at the source for the three different neutrino flavours. The fluxes are propagated following the same procedure as before, meaning that we consider oscillations over long distances. As can be seen in Fig. 4.1, even though the initial fluxes (dashed lines) are widely different, after standard oscillations the fluxes are almost identical within a factor 2 (solid lines). In other words, no matter the initial shape of the flavour spectra at the source, the end

[1] As a reminder, it is to be understood as $\nu_e + \bar{\nu}_e$ since IceCube cannot distinguish particles and antiparticles.
[2] See Appendix B

result will approximately always be a $1:1:1$ flavour ratio, which implies that all the spectra of the different flavours will eventually have roughly the same shape. Please note that for this plot to be made, widely different and arbitrary fluxes have been assumed. They bear no physical meaning. For instance, the break at 10^5 GeV exists only because of the assumed shape of the flavour fluxes at source, which has been built by part.

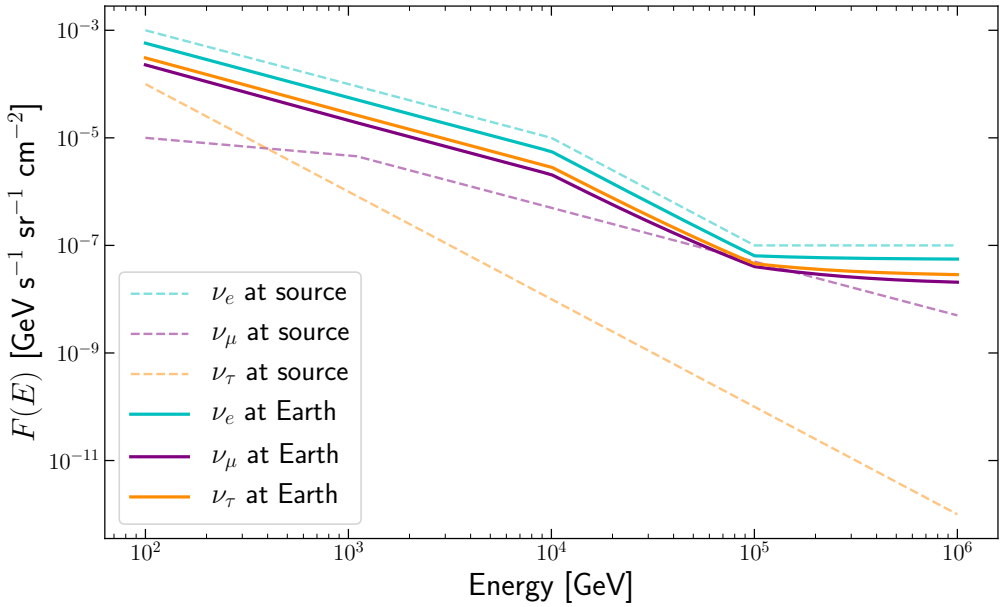

Figure 4.1: Fluxes at the source and after standard oscillations. The dashed lines refer to fluxes at the source, whereas the solid lines represent the flux at Earth, after oscillation. The fluxes related to respectively the electron, muon and tau flavour are in cyan, purple and orange.
Widely different arbitrary spectra are assumed, which are massaged out over long distances. They bear no physical meaning.

It means that flavour selection at the source is not a viable explanation for the lack of Glashow Resonance events, since any such mechanism will be hidden by oscillation over long baselines.

4.2 Flavour selection at Earth

Flavour selection at Earth would mean that there is a process through which neutrinos interacts with the Earth, altering significantly the final spectra. An example of a mechanism that would lead to significant modifications on the fluxes due to neutrino oscillations in matter was introduced in 1.3.2, the MSW resonance[3]. While it has already been studied for atmospheric [71] and solar neutrinos [72], at PeV energies the neutrinos can only travels tens of kilometers, which is not enough for the MSW resonance to occur.

[3]Please note that resonant oscillation in the Earth were considered before Mikheev-Smirnov-Wolfenstein (1986) by Cudell and Gaisser (1985).

4.3 Flavour selection during neutrino propagation

The final way through which there can be a modification of the neutrino spectra at Earth is if the selection occurs during the propagation itself. Several scenarios exist, for instance, neutrino decay, small violation of Lorentz invariance, or the existence of pseudo-Dirac neutrinos. The first one will be addressed in this work.

4.3.1 Neutrino decay: a Standard Model extension

Neutrino decay is a new physics scenario that states that these particles have a finite lifetime. In the realm of the Standard Model, neutrinos are stable particles because they are the lightest ones and can't interact with photons, which means they are forbidden to decay at tree level.

There are two approaches to this new physics. In both, the lightest mass eigenstate is stable. Either one can consider a total decay, *i.e.* disappearance, of the heavier mass eigenstates, or one can consider a partial decay that translates into a new factor in the oscillation probability, as it will be explained later. The latter will be discussed, and leads to an energy-dependent spectra after mixing, as opposed to before where the three flavours had the same spectra at all energies. Complete decay would modify the final ratio, but not in an energy-dependant way, thus it is of no interest here.

In the following, we will thus consider the lightest neutrino mass eigenstate to be stable by construction, since there isn't any lighter particle in which it can decay, whereas the two others will undergo a partial decay. These decays can go according to many channels. There are two families of decays: the visible and invisible ones. There are named following the detectability of the decay products.
Concerning the first family, examples are the radiative two-body decay of the form
$\nu_i \to \nu_j + \gamma$, and three-body decay of the form $\nu \to \nu\nu\bar{\nu}$ [73][74]. The former would lead to the detection of photons, which are not detected, and the latter would be linked to a hypothetical four-neutrinos interaction, constrained by the decay width of Z^0, which is known at a great precision [75] [76]. Both of these kinds of decays already bear tight constraints [74] and thus would not constitute possible decay channels [73][74]. As an example, a feynman diagram for the radiative two-body decay would be the following:

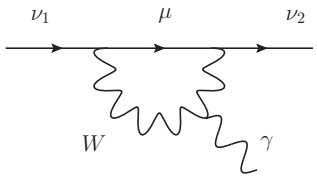

Figure 4.2: Feynman diagram at loop-level of a radiative 2-body neutrino decay.

On the other hand, invisible decays, *i.e.* decays that would not lead to detectable products, can only be weakly constrained by experience and thus better candidates. The products of such a processes are very lightweight and undetectable particles such as sterile neutrinos.

The decay channels of this family of decay have the form:

$$\nu_i \to \nu_j + X \tag{4.1}$$
$$\nu \to X \tag{4.2}$$

where ν_i is a mass eigenstate, and X an invisible, very light or massless particle like a sterile neutrino, or a new particle like a Majoron. In (4.1), the energy of the produced neutrino ν_j is assumed to be significantly reduced compared to the initial ν_i. That way, it does not fall in the IceCube energy range, does not contribute to the diffuse neutrino spectrum, thus the products of decay are indeed invisible.

Neutrino decay and oscillation: the new survival probability

Let us derive analytically the expression of the neutrino flux after decay. To obtain this result, one has to solve the evolution equation equation, in which the Hamiltonian contains a contribution related to decay. The equation can be written

$$i\frac{d\left|\nu\right\rangle}{dt} = \left(\mathcal{H}_0^m + \mathcal{H}_D\right)\left|\nu\right\rangle$$

with $\left|\nu\right\rangle = \left(\left|\nu\right\rangle_1, \left|\nu\right\rangle_2, \left|\nu\right\rangle_3\right)^T$, $\mathcal{H}_0^m$ the vacuum Hamiltonian in the mass basis, and $\mathcal{H}_D$ the decay Hamiltonian. For the normal mass hierarchy, the first mass eigenstate, ν_1, is stable, and the decay Hamiltonian has the form

$$\mathcal{H}_D = \begin{pmatrix} 0 & 0 & 0 \\ 0 & -i\lambda_2 & 0 \\ 0 & 0 & -i\lambda_2 \end{pmatrix}$$

For the inverted mass hierarchy, the third mass eigenstate is considered stable and the two others will decay. $\mathcal{H}_D$ will have the following expression:

$$\mathcal{H}_D = \begin{pmatrix} -i\lambda_1 & 0 & 0 \\ 0 & -i\lambda_2 & 0 \\ 0 & 0 & 0 \end{pmatrix}$$

For both hierarchy, $\lambda_i = \frac{m_i}{E\tau_i}$, with m_i, τ_i and E are the mass, the rest-frame lifetime and the energy of a flux of neutrino ν_i that propagates over a distance L. One can note that the shape of the decaying part of the equation is identical to the regular decay equation one could find for the population of radioactive particles, for instance. This comes as no surprise, since we "forced" this shape of equation by manually introducing a Hamiltonian with the above form, necessarily leading to an exponential decay of the mass eigenstates. The solution of this equation will be the same as in 1.3, only with an additional exponential factor translating the decay:

$$exp = (-\lambda_i \cdot t) = exp(-\frac{L}{E} \cdot \frac{m_i}{\tau_i})$$

in natural units ($c = 1$), with t is the time in the observer's frame.

To show it, let us consider once again the 2-flavour framework, in which the first mass eigenstate decays, and the second is stable. It bears no physical meaning, but it allows to easily show the consequence of the introduction of this decay Hamiltonian. The following reasoning is almost

identical in the 3-flavour framework. The evolution equation for the 2 mass eigenstates is

$$\begin{aligned} i\frac{d}{dt}\begin{pmatrix}|\nu_1\rangle\\|\nu_2\rangle\end{pmatrix} &= (\mathcal{H}_{0,2}+\mathcal{H}_{D,2})\begin{pmatrix}|\nu_1\rangle\\|\nu_2\rangle\end{pmatrix} \\ &= \begin{pmatrix}E_1|\nu_1\rangle\\E_2|\nu_2\rangle\end{pmatrix} + \begin{pmatrix}-i\lambda_1 & 0\\0 & 0\end{pmatrix}\begin{pmatrix}|\nu_1\rangle\\|\nu_2\rangle\end{pmatrix} \\ &= \begin{pmatrix}E_1-i\lambda_1 & 0\\0 & E_2\end{pmatrix}\begin{pmatrix}|\nu_1\rangle\\|\nu_2\rangle\end{pmatrix} \end{aligned}$$

where $\mathcal{H}^m_{0,2}$ and $\mathcal{H}_{D,2}$ denote the vacuum and decay hamiltonian where the first mass eigenstate decay, in the 2-flavour framework. To this, the solution is obtain straightforwardly:

$$\begin{aligned} |\nu_1(t)\rangle &= |\nu_1(t=t_0)\rangle \cdot exp((-iE_1-\lambda)t) \\ |\nu_2(t)\rangle &= |\nu_2(t=t_0)\rangle \cdot exp(-iE_2t) \end{aligned}$$

One can note the appearance of an exponential decrease in the first mass eigenstate. To obtain the flavour eigenstates, one simply has to multiply $|\nu\rangle = (|\nu_1\rangle, |\nu_2\rangle, |\nu_3\rangle)^T$ by the PMNS matrix, as was done before, in the 3-flavour framework.

The probability that a neutrino ν_α oscillates in a ν_β over long distances is then given by

$$P_{\alpha\beta} = \sum_i |U_{\alpha i}|^2 |U_{\beta i}|^2 e^{-\frac{L}{E}\frac{m_i}{\tau_i}}$$

We will work under the simplifying assumption $\tau_i/m_i = \tau/m$ for the decaying neutrinos. In the normal mass hierarchy, the lightest one is ν_1, which will be assumed stable, and we will assume $\tau_2/m_2 = \tau_3/m_3 = \tau/m$. For the inverted one, we will work with ν_3 as the stable neutrino, and $\tau_1/m_1 = \tau_2/m_2 = \tau/m$. Generalising these assumptions will however not change the conclusions of our analysis. In the following, we will use the appellation "lifetime" for τ/m instead of τ. We work with the former rather than the latter, because when trying to determine the neutrino lifetimes, we only have access to the ratio τ/m, since the neutrino masses are unknown.

One can then wonder which value of the lifetime must be considered. There are two extreme cases. The "no decay" case corresponds to lifetimes such that all the neutrinos within the IceCube energy range arrive intact. To know when this is the case, as the effective areas of the detector are given for energy ranging from $10^{4.78}$ GeV to 10^7 GeV, we made plots of the final fluxes for the different flavours in [$10^{4.78}$ GeV, 10^8 GeV]. Since the region of interest is the vicinity of the Glashow Resonance Energy (6.3 PeV), there is no point in extending the region towards lower energy, but extending it towards higher energy could allow us to have a more global picture of what is happening. The minimum lifetime for the neutrinos to arrive unscathed in this range is $\tau/m \approx 10^3$ s/eV. The other extreme case naturally corresponds to the one where all the neutrino within that range have decayed. This happens for a lifetime smaller than 10^{-4} s/eV. The region of interest for lifetime is naturally chosen as [10^{-4} s/eV, 10^3 s/eV].

In the following, we will consider once again a power law flux. We will integrate over the redshift, in other words, we will consider all the sources from our vicinity $z = 0$ to a certain z_{max}. Rigorously, it should be taken as $z_{max} \to +\infty$, but we chose $z_{max} = 10$ as the integrand above this value will approximately be zero. The redshift z can be described by

$$\frac{\lambda}{\lambda_0} = 1 + z$$

with λ_0 and λ being the wavelength of a signal at source and at detection. This can be re-expressed as a function of the energy of a particle at source E_0 and at the detector E in the

form

$$\frac{E_0}{E} = 1 + z$$

To introduce the redshift dependence inside the probabilities and the flux, we will simply replace E by $E(1+z)$ wherever the energy appears. Moreover, since we are considering different redshifts, we are considering different sources at different distances. The distance L that appears inside the exponential cannot be constant and must also depend on z. $L(z)$ is the light-travelled distance, defined by

$$L(z) = L_H \int_0^z \frac{dz'}{(1+z')h(z')}$$

with $L_H \equiv c/H_0 \approx 4.55\ Gpc$, $h(z) \equiv H(z)/H_0$, H_0 the Hubble constant chosen as 65.89 $\frac{\text{km}}{\text{s·Mpc}}$, and $H(z) \equiv H_0\sqrt{\Omega_m(1+z)^3 + \Omega_\Lambda}$ the Hubble parameter, assuming a flat Universe with $\Omega_m = 0.27$ and $\Omega_\Lambda = 0.73$. Considering the light-travelled distance means that the trigger of neutrino decay "clock" is directly related to the distance it has crossed since its creation [77].

Taking all this into account, and assuming a homogeneous distribution of sources, the diffuse flux of a flavour α at the Earth as a function of the energy is given by [73]

$$\frac{d\Phi_{\nu_\alpha}}{dE_\nu} = \int_{z_{min}}^{z_{max}} dz \sum_{i\beta} \frac{d\Phi_{\nu_\beta}^{source}(E,z)}{dE_\nu} |U_{\alpha i}|^2 |U_{\beta i}|^2 e^{-\frac{L(z)}{E}\frac{m_i}{\tau_i}} \tag{4.3}$$

Please note that at this point, the code used to compute the flux has to be parallelised in order to be able to run in a realistic amount of time.

One can then compute the different neutrinos fluxes at Earth, depending on the hierarchy, considering different lifetimes. For the following plots, the flux that was used is the one obtained from the through-going muon analysis, with the best-fit values, considering in addition the redshift dependance of the energy:

$$\frac{d\phi}{dE_\nu} = \phi_0 \left(\frac{E_\nu(1+z)}{100\ TeV}\right)^\gamma,$$

with $\phi_0 = 1.1\ 10^{-18}\ \text{GeV}^{-1}\text{s}^{-1}\text{sr}^{-1}\text{cm}^{-2}$, and $\gamma = -2.1$. We chose the Thμ best-fit flux rather than the HESE one because we want to be able to explain both Thμ and HESE fit fluxes considering neutrino decay. We thus kept the higher of the two, and see if we could make the two agree this by reducing it through decay.

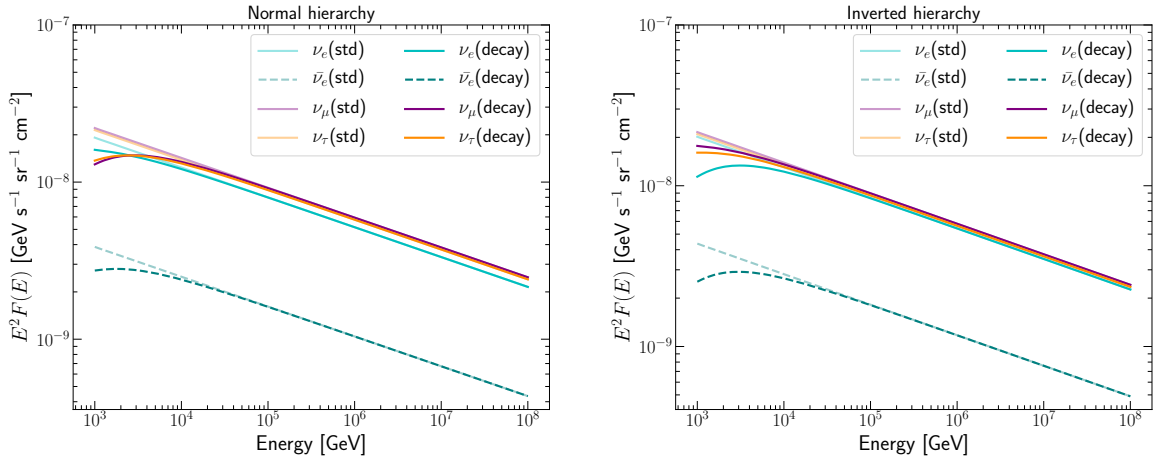

Figure 4.3: Final $\nu + \bar{\nu}$ fluxes after propagation over long distances considering neutrino decay, for the normal (left) and inverted (right) mass hierarchy, for a lifetime $\tau/m = 10^2$ s/eV. The ν_α, $\alpha = e, \mu, \tau$ fluxes are actually the $\nu_\alpha + \bar{\nu}_\alpha$ fluxes, and are shown in respectively light blue, purple and orange, whereas the $\bar{\nu}_e$ one is solely the electron antineutrino one, and is shown in a darker shade of blue.

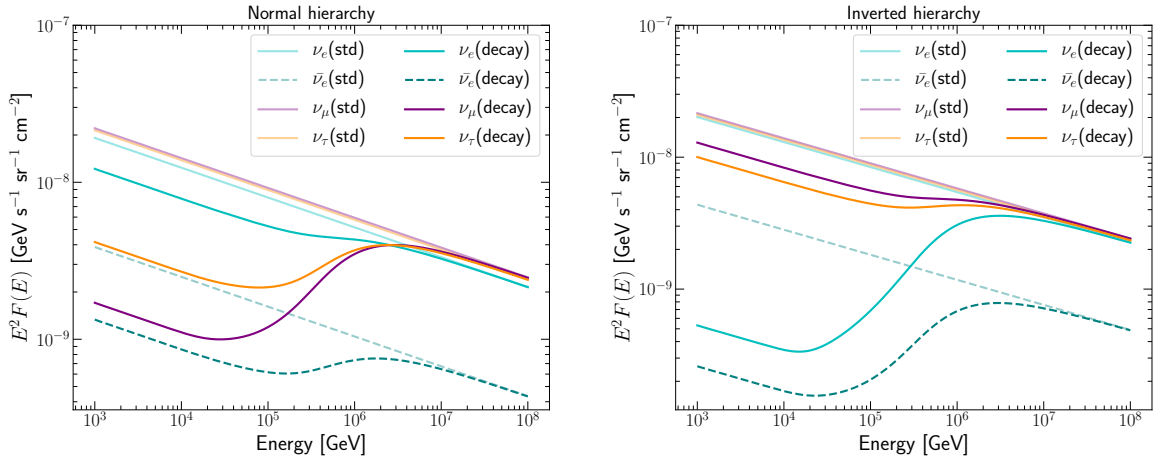

Figure 4.4: Final $\nu + \bar{\nu}$ fluxes after propagation over long distances considering neutrino decay, for the normal (left) and inverted (right) mass hierarchy, for a lifetime $\tau/m = 10^{-1}$ s/eV. The ν_α, $\alpha = e, \mu, \tau$ fluxes are actually the $\nu_\alpha + \bar{\nu}_\alpha$ fluxes, and are shown in respectively light blue, purple and orange, whereas the $\bar{\nu}_e$ one is solely the electron antineutrino one, and is shown in a darker shade of blue.

In Fig. 4.3 and Fig. 4.4 are shown the final $\nu_\alpha + \bar{\nu}_\alpha$, $\alpha = e, \mu, \tau$ and $\bar{\nu}_e$ fluxes at Earth, considering standard oscillations only, and standard oscillation plus neutrino decay. If the lifetime is high, almost no effects are noticeable in IceCube energy range, and there is no change whatsoever in the resonant bin[4]. It comes from the fact that the higher the lifetime, the more stable the neutrinos, thus the less effects due to decay. This can be further confirmed by computing the

[4] As a reminder, the resonant bin was defined as $[4.75\ PeV,\ 8\ PeV]$ and was chosen to encompass the full spike in the ν_e effective area due to Glashow Resonance, according to IceCube's binning

expected number of events with or without decay in this particular bin, which remains the same in both hierarchies. The number of events are shown in Tables 4.1 and 4.2.

At a lifetime of 10^{-1} s/eV, effects are starting to manifest inside the resonant bin. They do so starting from the lower energy end. It comes from the fact that the higher the energy, the smaller the effects of decay, since the energy appears on the denominator of the exponential in 4.3. These are not extremely important in the normal mass hierarchy, even for shorter lifetimes, at least for the ν_e, which is the flavour we are interested in since it is the one leading to Glashow Resonance. Thus, plots for lower lifetimes will be considered for the inverted hierarchy only.

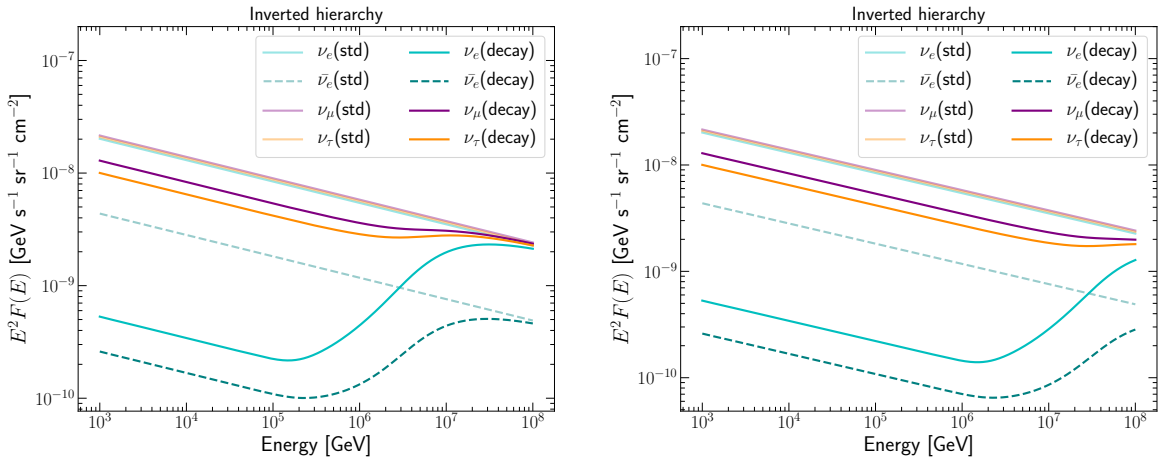

Figure 4.5: Final $\nu + \bar{\nu}$ fluxes after propagation over long distances considering neutrino decay, in the inverted mass hierarchy, for different lifetimes.
On the left: $\tau/m = 10^{-2}$ s/eV.
On the right: $\tau/m = 10^{-3}$ s/eV.
The $\nu_\alpha,\ \alpha = e, \mu, \tau$ fluxes are actually the $\nu_\alpha + \bar{\nu}_\alpha$ fluxes, and are shown in respectively light blue, purple and orange, whereas the $\bar{\nu}_e$ one is solely the electron antineutrino one, and is shown in a darker shade of blue.

On Fig.4.5, the effects are getting more important in the resonant bin. This can also be seen in the number of events.

The table below sums up the expected number of ν_e, ν_μ, ν_τ and Glashow resonance events in the resonant bin, for both hierarchy, for different lifetimes. Please bear in mind that the number of resonant events is computed using the analytical cross section, whereas the others are obtained using IceCube effective areas. The consequence is that the former is always bigger than the others, but this is however not a discrepancy, as it has already been discussed before.

		Lifetime (s/eV)						
Hierarchy	Events	10^2	10^1	10^0	10^{-1}	10^{-2}	10^{-3}	∞
Normal	ν_e	0.295	0.295	0.294	0.284	0.231	0.191	0.295
	GR	0.597	0.597	0.593	0.559	0.365	0.218	0.597
	ν_μ	0.040	0.040	0.039	0.036	0.018	0.004	0.040
	ν_τ	0.043	0.043	0.042	0.039	0.022	0.009	0.043
Inverted	ν_e	0.310	0.310	0.307	0.281	0.131	0.018	0.310
	GR	0.674	0.673	0.667	0.612	0.298	0.060	0.674
	ν_μ	0.039	0.039	0.039	0.037	0.039	0.024	0.039
	ν_τ	0.042	0.042	0.042	0.040	0.029	0.021	0.042

Table 4.1: Number of expected events in the resonant bin considering neutrino decay and standard oscillations for both hierarchies. ν_α where $\alpha = e, \mu, \tau$ refers to events involving $\nu_\alpha + \bar{\nu}_\alpha$, computed using effective areas. Glashow Resonance (GR) events were computed using the analytical cross section, which involves $\bar{\nu}_e$ only. The lifetime ∞ corresponds to standard oscillations only, *i.e.* no decay.

		Lifetime (s/eV)						
Hierarchy	Events	10^2	10^1	10^0	10^{-1}	10^{-2}	10^{-3}	∞
Normal	ν_e	2.399	2.368	2.168	1.798	1.591	1.530	2.403
	ν_μ	1.269	1.242	1.039	0.504	0.162	0.101	1.272
	ν_τ	1.703	1.663	1.382	0.740	0.392	0.335	1.708
Inverted	ν_e	2.517	2.428	1.868	0.829	0.248	0.078	2.527
	ν_μ	1.241	1.230	1.144	0.916	0.770	0.744	1.243
	ν_τ	1.667	1.642	1.464	1.058	0.838	0.801	1.670

Table 4.2: Number of expected events in the whole IceCube energy range ($[10^5$ GeV, 10^7 GeV$]$) considering neutrino decay and standard oscillations for both hierarchies. IceCube's binning starts at 10^3 GeV, but the effective area is zero under 10^5 GeV.

It is important to mention that these numbers were computed using a flux that has been fitted without considering neutrino decay. Therefore, the normalisation factor has to be modified if it is taken into account. As they are, these numbers of events do not mean much, since we haven't corrected the flux. However, it still allows, for a given lifetime, to assess the relative importance of this non-standard physics interaction.

Finally, showing plots of the track to cascade ratio in the PeV range allows us to determine more directly the effects of the decay on the importance of one with respect to the other at high energy. They were obtained by defining two bins, $[10^6$ GeV, $10^{6.5}$ GeV$]$ which we shall call bin A, and $[10^{6.5}$ GeV, 10^7 GeV$]$ which we shall call bin B. We computed the number of track (ν_μ) and cascade (ν_e, ν_τ) events in each bin, and took the ratio. This binning, different from IceCube binning, has been chosen for several reasons. First, sticking to IceCube binning is not necessarily ideal since it is bound to change over time[5]. Thus, for simplicity, we decided to divide the PeV range in two logarithmically equal parts. Moreover, the separation between the two bins marks

[5]As a reminder, the binnings for HESE and PEPE effective areas are different.

the energy above which no HESE are detected. In addition, it is possible to resolve both cascades of a ν_τ double band event in bin B if both are at least partially within the detector, allowing to distinguish it from a ν_e. The track to cascade ratio is important to consider, since there is a discrepancy between the neutrino diffuse flux obtained with through-going muons and the one fitted with starting events. The former is harder than the latter, and it is so far unexplained. Finding a lifetime and a hierarchy that would lead to a higher track-to-cascade ratio would be a step in the right direction, since it would explain the reason why we observe more tracks than cascades at high energy.

Let us first consider the normal mass hierarchy. Let us denote the number of ν_α ($\alpha = e, \mu, \tau$) induced events by n_{ν_α}. It was seen before that the electron flavour remains rather unaffected, whereas the muon and tau flavours decay more importantly. Since we are plotting $n_{\nu_\mu}/(n_{\nu_e}+n_{\nu_\tau})$ with n_{ν_μ} and n_{ν_τ} that decrease, the numerator will continue to decrease while the denominator won't go below n_{ν_e}. The ratio continues to decrease until total decay in the PeV range, which occurs between $\tau/m = 10^{-3}$ and 10^{-4}. Thus, the righ-hand plot of Fig. 4.6 will not be modified much for lower lifetimes.

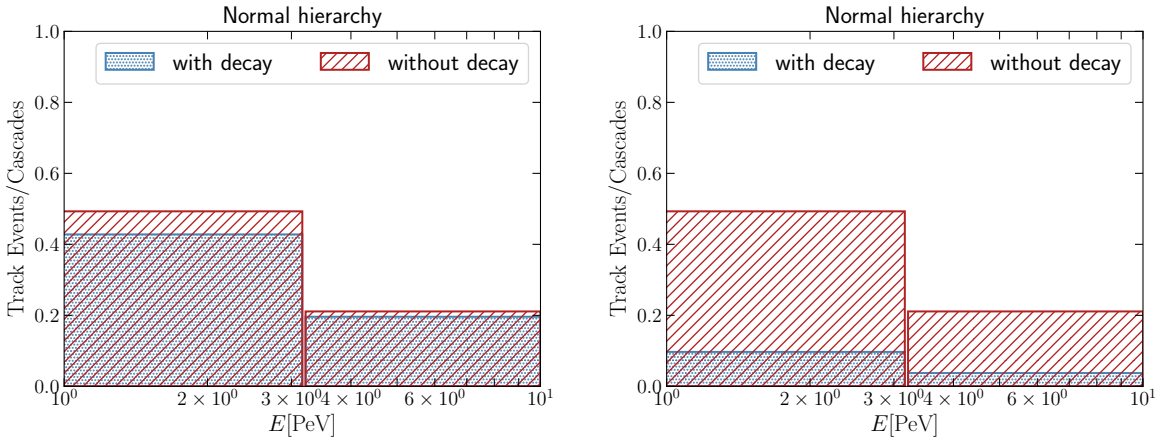

Figure 4.6: Track-to-cascade ratio in the different bins of IceCube in the normal mass hierarchy when the effects of decay start to manifest themselves in the IceCube energy range, *i.e* with a lifetime of $\tau/m = 10^{-1}$ s/eV (left), and when the decay is almost complete, *i.e*. 10^{-3} s/eV (right). The blue areas correspond to the ratio after decay, whereas the red ones are those without decay.

Even with neutrino decay, the track-to-cascade ratio will always be smaller than 1 in the normal hierarchy. This is another reason not to favour it, since in practice we observe more tracks than cascades at high energy.

In the inverted hierarchy, the opposite occurs. The number of ν_μ and ν_τ stay rather unaffected, and the number of ν_e decreases sharply. Thus, the ratio will this time tend towards $n_{\nu_\mu}/(\epsilon + n_{\nu_\tau}) \approx n_{\nu_\mu}/n_{\nu_\tau}$ with ϵ small, representing the number of ν_e events this time. The shorter the lifetime, the bigger the ratio, in each bin. Moreover, it can be larger than 1, which is an argument in favour of this hierarchy.

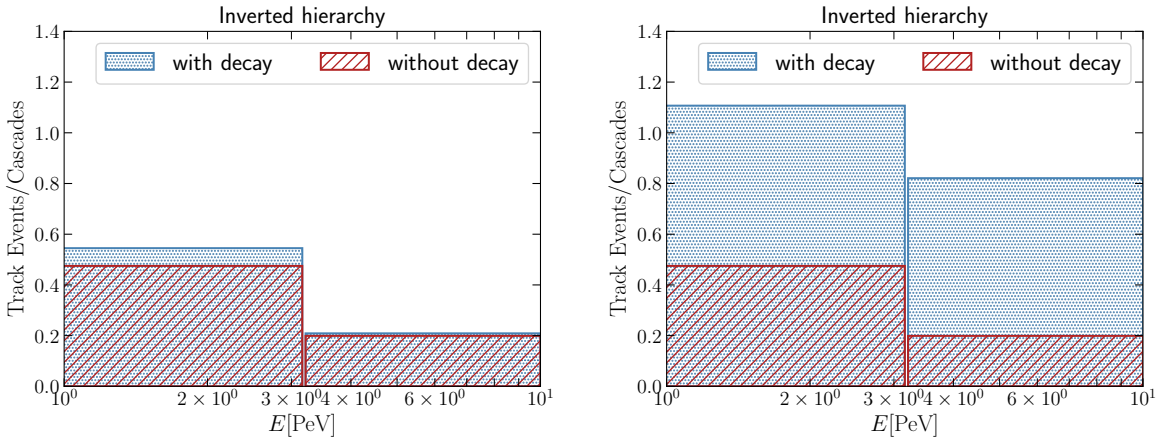

Figure 4.7: Track-to-cascade ratio in the different bins of IceCube in the inverse mass hierarchy when the effects of decay start to manifest themselves in the IceCube energy range, *i.e.* with a lifetime of $\tau/m = 10^{-1}$ s/eV (left) and when decay is almost complete, *i.e.* 10^{-3} s/eV (right). The blue areas correspond to the ratio after decay, whereas the red ones are those without decay.

In both hierarchies, there is a decrease of the track to cascade ratio in the high-energy end. This comes from the Glashow Resonance, which will increase the number of electron neutrino events no matter how much the ν_e flavour has decayed.

4.3.2 CP violating phase and θ_{13} variation

In Chapter 1, the PMNS matrix was given for the two mass hierarchies, as well as the 3σ range for all its elements. When [73] was written, the mixing angle θ_{13} and the CP violating phase δ were less constrained than now. They studied the effects of a mixing angle varying in $[0°, 9.1°]$ and a phase varying in $[0, \pi]$. In this work, we will restrain these θ_{13} domains to $[8.22°, 8.99°]$ ($[8.26°, 9.02°]$) for the normal (inverted) mass hierarchy. The phase δ will be taken inside $[141°, 370°]$ ($[205°, 354°]$). At first, we will only consider the mixing angle to vary, and consider a δ fixed at 222° (285°), before making both vary. It should be noted that even though now θ_{13} is as well constrained as the other angles, it is the one that has the biggest effect of the three. This is due to the shape of the PMNS matrix. Therefore, its variation is still worth considering now. Let us also stress the fact that, similarly to 2.7.5, we are not computing the 3σ interval of the neutrino flux after mixing, but rather the maximum interval in which it can vary, considering the θ_{13} angle and the δ phrase varying within their respective 3σ interval. We will nonetheless use the appellation "3σ interval" in the following.

Effects of the variation of θ_{13}

To obtain the following plots, θ_{13} has been considered to vary within the previously specified interval. The final flux after decay was computed exactly as before, for different values of the angle. The upper and lower boundaries were kept and are shown as the border of the shaded areas. Similarly to the previous situation, the effects of decay start to become noticeable in the resonant bin for a lifetime lower than 10^{-1} s/eV. The influence of the variation of θ_{13} is mainly localised on the low-energy part of the spectrum. The variation of the angle has only a small influence in the inverted mass hierarchy, and almost nothing is perceivable in the normal one.

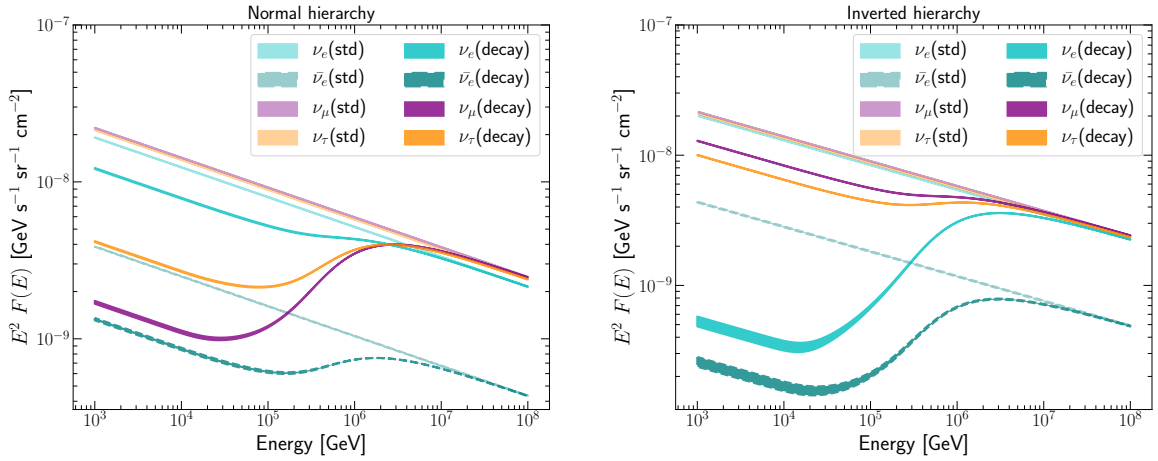

Figure 4.8: Final $\nu + \bar{\nu}$ fluxes after propagation over long distances considering neutrino decay and θ_{13} varying within its 3σ range, for a lifetime $\tau/m = 10^{-1}$ s/eV.
On the left: Normal mass hierarchy.
On the right: Inverted mass hierarchy.
The $\nu_\alpha,\ \alpha = e, \mu, \tau$ fluxes are actually the $\nu_\alpha + \bar{\nu}_\alpha$ fluxes, and are shown in respectively light blue, purple and orange, whereas the $\bar{\nu}_e$ one is solely for the electron antineutrino, and is shown in a darker shade of blue.

Since there are almost no change in the normal mass hierarchy, it is once again not worth showing plots for smaller lifetimes. The following graphs, which concern the inverted hierarchy only, show a clear modification compared to before. However, the consequences remain rather small, as can be seen in the predicted number of events in the following tables.

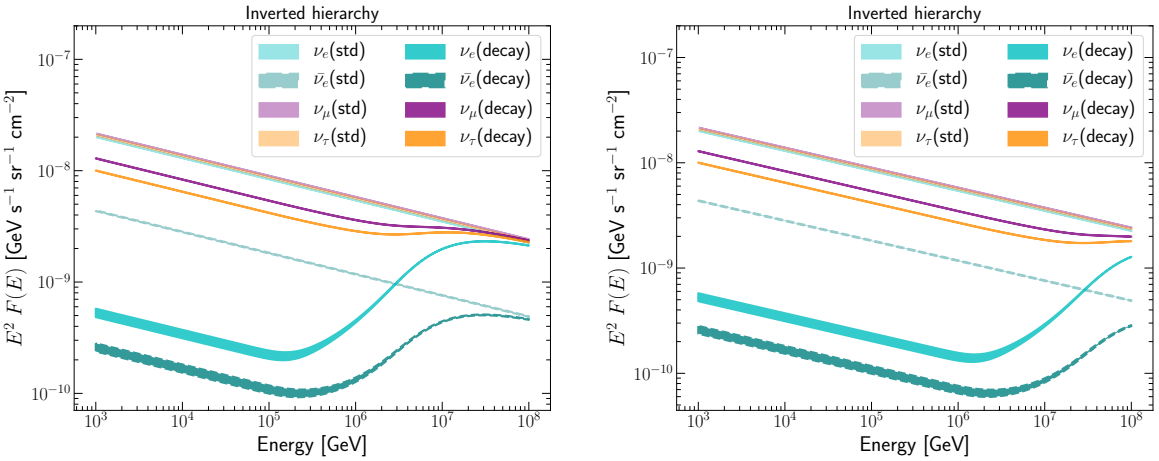

Figure 4.9: Final $\nu+\bar{\nu}$ fluxes after propagation over long distances considering neutrino decay and θ_{13} varying within its 3σ range, in the inverted mass hierarchy, for different lifetimes.
On the left: $\tau/m = 10^{-2}$ s/eV.
On the right: $\tau/m = 10^{-3}$ s/eV.
The $\nu_\alpha,\ \alpha = e, \mu, \tau$ fluxes are actually the $\nu_\alpha + \bar{\nu}_\alpha$ fluxes, and are shown in respectively light blue, purple and orange, whereas the $\bar{\nu}_e$ one is solely for the electron antineutrino, and is shown in a darker shade of blue.

		Lifetime (s/eV)			
Hierarchy	Events	10^{-1}	10^{-2}	10^{-3}	∞
Normal	ν_e	[0.284, 0.285]	[0.230, 0.232]	[0.189, 0.192]	[0.294, 0.295]
	GR	[0.558, 0.560]	[0.364, 0.367]	[0.215, 0.222]	[0.596, 0.599]
	ν_μ	[0.036, 0.036]	[0.018, 0.018]	[0.004, 0.004]	[0.043, 0.043]
	ν_τ	[0.039, 0.039]	[0.022, 0.022]	[0.009, 0.009]	[0.043, 0.043]
Inverted	ν_e	[0.280, 0.281]	[0.131, 0.132]	[0.017, 0.018]	[0.310, 0.310]
	GR	[0.608, 0.617]	[0.294, 0.302]	[0.056, 0.063]	[0.669, 0.679]
	ν_μ	[0.037, 0.037]	[0.029, 0.029]	[0.024, 0.024]	[0.039, 0.039]
	ν_τ	[0.040, 0.040]	[0.029, 0.029]	[0.021, 0.021]	[0.042, 0.042]

Table 4.3: Number of expected events in the resonant bin considering neutrino decay plus θ_{13} varying in its 3σ range, and standard oscillations for both hierarchies. ν_α where $\alpha = e, \mu, \tau$ refers to events involving $\nu_\alpha + \bar{\nu}_\alpha$, computed using effective areas. Glashow Resonance (GR) events were computed using the analytical cross section.

In Table 4.3 are shown the upper and lower boundaries of the expected number of events, considering θ_{13} varying in its 3σ interval, once again for the resonant bin and the whole IceCube range.

		Lifetime (s/eV)		
Hierarchy	Events	10^{2}	10^{1}	10^{0}
Normal	ν_e	[0.294, 0.295]	[0.294, 0.295]	[0.293, 0.294]
	GR	[0.596, 0.599]	[0.595, 0.598]	[0.592, 0.595]
	ν_μ	[0.040, 0.040]	[0.040, 0.040]	[0.039, 0.039]
	ν_τ	[0.043, 0.043]	[0.043, 0.043]	[0.042, 0.042]
Inverted	ν_e	[0.310, 0.310]	[0.309, 0.310]	[0.307, 0.307]
	GR	[0.669, 0.679]	[0.668, 0.678]	[0.662, 0.672]
	ν_μ	[0.039, 0.039]	[0.039, 0.039]	[0.039, 0.039]
	ν_τ	[0.042, 0.042]	[0.042, 0.042]	[0.042, 0.042]

		Lifetime (s/eV)		
Hierarchy	Events	10^2	10^1	10^0
Normal	ν_e	[2.397, 2.403]	[2.365, 2.372]	[2.164, 2.174]
	ν_μ	[1.268, 1.271]	[1.241, 1.244]	[1.039, 1.041]
	ν_τ	[1.704, 1.704]	[1.664, 1.664]	[1.382,1 .383]
Inverted	ν_e	[2.515, 2.520]	[2.426, 2.432]	[1.865, 1.872]
	ν_μ	[1.242, 1.243]	[1.230, 1.231]	[1.144, 1.145]
	ν_τ	[1.667, 1.669]	[1.642, 1.644]	[1.463, 1.466]

		Lifetime (s/eV)			
Hierarchy	Events	10^{-1}	10^{-2}	10^{-3}	∞
Normal	ν_e	[1.790, 1.807]	[1.581, 1.602]	[1.520, 1.542]	[2.401, 2.407]
	ν_μ	[0.503, 0.505]	[0.160, 0.164]	[0.099, 0.103]	[1.272, 1.275]
	ν_τ	[0.738, 0.742]	[0.390, 0.395]	[0.332, 0.337]	[1.709, 1.709]
Inverted	ν_e	[0.825, 0.834]	[0.243, 0.254]	[0.072, 0.084]	[2.525, 2.525]
	ν_μ	[0.915, 0.917]	[0.769, 0.772]	[0.743, 0.746]	[1.243, 1.243]
	ν_τ	[1.056, 1.060]	[0.836, 0.840]	[0.800, 0.803]	[1.670, 1.670]

Table 4.4: Number of expected events in the whole IceCube energy range ([10^5 GeV, 10^7 GeV]) considering decay plus θ_{13} varying in its 3σ range, and standard oscillation for both hierarchies. IceCube's binning starts at 10^3 GeV, but the effective area is zero under 10^5 GeV.

Effects of the variation of δ_{CP}

The other varying parameter is the CP violating phase. Whereas θ_{13} did not yield much of a difference, the influence of the CP violating phase is more important, especially in the normal hierarchy. This is notably due to the fact that the 3σ range is much higher than for any other parameter. One can note that while θ_{13} had most of its effects in the low-energy end of the IceCube spectrum, δ also has an influence on the higher energies.

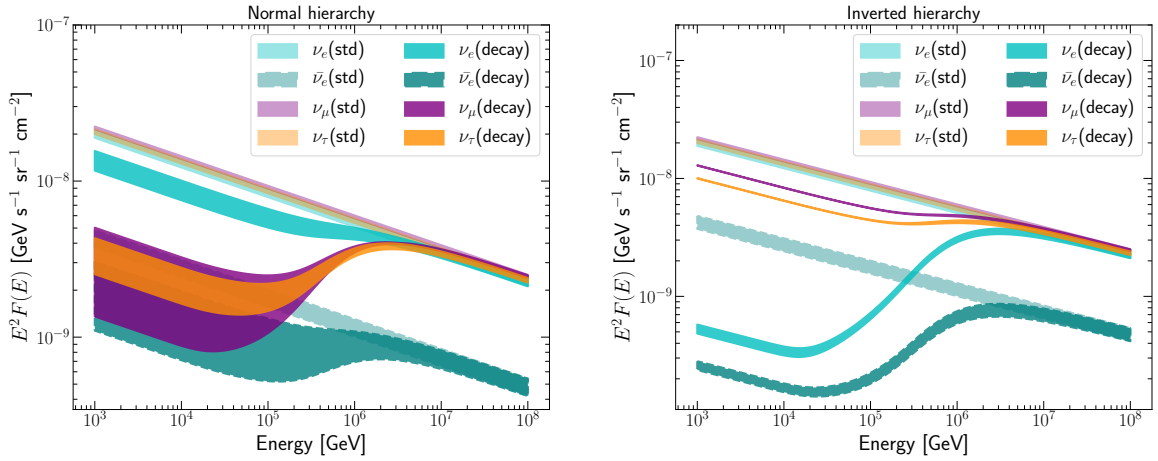

Figure 4.10: Final $\nu + \bar{\nu}$ fluxes after propagation over long distances considering neutrino decay and θ_{13}, δ varying within their 3σ range, for a lifetime $\tau/m = 10^{-1}$ s/eV.
On the left: Normal mass hierarchy.
On the right: Inverted mass hierarchy.
The ν_α, $\alpha = e, \mu, \tau$ fluxes are actually the $\nu_\alpha + \bar{\nu}_\alpha$ fluxes, and are shown in respectively light blue, purple and orange, whereas the $\bar{\nu}_e$ one is solely for the electron antineutrino, and is shown in a darker shade of blue.

While the effects of varying the phase within its uncertainty range are most noticeable in the normal hierarchy, they are not sufficient to significantly alter the ν_e flux. Once again, the inverted hierarchy seems more promising in doing so. One can note than in this one, the effects are not important, at least not with respect with neutrino decay.

Finally, Table 4.5 shows the upper and lower boundaries of expected number of events, with θ_{13} and δ_{CP} varying in their respective 3σ range.

		Lifetime (s/eV)		
Hierarchy	Events	10^2	10^1	10^0
Normal	ν_e	[0.291, 0.324]	[0.291, 0.324]	[0.290, 0.323]
	GR	[0.579, 0.747]	[0.579, 0.747]	[0.575, 0.744]
	ν_μ	[0.039, 0.040]	[0.039, 0.040]	[0.038, 0.040]
	ν_τ	[0.040, 0.043]	[0.040, 0.043]	[0.040, 0.042]
Inverted	ν_e	[0.290, 0.323]	[0.290, 0.323]	[0.288, 0.320]
	GR	[0.576, 0.742]	[0.576, 0.742]	[0.571, 0.735]
	ν_μ	[0.039, 0.040]	[0.039, 0.040]	[0.039, 0.040]
	ν_τ	[0.040, 0.043]	[0.040, 0.043]	[0.040, 0.043]

		Lifetime (s/eV)			
Hierarchy	Events	10^{-1}	10^{-2}	10^{-3}	∞
Normal	ν_e	[0.280, 0.316]	[0.225, 0.274]	[0.183, 0.242]	[0.291, 0.324]
	GR	[0.541, 0.721]	[0.337, 0.584]	[0.183, 0.480]	[0.579, 0.747]
	ν_μ	[0.036, 0.036]	[0.017, 0.021]	[0.004, 0.010]	[0.039, 0.040]
	ν_τ	[0.037, 0.039]	[0.019, 0.022]	[0.006, 0.010]	[0.040, 0.043]
Inverted	ν_e	[0.263, 0.293]	[0.123, 0.137]	[0.016, 0.019]	[0.290, 0.323]
	GR	[0.524, 0.675]	[0.256, 0.328]	[0.054, 0.065]	[0.577, 0.742]
	ν_μ	[0.037, 0.039]	[0.029, 0.030]	[0.024, 0.024]	[0.039, 0.040]
	ν_τ	[0.038, 0.041]	[0.028, 0.029]	[0.021, 0.021]	[0.040, 0.043]

Table 4.5: Number of expected events in the resonant bin considering neutrino decay plus θ_{13} varying in its 3σ range, and standard oscillations for both hierarchies. ν_α where $\alpha = e, \mu, \tau$ refers to events involving $\nu_\alpha + \bar{\nu_\alpha}$, computed using effective areas. Glashow Resonance (GR) events were computed using analytical cross section.

		Lifetime (s/eV)		
Hierarchy	Events	10^2	10^1	10^0
Normal	ν_e	[2.374,2.645]	[2.341,2.620]	[2.134,2.463]
	ν_μ	[1.240,1.290]	[1.217,1.262]	[1.030,1.073]
	ν_τ	[1.600,1.711]	[1.559,1.670]	[1.273,1.390]
Inverted	ν_e	[2.363,2.629]	[2.281,2.537]	[1.757,1.953]
	ν_μ	[1.247,1.293]	[1.235,1.280]	[1.149,1.186]
	ν_τ	[1.600,1.713]	[1.576,1.687]	[1.412,1.500]

		Lifetime (s/eV)			
Hierarchy	Events	10^{-1}	10^{-2}	10^{-3}	∞
Normal	ν_e	[1.749,2.172]	[1.534,2.009]	[1.471,1.961]	[2.378,2.648]
	ν_μ	[0.494,0.622]	[0.144,0.343]	[0.081,0.293]	[0.081,0.293]
	ν_τ	[0.618,0.750]	[0.264,0.405]	[0.205,0.347]	[1.605,1.715]
Inverted	ν_e	[0.779,0.868]	[0.232,0.262]	[0.072,0.084]	[2.373,2.639]
	ν_μ	[0.919,0.936]	[0.772,0.778]	[0.746,0.750]	[1.248,1.295]
	ν_τ	[1.038,1.074]	[0.836,0.844]	[0.802,0.806]	[1.602,1.716]

Table 4.6: Number of expected events in the whole IceCube energy range ([10^5 GeV, 10^7 GeV]) considering decay plus θ_{13} varying in its 3σ range, and standard oscillation for both hierarchies. IceCube's binning starts at 10^3 GeV, but the effective area is zero under 10^5 GeV.

It can be noted that these tables are fairly similar to the previous ones, especially for the inverted hierarchy, which is to be expected considering the previous plots.

4.4 IceCube flux: refitting the flux after decay

The power-law flux used until now has been normalised considering only standard oscillations. This means that the normalisation was chosen so that the power law model is consistent with the number of events observed by IceCube. When adding non-standard physics interactions, the normalisation factor is bound to change.

Over 6 years of HESE observation by IceCube, 3 HESE have been found in bin A, *i.e.* in $[10^6$ GeV, $10^{6.5}$ GeV$]$, and none above these energies. These HESE originated from ν_e and ν_τ, but not ν_μ since no track was observed. Over 4.6 years of PEPE observation, 1 cascade event has been found in the bin B, *i.e.* $[10^{6.5}$ GeV, 10^7 GeV$]$. At such high energies, it is possible to distinguish between cascade and double cascade events. The PEPE looks like a single cascade event, therefore it should be a Glashow Resonance. However, it is important to mention that this cascade may actually be the second one of a much higher energy ν_τ event that would have occured further outside the instrumented volume, at roughly two times the reconstructed energy [78]. In that case, it would mean no Glashow Resonance event would have been observed yet. In the following, we will consider the detected partially-contained event to be from a ν_e[6].

	HESE (6 years)		ν_e PEPE (4.6 years)
Model	Bin A (ν_e, ν_τ)	Bin B(ν_e)	Bin B (ν_e)
$\gamma = -2.1$	3.124	2.467	3.154
$\gamma = -2.9$	0.925	0.287	0.367
Observations	3	0	1

Table 4.7: Table showing the expected number of events using a power law flux for the first two lines, with a normalisation $\phi_0 = 1.01 \times 10^{-18}$ GeV^{-1}s^{-1}sr^{-1}cm^{-2} for $\gamma = -2.19$ (Thμ best-fit flux), and $\phi_0 = 2.19 \times 10^{-18}$ GeV^{-1}s^{-1}sr^{-1}cm^{-2} for $\gamma = -2.91$ (HESE best-fit flux), and the observations. Since no starting track-like events are observed in bin A, only the number of expected starting events during 6 years for ν_e and ν_τ are shown. In addition, since the detected event in bin B is supposed to be a Glashow Resonance event, only the number of ν_e events is shown.

To refit the flux, the number of expected events in the bin A has been computed. The flux was then multiplied so that this number is equal to 3, as it is what has been observed. The number of ν_e HESE and PEPE in bin B is then computed. With a suitable set of hierarchy, lifetime, spectral index and normalisation, one should have 1 PEPE and no HESE, *i.e.* less than 1. What we are searching for is a combination of these parameters such that sufficient ν_e decay occurs in the first bin, and fewer decay effects lie in the second bin to be able to still observe 1 PEPE.

Let us explain why too high or too low a lifetime is not suitable. If it is too high, too many Glashow Resonances would be expected, be it with the HESE or PEPE effective areas. One could think that the problem with a lifetime too large is that not enough decay would occur within the first bin to explain the 3 cascade events. It is however not a problem, since the flux will not matter as it is normalised to satisfy this 3-event requirement. The problem lies in the fact that too high a lifetime would not lead to enough decays in bin A *with respect to* bin B. Also, since lifetimes that do not give decays inside the considered bins are to be discarded, there is no need to consider $\tau/m > 1$ s/eV The problems related to too small lifetimes depend on the hierarchy, and will be explained later.

The next parameter is the spectral index. It has been seen before that there is a discrepancy between the flux fitted using starting events and the one using through-going muons. The latter was harder than the former, with a spectral index in $[-2.3, -2.1]$ rather than $[-2.9, -2.7]$. The

[6]The event could also be due to a ν_e — not the antiparticle —, but since the resonant event rate is much higher than the non-resonant ones, we assume this event to be due to a $\bar{\nu}_e$. However, it won't change anything in the following, since IceCube can't distinguish particles and antiparticles

right spectral index must then be in the first interval, to be able to explain the through-going muons at high energies. However, the decay must be such that it affects mostly the neutrinos that induce cascade events, namely ν_e and ν_τ.

Let us consider the normal mass hierarchy. As has been seen above, the decay effects are more important on the muon and tau flavours rather than on the electron one. The consequences are the following: to account for the 3 cascades in the first bin, the more decay effects, the bigger the flux normalisation. However, since ν_e haven't decayed much in the energy range of the second bin, they will basically only increase the number of GR events, *i.e.* ν_e events in the second bin. The initial problem, which was that too few resonant events are observed compared to predictions, is then only magnified. Moreover, the too important decay of the muon flavour could also be inconsistent with the number of detected ν_μ events. To illustrate this, the number of expected ν_e HESE and PEPE in the second bin for a renormalised flux for different lifetimes are shown in the table below. The smaller the lifetime, the more ν_τ decay, the bigger the normalisation factor, and thus the more Glashow Resonant events, since ν_e are essentially unaltered.

Spectral index γ	Lifetime τ/m (s/eV)	ν_e HESE	ν_e PEPE
-2.1	∞	2.463	3.136
	10^{-1}	2.919	3.717
	10^{-2}	4.089	5.207
	10^{-3}	3.927	5.001
-2.2	∞	2.340	2.991
	10^{-1}	2.779	3.552
	10^{-2}	3.876	4.955
	10^{-3}	3.276	4.763
-2.3	∞	2.058	2.631
	10^{-1}	2.453	3.135
	10^{-2}	3.420	4.372
	10^{-3}	3.278	4.190

Table 4.8: Number of expected ν_e HESE and PEPE in [$10^{6.5}$ GeV, 10^7 GeV], for the normal mass hierarchy, for the refitted decayed flux.

As it was stated, the ν_e never decay enough in the energy range of the first bin, nor in the second. Therefore, the smaller the lifetime, the fewer ν_τ and so the fewer cascade events. To still account for the 3 detected HESE, the normalisation factor must be higher and higher, hence the increasing number of events in the second bin. However, one can see that for the shortest considered lifetime, the number of events starts to decrease. This comes from the fact that for a lifetime not small enough, there is still a part of the flux in the second bin that isn't affected by decay, which explains the increasing number of events as the factor increases. For a certain lifetime, the decay is roughly complete in the two bins, so the number of events decreases. In other words, the flux decreases more due to decay than it is scaled up thanks to the new normalisation. To sum up, the ν_e decay is never enough to be able to explain 1 PEPE and no HESE during the observation period in the normal hierarchy. Therefore, neutrino decay in the normal mass hierarchy is not an explanation for the absence of Glashow resonance using High-Energy starting events effective area, nor for the only 1 Partially-contained PeV events.

Let us now consider the inverted mass hierarchy. The number of events for different spectral

indices and lifetimes for a renormalised flux are shown in the Table 4.9.

Spectral index γ	Lifetime τ/m (s/eV)	ν_e HESE	ν_e PEPE
-2.1	∞	2.556	3.255
	10^{-1}	3.016	3.841
	10^{-2}	3.181	4.055
	10^{-3}	0.571	0.728
-2.2	∞	2.241	2.853
	10^{-1}	2.654	3.379
	10^{-2}	2.784	3.548
	10^{-3}	0.492	0.627
-2.3	∞	2.138	2.733
	10^{-1}	2.527	3.229
	10^{-2}	2.567	3.281
	10^{-3}	0.453	0.578

Table 4.9: Number of expected ν_e HESE and PEPE in $[10^{6.5}$ GeV, 10^7 GeV], for the inverted mass hierarchy, for the refitted decayed flux.

For lifetimes not small enough, the decay occurs mainly in the first bin. Therefore, the same problem as above arises: to account for the same number of HESE in this bin, the normalisation must be larger than one. However, since almost no decay occurs in the second bin at these lifetimes, the number of GR events only increases, further increasing the problem as written before. Concerning too short lifetimes, the problem in this hierarchy is different from in the other one. Previously, the ν_e decay was never enough to account for 1 PEPE and no HESE. Here, on the contrary, the ν_e decay is so important that a lifetime too small leads to no events, either HESE or PEPE. By looking at the number of events for a lifetime $\tau/m = 10^{-2}$ and 10^{-3} s/eV, since modifying continuously the lifetime leads to continuous change in the flavour spectra, there must be a lifetime for which the number of ν_e PEPE is equal to 1, the number of ν_e HESE smaller than 1. Depending on the spectral index, the lifetime favoured by neutrino decay to explain the number of observed Glashow Resonance is $\tau/m = 1.43 \times 10^{-3}$ s/eV for an index of $\gamma = -2.1$, $\tau/m = 1.75 \times 10^{-3}$ s/eV for $\gamma = -2.2$, and $\tau/m = 2.1 \times 10^{-3}$ s/eV for $\gamma = -2.3$. In all these situations, 1 ν_e PEPE event is expected in the bin $[10^{6.5}$ GeV, 10^7 GeV$]$[7], which corresponds to the observed GR event, and less than 1 HESE, *i.e.* no starting event. One could expect that there would be a spectral index for which the ratio PEPE/HESE is maximum, which would then be favoured, but it is not the case. Instead, the number of expected HESE is always 0.78. Therefore, one cannot conclude decisively that there is a combination of spectral index and lifetime that is the most suitable. Rather, given the 1σ range of the best fit spectral index, one can narrow down the range of the lifetime.

Finally, the fluxes at the sources that could explain the observed number of events consider-

[7] As a reminder, in this bin, it is possible to distinguish resolve the two cascades in a ν_τ event, allowing to distinguish it from a ν_e interaction.

ing neutrino decay are

$$\frac{d\phi}{dE_\nu} = \begin{cases} 3.38 \times 10^{-18} \ \left(\frac{E_\nu}{100\ TeV}\right)^{-2.1}, \ \tau/m = 1.43 \times 10^{-3} \text{ s/eV} \\ 4.76 \times 10^{-18} \ \left(\frac{E_\nu}{100\ TeV}\right)^{-2.2}, \ \tau/m = 1.75 \times 10^{-3} \text{ s/eV} \\ 6.67 \times 10^{-18} \ \left(\frac{E_\nu}{100\ TeV}\right)^{-2.3}, \ \tau/m = 2.10 \times 10^{-3} \text{ s/eV} \end{cases}$$

Please bear in mind that these are the sources. To obtain the fluxes at the Earth, one must consider the effect of standard oscillation over long distances, coupled to neutrino decay.

4.4.1 Another neutrino production mechanism: neutron decay

A thorough analysis of the neutrino spectra at Earth given that the process at their origin was the $p\gamma$ mechanism has been done. It is nonetheless important to realise that the actual process is not known. Another possibility that was presented in Sections 1.5.5 and 3.2.2 is neutron decay. We will give insights as to how important this other mechanism will influence our results.

Neutron decay would lead to a flavour ratio of $0 : 0 : 0$ and $1 : 0 : 0$, meaning that only antineutrinos would be present in the diffuse flux. We would however not realise it since IceCube does not distinguish between particles and antiparticles. In Fig. 3.5, the number of expected resonant events as a function of the initial fraction of $\bar{\nu}_e$ is shown. The left end of the plot corresponds to the $p\gamma$ case, when no $\bar{\nu}_e$ are created at the source, whereas the right end corresponds to the neutrino decay. Between the two extremes, there is about a factor 2 in the expected number of electron antineutrino interactions. As a reminder, the spectral averaging will take place and massage the flavour spectra, which explains the small difference. However, nothing guarantees that the effects of decay will be the same.

Neutrino decay

The same procedure as before has been adopted to obtain the final spectra. Only the initial flavour ratio has been modified. While the importance of the decay might change, since the composition of the initial flux is different, the position of the transition between full and absent of decay depends only on the energy, and thus remains unaffected by the change of mechanism at the source. The region of interest for the lifetimes is still $[10^{-4}$ s/eV, 10^3 s/eV$]$. Larger or smaller values will simply correspond to no decay or full decay within the IceCube energy range, as already explained.

As before, lifetimes of 10^2 s/eV and above do have an effect in the IceCube range, but the effects are barely visible, and there is no influence in the PeV range. One must go as low as 10^{-1} s/eV to start seeing effects at a such high energy.

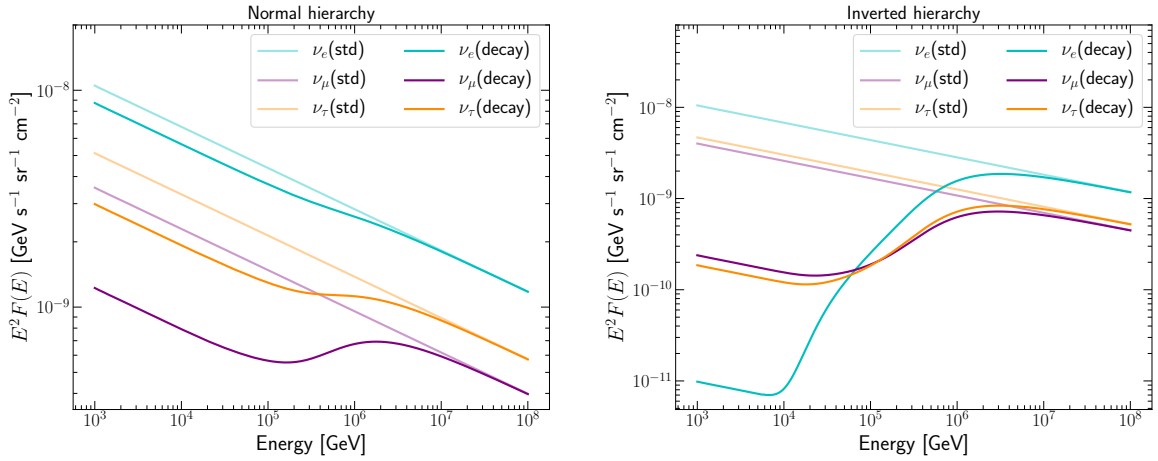

Figure 4.11: Final $\nu + \bar{\nu}$ fluxes after propagation over long distances considering neutrino decay, for a lifetime $\tau/m = 10^{-1}\ s/eV$.
On the left: Normal mass hierarchy.
On the right: Inverted mass hierarchy.
The $\nu_\alpha,\ \alpha = e, \mu, \tau$ fluxes are actually the $\nu_\alpha + \bar{\nu}_\alpha$ fluxes, and are shown in respectively light blue, purple and orange, whereas the $\bar{\nu_e}$ one is solely the electron antineutrino one, and is shown in a darker shade of blue.

The effects for the normal mass hierarchy are similar to what was obtained for the $p\gamma$ mechanism, although there is a bigger difference in the relative importance of the different flavour spectra. The effects of neutrino decay on the electron are rather small, thus the same conclusions as for the other mechanism are still valid. Similarly, the electron flavour undergoes the biggest decay for the other hierarchy. The main difference lies in the magnitude. Previously, there was roughly 1 order of magnitude between decay and standard oscillations only. Here, there are 3 orders of magnitude between the two situations, which is far more important. This, of course, will have consequences on the number of events one would expect, that are summed up in Tables 4.10 and 4.11.

		Lifetime (s/eV)						
Hierarchy	Events	10^2	10^1	10^0	10^{-1}	10^{-2}	10^{-3}	∞
Normal	ν_e	0.161	0.161	0.161	0.159	0.145	0.135	0.161
	GR	1.621	1.621	1.618	1.594	1.459	1.356	1.621
	ν_μ	0.006	0.006	0.006	0.006	0.004	0.002	0.006
	ν_τ	0.010	0.010	0.010	0.010	0.008	0.006	0.010
Inverted	ν_e	0.161	0.161	0.160	0.146	0.066	0.005	0.161
	GR	1.620	1.618	1.604	1.463	0.661	0.052	1.620
	ν_μ	0.007	0.007	0.007	0.007	0.003	0.001	0.007
	ν_τ	0.009	0.009	0.009	0.0080	0.004	0.001	0.09

Table 4.10: Number of expected events in the resonant bin considering neutrino decay and standard oscillations for both hierarchies. ν_α where $\alpha = e, \mu, \tau$ refers to events involving $\nu_\alpha + \bar{\nu}_\alpha$, computed using effective areas. Glashow Resonance (GR) events were computed using analytical cross section, which involves $\bar{\nu}_e$ only.

		Lifetime (s/eV)						
Hierarchy	Events	10^2	10^1	10^0	10^{-1}	10^{-2}	10^{-3}	∞
Normal	ν_e	1.315	1.307	1.257	1.163	1.111	1.095	1.316
	ν_μ	0.204	0.201	0.178	0.117	0.078	0.071	0.205
	ν_τ	0.408	0.403	0.368	0.289	0.246	0.238	0.409
Inverted	ν_e	1.310	1.263	0.964	0.409	0.098	0.007	1.316
	ν_μ	0.230	0.225	0.188	0.089	0.026	0.014	0.231
	ν_τ	0.372	0.361	0.288	0.121	0.031	0.015	0.373

Table 4.11: Number of expected events in the whole IceCube energy range ([10^5 GeV, 10^7 GeV]) considering neutrino decay and standard oscillations for both hierarchies. IceCube's binning starts at 10^3 GeV, but the effective area is zero under 10^5 GeV.

The track-to-cascade ratio in IceCube can also be shown for the neutron decay mechanism.

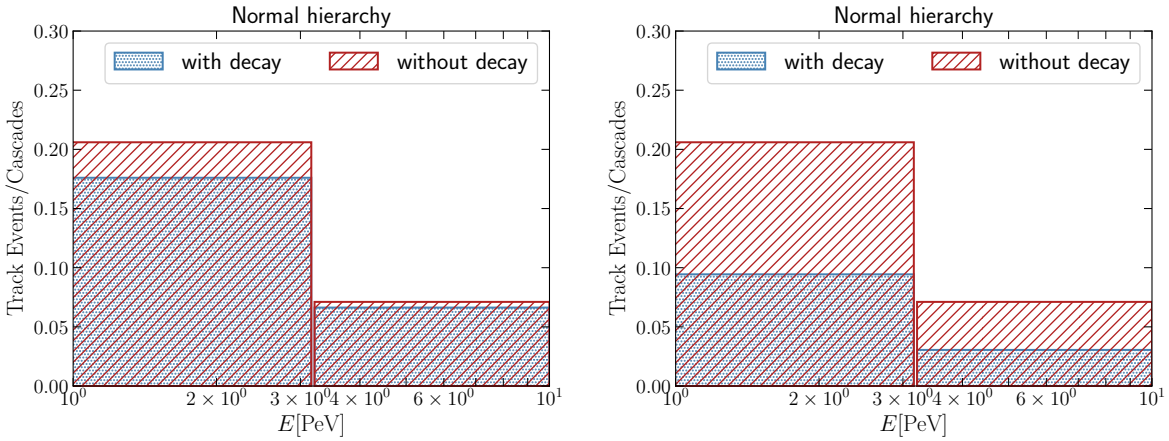

Figure 4.12: Track-to-cascade ratio in the different bins of IceCube in the normal mass hierarchy, with a lifetime of $\tau/m = 10^{-1}$ s/eV (left) and 10^{-4} s/eV (right). The blue areas correspond to the ratio after decay, whereas the red ones are those without decay.

For the normal hierarchy, the initial ratio is smaller than in the $p\gamma$ scheme, by about a factor 2. A similar decrease is observed when the lifetime gets shorter. As before, this comes from the fact that the electron neutrino flux does not decay much in either bin, whereas the muon flavour flux decays more. Although the decrease of the track-to-cascade ratio is less important than with the other mechanism, about a factor 2 compared to a factor 5 before, the ratio after total decay is very similar.

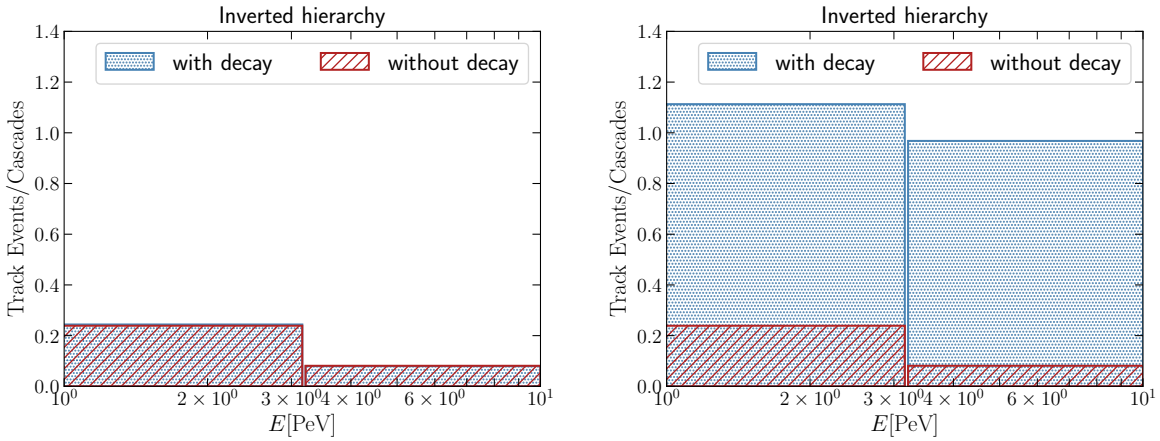

Figure 4.13: Track-to-cascade ratio in the different bins of IceCube in the inverse mass hierarchy, with a lifetime of $\tau/m = 10^{-1}$ s/eV (left) and 10^{-4} s/eV (right). The blue areas correspond to the ratio after decay, whereas the red ones are those without decay.

In the inverted mass hierarchy, one can also see an increase of the ratio as the lifetime decreases. The relative increase is much more important than in the $p\gamma$ case. The ratio is multiplied by a factor 4, rather than a factor 2 before. Similarly to the normal hierarchy, the ratio after total decay is very similar to the other scheme.

IceCube flux: refitting the flux after decay

Similarly to what was done for the $p\gamma$ mechanism, we will refit IceCube flux considering this time neutron decay at the source. 3 HESE have been observed in [10^6 GeV, $10^{6.5}$ GeV], no ν_e event in [$10^{6.5}$ GeV, 10^7 GeV], but 1 ν_e PEPE in this second bin have been detected.

The same tables that were shown before can be given in this scheme as well. However, only one spectral index will be considered, since the aim of this section is more to see how much of an impact the mechanism at the source has. Naturally, the through-going muon best-fit index is used, which is $\gamma = -2.19$.

Spectral index γ	Lifetime τ/m (s/eV)	ν_e HESE	ν_e PEPE
-2.19	∞	3.363	4.299
	10^{-1}	3.589	4.587
	10^{-2}	3.880	4.959
	10^{-3}	3.746	4.788
	10^{-4}	3.728	4.765

Table 4.12: Number of expected ν_e HESE and PEPE in [$10^{6.5}$ GeV, 10^7 GeV], for the normal mass hierarchy, for the refitted decayed flux, considering this time neutron decay as source mechanism.

The same conclusion as for the $p\gamma$ mechanism holds. Basically, the ν_e flux remains unaffected by decay. The ν_τ one, on the other hand, is reduced. To compensate for this, the normalisation factor of the flux has to be larger, which will simply lead to an increase in the number of ν_e starting and partially-contained events. Moreover, when the lifetime is small enough, the rescaling factor won't change anymore, but the decay will be complete in the second bin, hence the reduction of the number of events at the last line of Table 4.13.

Spectral index γ	Lifetime τ/m (s/eV)	ν_e HESE	ν_e PEPE
-2.1	∞	3.462	4.425
	10^{-1}	4.522	5.779
	10^{-2}	11.128	14.220
	10^{-3}	6.751	8.629
	10^{-4}	0.258	0.330

Table 4.13: Number of expected ν_e HESE and PEPE in [$10^{6.5}$ GeV, 10^7 GeV], for the inverted mass hierarchy, considering this time neutron decay as source mechanism.

Once again, the same conclusion as for the other mechanism holds. The main difference lies in the decay of the ν_e flux, which is far more important here. It means that the rescaling factor has to be much bigger to account for the 3 HESE in the first bin. The consequence is that one must consider even smaller lifetimes to reach the point where the decay is important enough. For a lifetime of $\tau/m = 2.6 \times 10^{-4}$ s/eV, one expects 1 ν_e PEPE and no HESE in the second bin. The lifetime is one order of magnitude lower than before, meaning that it is right at the verge of full decay. Please note again that no event doesn't mean that the prediction is simply 0. Rather, the prediction is comprised between 0 and 1.

One would expect the ratio of the number of ν_e HESE over the number of PEPE in the second to be different with this mechanism. However, it still is 0.78. This means that this ratio is not dependent on the mechanism through which neutrinos are produced, nor on the spectral index.

The flux favoured by neutrino decay with a neutron decay mechanism at source is

$$\frac{d\phi}{dE_\nu} = 2.35\ 10^{-16} \left(\frac{E_\nu}{100\ TeV}\right)^{-2.19},\ \frac{\tau}{m} = 2.6\ 10^{-4}\ \text{s/eV}$$

To sum up this section, one can say that no matter the mechanism at the source, a lifetime of the order of 10^{-4} to 10^{-3} s/eV can be an explanation to the observed event rate, hence solving the problem of the (partial) disappearance of the Glashow Resonance. However, it is important to note that no lifetime seems to be favoured amongst all the possible ones.

Summary and Conclusions

In this thesis, we have investigated one of the most striking features in the ultrahigh energy neutrino data observed at IceCube: the conflict between the best-fit fluxes estimated using two different sets of events, HESE and Thμ, distinguished only by the experimental cuts imposed on them. The HESE sampling consists of events whose initial interaction takes place within IceCube's instrumented volume while the Thμ sampling exclusively comprises muon tracks originating from neutrino interactions in rocks outside the detector and then streaming across it. Despite detecting the same incoming flux of neutrinos, the former suggests a much softer (*i.e* steeply falling) best-fit for the flux ($\propto E^{2.91}$) as opposed to the much harder spectrum suggested by the latter ($\propto E^{-2.19}$). We examined this difference particularly with an eye on the Glashow Resonance — a resonant enhancement of the interaction strengths for the $\bar{\nu}_e$ in a narrow energy window around 6.3 PeV.

To set up the premise for our investigation, we reviewed some of the basic concepts of neutrino physics relevant to our requirements in Chapter 1 and then, in Chapter 2, the origins and detection of ultrahigh energy neutrinos. In Chapter 3, we discussed the Glashow Resonance in detail, highlighting its unique properties. Theoretically, one expects a large increase in the number of events due to this resonance around energies of 6.3 PeV; in practice, the 6-year HESE data coming from IceCube contains no events beyond 2.1 PeV. A different sampling of events, called PEPE, uses partial cascades originating just outside the detector's instrumented volume, thereby effectively increasing its apparent detection volume; it finds a solitary event, initiated by a neutrino with an energy of 6.3 PeV, undetected by HESE.

It is important to remind that although the mechanism at the origin of high-energy neutrino is often assumed to be the $p\gamma$, leading to a flux ratio of $1:1:0+0:1:0=1:2:0$, with initially no $\bar{\nu}_e$, it is not confirmed. Another possible neutrino production channel that was discussed in this work is neutron decay, which would lead to $0:0:0$ and $1:0:0$, *i.e.* only one electron antineutrino is produced. These two mechanisms can be considered as the two extremes, in the sense that one would not lead to any $\bar{\nu}_e$ at source, whereas the other would be entirely made of it. Therefore, it might be that the absence of Glashow resonance is a natural consequence of the true composition of the neutrino flux, dictated mainly by the spectral index and the flavour ratio. To investigate this, we computed the expected number of events considering the extremes and everything between (an initial $\bar{\nu}_e$ fraction between 0 and 1). We saw that when working with cross section, which means when being able to distinguish particles from antiparticles, this should only affect the GR events and not the non-resonant ones. In practice, this modification would be hidden in $\nu_e + \bar{\nu}_e$ flux, leading to a modification of electron neutrino event in IceCube. The mechanism at source being unknown, the spectral index also remains an uncertainty. Thus, its importance on the number of event was assessed. If it is too low, the neutrino spectrum will be so soft than the event rate in the resonant bin will be extremely low, leading to far less than 1 event per year.

Next, we discussed the best-fit neutrino fluxes obtained using HESE and through-going muons. We also computed the expected number of PEPE as a function of the initial content of the

neutrino flux in ν_e and $\bar{\nu}_e$, for the two models. No matter the initial ratio, the two models never agree within their 1σ error range. The problem comes from the fact that the flux obtained with through-going muons ($\propto E^{-2.19}$) is much harder than the one using HESE ($\propto E^{-2.91}$). This is a surprise since we are essentially observing the same diffuse neutrino flux. The only difference lies in the fact that the two kinds of event considered in the two models, which are the track events originating outside the detector for the Thμ, and starting events for the HESE. This suggests that there must be a flavour dependent interaction that acts as a kind of sieve, reducing the amount of ν_e and ν_τ in favour of ν_μ.

After establishing that standard model based explanations do not work, we decided to investigate non-standard physics, focusing on neutrino decay. The three possible places where the flavour selection can occur are at the neutrino source, during propagation, or at Earth; only the second one leads to observable differences in the neutrino flavour spectra. A modification at source is massaged out by neutrino oscillation, and no selection can occur within the Earth since it is opaque to neutrinos at above 1 PeV energies. In this work, we specifically focused on neutrino decay. Standard oscillation does not lead to difference between the normal and inverted mass hierarchy. However, the differences will be crucial when inducing non-standard effects, since neutrino decay will affect both of them differently. We find that the normal hierarchy does not lead to an important enough modification of the ν_e flux to explain the discrepancy between the HESE and Thμ fitted fluxes, nor the so few observations of Glashow Resonance. The inverted hierarchy, on the other hand, seems more promising, since there is a significant decay of the ν_e flux with respect to the other flavours. Please note that the mechanism at source, *i.e.* $p\gamma$ or neutron decay, leads to a different importance of decay in $10^6 - 10^{6.5}$ PeV. For the former, there is a decrease of an about 1 order of magnitude for the ν_e flux. For the latter, the decay is more important and reaches 3 orders of magnitude. In both cases, it means that the ν_e flavour has completely decayed, at least with respect to the other flavours. In bin B, on the other hand, the flux remains partially untouched, which could explain the lack of HESE as well as the only ν_e PEPE that was observed in bin B. In the $p\gamma$ case, the importance of the mixing angle θ_{13} as well as the CP violating phase δ were assessed by making them vary within their 3σ range. The effects are more important in the normal hierarchy, but not enough to be a suitable explanation for the problem of this work. The effects are found to be minimal in the inverted hierarchy.

The final step of this thesis was to refit the power law flux to account for IceCube's data. In other words, the flux was refitted considering that 3 HESE (events initiated by ν_e or ν_τ) were observed in bin A, none in bin B, and 1 ν_e PEPE in bin B. It was possible to claim that the PEPE is from an electron (anti)neutrino since the two cascades of a tau neutrino event can be resolved at these energies[8]. As expected, the normal hierarchy does not provide a sufficient decay of the ν_e flux with respect to the other flavours, and thus it is not possible to refit the flux as explained above. If one chose to refit the flux to obtain the 3 HESE in bin A, there would be too many expected Glashow resonance events in bin B. Similarly, fitting the flux to have 1 resonant event in bin B leads to too few HESE in bin A. Basically, the decaying being not important enough, it is as if it doesn't happen, and we still encounter the problems we aim to solve, *i.e.* the discrepancy between the HESE and Thμ fluxes, and the observed event rates. Thus, one can conclude that the normal hierarchy, considering that neutrino can decay, and either a $p\gamma$ or a neutron decay mechanism at source, fails to explain the observed event rates, thus fails to make the HESE and Thμ flux agree. The inverted hierarchy, on the other hand, allows to obtain a flux that explains the discrepancy between the two. For a spectral index comprised in $[-2.3,\ -2.1]$, *i.e.* compatible with the Thμ flux, a lifetime between $[1.43 \times 10^{-3}$ s/eV, 2.1×10^{-3} s/eV$]$ seems to be a suitable explanation if the mechanism at source is a $p\gamma$ interaction. If the neutrinos

[8]Let us nonetheless mention that we might actually only have observed the second cascade of a ν_τ event, the first one being outside the detector. This would mean that no Glashow Resonance event has been observed yet.

originate from neutron decay, the required lifetime would be one order of magnitude smaller. Our goal is to examine if we can get the HESE event rates to agree with the Thμ flux, therefore the fitting was done only for the best-fit spectral index, -2.19, and would correspond to a lifetime of 2.6×10^{-4} s/eV. As stated, all the fittings were done to account for 1 ν_e PEPE and no ν_e HESE in bin B, while also accounting for the 3 HESE observed in bin A. In all the cases where it was possible, there was actually 0.78 ν_e HESE observed in the higher energy bin during the 6 years of observation. This is a surprise, since we would have expected that number to vary depending on the spectral index or the mechanism at source. While it is smaller than 1, which implies no event was detected, it is statistically within the realm of detection.

To summarise, the problem studied in this work can be split into two key elements: a too low Glashow Resonance rate, and the disagreement between the HESE and Thμ fit fluxes. We focused on non-standard physics to try to explain the flavour discrepancies. The latter flux being much harder than the former, we focused on neutrino decay to see if it was possible, considering the Thμ flux at the source, to deplete significantly at least the ν_e component in order to explain the harder flux using through-going muons, *i.e.* the disappearance of HESE in bin B, and the partial disappearance of Glashow Resonance. It appears that it is possible to explain the observed event rates starting from the Thμ flux at the source, which undergoes neutrino decay in the inverted mass hierarchy, decreasing significantly the ν_e flavour up to $\sim 10^{6.5}$ GeV.

Results from future neutrino detectors operating at nearly the same energies and from further runs of IceCube itself will be crucial to resolving whether non-standard effects in ultrahigh energy neutrino propagation — and in what form — may explain the puzzles around flavour selectivity clearly seen with the current data. The planned KM3Net detector holds particular promise in this regard. It will be located in the northern hemisphere and, therefore, in consort with IceCube help conduct full-sky surveys of potential neutrino sources. In addition, KM3Net will be in a volume of approximately 5 km^3, meaning it will observe much more neutrinos that IceCube does. Both the complementary and the higher event rates will undoubtedly gives us more insight into to the mechanism at the origin of neutrinos. It would estimate the neutrino flux more accurately therefore potentially leading to the observation of non-standard physics or, in the absence of such, tighter constraint on them.

We have entered an unprecedented era of multimessenger physics involving ultrahigh energy cosmic rays and neutrinos on one hand and gravitational waves on the other. Our understanding of fundamental particle interactions will no doubt be guided by what secrets these multiple avenues uncover in the future and how they correlate, potentially leading to a unified theory of interactions. The study of ultrahigh energy neutrino will continue to be a key player in this venture.

Appendices

Appendix A

Feynman rules

In order to write cross section for different processes, some very useful rules exist. They allow us to reduce and simplify the computation one must do to obtain the cross section or the decay width of a process. Even though they will not be explained, they will be used in the following and therefore it is important to introduce them.

The Feynman diagrams that are shown in this work can be split into 2 parts: the vertices and the propagator(s). A vertex is the diagram that corresponds to a term in the interaction Lagrangian. For instance, if there is a term related to the interaction of 2 fermions and 1 boson in the Lagrangian, the corresponding vertew will consist in 2 fermionic lines (solid lines) and one bosonic line (wavy lines) that are linked at a given point. A propagator will be a line that links two vertices (e.g. the two bosonic lines of two vertices). In this section, we will present the different vertices and propagators used in this work.

A.1 Vertex of quantum electrodynamics

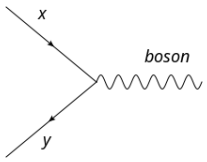

Figure A.1: Vertex of quantum electrodynamic. x and y can represent different particles and antiparticles, e.g. electron and positron respectively.

One can note that the direction of the arrow indicates if the line refers to a particle or an antiparticle. If one were to read the diagram from left to right, x would be a particle, whereas y would refer to an antiparticle. Please note some books consider that the diagram must be read differently, for instance from bottom to top. The bosonic line represents a boson that is involved in quantum electrodynamic process, *i.e.* a photon. The mathematical expression of such a vertex is

$$-ie\gamma^{\mu}$$

where e is the charge of the electron, and μ is and index that will be attributed to the intersection of several lines (here, the intersection between the three lines).

A.2 Vertex of weak interaction

The second vertex that we will use is the one with two fermionic lines and one bosonic line, the difference being that the boson belongs to the realm of the electroweak theory, so it can be a W^+, a W^- or a Z^0.

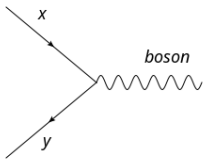

Figure A.2: Vertex of weak interaction. x and y can represent different particles, e.g. electron and positron respectively.

Even if the diagram looks the same, it actually represents different phenomena. As will be seen later, here the x and y can respectively be an electron and an antineutrino, and the boson can be a W^-, which wasn't possible before. The mathematical expression is

$$i\frac{g}{\sqrt{2}}\gamma^\mu\frac{1-\gamma^5}{2}$$

where g is the coupling constant of the weak interaction. [79]

A.3 Propagator

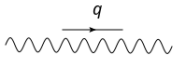

Figure A.3: Propagator of a boson. q is the four-momentum.

Once again, the diagram representing the propagator of a boson is the same no matter the boson, at least in QED and electroweak theory. However, the mathematical expression will differ. In the case of a photon, *i.e.* a massless boson, the propagator in Feynman's gauge would be

$$\frac{-ig^{\mu\nu}}{q^2}$$

where q is the four-current [80]. In this work, the propagator that will be used is the Proca's propagator. It describes a massive boson. We use it as, in the Glashow Resonance, the involved boson is a massive W^-. Its expression is

$$-i\frac{g^{\mu\nu}-\frac{q^\mu q^\nu}{M^2}}{q^2-M^2+iM\Gamma}$$

where M is the mass of the heavy boson, and Γ its decay width [80]. The appearance of the decay width implies that the particle is unstable.

Appendix B

Neutrino mixing and flavour ratio

In this part of the appendix, the theoretical prediction of the neutrino flavour ratio starting with an arbitrary one will be derived. In particular, the expected $\nu_e : \nu_\mu : \nu_\tau = 1 : 1 : 1$ starting from $1 : 2 : 0$ will be predicted analytically.

B.1 Flavour ratio after mixing

The three observed flavour of neutrinos, which are electron, muon and tau neutrino (written ν_e, ν_μ and ν_τ), are actually combinations of three mass eigenstates, written ν_1, ν_2 and ν_3. The link between the flavour and mass eigenstates, given by the PMNS matrix, is as follows:

$$\begin{pmatrix} \nu_e \\ \nu_\mu \\ \nu_\tau \end{pmatrix} = \begin{pmatrix} U_{e1} & U_{e2} & U_{e3} \\ U_{\mu 1} & U_{\mu 2} & U_{\mu 3} \\ U_{\tau 1} & U_{\tau 2} & U_{\tau 3} \end{pmatrix} \begin{pmatrix} \nu_1 \\ \nu_2 \\ \nu_3 \end{pmatrix}$$

What we are interested in is the probability of observing a neutrino ν_α when one has started with an initial state ν_β, where $\alpha, \beta = e, \mu, \tau$.

By using the above notation, the initial and final states can be written with the PMNS matrix:

$$|\nu_\alpha\rangle = \sum_{j=1}^{3} U_{\alpha j} |\nu_j\rangle , \quad |\nu_\beta\rangle = \sum_{k=1}^{3} U_{\beta k} |\nu_k\rangle$$

From the time evolution equation, the initial state will evolve as follows:

$$|\nu_\beta(t)\rangle = \sum_{k=1}^{3} U_{\beta k} |\nu_k\rangle e^{-iE_k t}$$

where E_k is the energy corresponding with the eigenstate k, and t the time.

The probability to observe a state $|\nu_\alpha\rangle$ while having started with a state $|\nu_\beta\rangle$ is given by:

$$P(\nu_\beta \to \nu_\alpha) = \left| \left(\sum_{j=1}^{3} U_{\alpha j} \langle \nu_j | \right) \left(\sum_{k=1}^{3} U_{\beta k} |\nu_k\rangle e^{-iE_k t} \right) \right|^2 \tag{B.1}$$

$$= \left| \sum_j U^*_{\alpha j} U_{\beta j} e^{-iE_j t} \right|^2 \tag{B.2}$$

$$= \sum_j U^*_{\alpha j} U_{\beta j} e^{-iE_j t} \sum_k U_{\alpha k} U^*_{\beta k} e^{iE_k t} \tag{B.3}$$

$$= \sum_{j,k} U^*_{\alpha j} U_{\beta j} U_{\alpha k} U^*_{\beta k} e^{-i\Delta E_{jk} t} \tag{B.4}$$

$$= \sum_j |U_{\alpha j}|^2 |U_{\beta j}|^2 + \sum_{j \neq k} U^*_{\alpha j} U_{\beta j} U_{\alpha k} U^*_{\beta k} e^{-i\Delta E_{jk} t} \tag{B.5}$$

with $\Delta E_{jk} = E_j - E_k$. Then, one adds and subtract the same quantity:

$$P(\nu_\beta \to \nu_\alpha) = \sum_j |U_{\alpha j}|^2 |U_{\beta j}|^2 + \sum_{j \neq k} U^*_{\alpha j} U_{\beta j} U_{\alpha k} U^*_{\beta k} e^{-i\Delta E_{jk} t} \pm \sum_{j \neq k} U^*_{\alpha j} U_{\beta j} U_{\alpha k} U^*_{\beta k} \tag{B.6}$$

$$= \sum_j |U_{\alpha j}|^2 |U_{\beta j}|^2 + \sum_{j \neq k} U^*_{\alpha j} U_{\beta j} U_{\alpha k} U^*_{\beta k} - \sum_{j \neq k} U^*_{\alpha j} U_{\beta j} U_{\alpha k} U^*_{\beta k} (1 - e^{-i\Delta E_{jk} t}) \tag{B.7}$$

The first two sums can be rewritten in a Kronecker delta:

$$\sum_j |U_{\alpha j}|^2 |U_{\beta j}|^2 + \sum_{j \neq k} U^*_{\alpha j} U_{\beta j} U_{\alpha k} U^*_{\beta k} = \sum_{j,k} U^*_{\alpha j} U_{\beta j} U_{\alpha k} U^*_{\beta k} \tag{B.8}$$

$$= \sum_j U^*_{\alpha j} U_{\beta j} \sum_k U_{\alpha k} U^*_{\beta k} \tag{B.9}$$

$$= |\sum_j U_{\alpha j} U_{\beta j}|^2 \tag{B.10}$$

$$= \delta_{\alpha\beta} \tag{B.11}$$

since the PMNS matrix is unitary. Therefore, the probability to observe a state $|\nu_\alpha\rangle$ if one started with $|\nu_\beta\rangle$ is, by taking $t = L$ where L[1] is the travelled distance:

$$P(\nu_\beta \to \nu_\alpha) = \delta_{\alpha\beta} - \sum_{j \neq k} U^*_{\alpha j} U_{\beta j} U_{\alpha k} U^*_{\beta k} (1 - e^{-i\Delta E_{jk} L})$$

If we consider that the traveled distance tends to infinity, the oscillatory part, *i.e.* the complex exponential is average and thus disappears. Hence the probability when $L \to \infty$ is:

$$P(\nu_\beta \to \nu_\alpha) = \sum_j |U_{\alpha j}|^2 |U_{\beta j}|^2$$

It can easily be seen that this probability is symmetric in α and β, meaning that $P(\nu_\beta \to \nu_\alpha) = P(\nu_\alpha \to \nu_\beta)$ We can then represent the different probabilities in a matrix P, which can be written

$$P \equiv \begin{pmatrix} P_{ee} & P_{e\mu} & P_{e\tau} \\ P_{e\mu} & P_{\mu\mu} & P_{\mu\tau} \\ P_{e\tau} & P_{\mu\tau} & P_{\tau\tau} \end{pmatrix} \equiv AA^T$$

[1] As we are in natural units, $c = 1$

where $A \equiv \begin{pmatrix} |U_{e1}|^2 & |U_{e2}|^2 & |U_{e3}|^2 \\ |U_{\mu 1}|^2 & |U_{\mu 2}|^2 & |U_{\mu 3}|^2 \\ |U_{\tau 1}|^2 & |U_{\tau 2}|^2 & |U_{\tau 3}|^2 \end{pmatrix}$

With the reasoning above, one is then able to determine the final neutrino flux, given an initial flux:

$$\begin{pmatrix} F(\nu_e) \\ F(\nu_\mu) \\ F(\nu_\tau) \end{pmatrix} = P \begin{pmatrix} F^0(\nu_e) \\ F^0(\nu_\mu) \\ F^0(\nu_\tau) \end{pmatrix} = AA^T \begin{pmatrix} F^0(\nu_e) \\ F^0(\nu_\mu) \\ F^0(\nu_\tau) \end{pmatrix}$$

B.2 Flavour ratio $\nu_e : \nu_\mu : \nu_\tau = 1 : 1 : 1$

In the following, an initial flux ratio of $F^0(\nu_e) : F^0(\nu_\mu) : F^0(\nu_\tau) = 1 : 2 : 0$ will be assumed. Let us first compute $A^T F^0$, where F^0 is the column vector of initial flux. One has:

$$A^T \begin{pmatrix} F^0(\nu_e) \\ F^0(\nu_\mu) \\ F^0(\nu_\tau) \end{pmatrix} = \begin{pmatrix} |U_{e1}|^2 & |U_{e2}|^2 & |U_{e3}|^2 \\ |U_{\mu 1}|^2 & |U_{\mu 2}|^2 & |U_{\mu 3}|^2 \\ |U_{\tau 1}|^2 & |U_{\tau 2}|^2 & |U_{\tau 3}|^2 \end{pmatrix} \begin{pmatrix} 1 \\ 2 \\ 0 \end{pmatrix} F^0(\nu_e) \tag{B.12}$$

$$= \begin{pmatrix} 1 \\ 1 \\ 1 \end{pmatrix} F^0(\nu_e) + \begin{pmatrix} |U_{\mu 1}|^2 - |U_{\tau 1}|^2 \\ |U_{\mu 2}|^2 - |U_{\tau 2}|^2 \\ |U_{\mu 3}|^2 - |U_{\tau 3}|^2 \end{pmatrix} \tag{B.13}$$

using the fact that the PMNS matrix is unitary [81]. Moreover, the experience tells us that the different terms $|U_{\mu i}|^2 - |U_{\tau i}|^2,\ i = 1, 2, 3$ are $\ll 1$. The second term can therefore be neglected. Finally, to obtain the final flux, one needs to multiply by the matrix A. Using the fact that the PMNS matrix is unitary once again, one has

$$A \begin{pmatrix} 1 \\ 1 \\ 1 \end{pmatrix} = \begin{pmatrix} 1 \\ 1 \\ 1 \end{pmatrix}$$

hence

$$\begin{pmatrix} F(\nu_e) \\ F(\nu_\mu) \\ F(\nu_\tau) \end{pmatrix} = \begin{pmatrix} 1 \\ 1 \\ 1 \end{pmatrix} F^0(\nu_e)$$

The column vector in front of $F^0(\nu_e)$ tells us that if one starts with a flux ratio of $1 : 2 : 0$, one will end up with one of $1 : 1 : 1$.

Appendix C

Narrow-Width Approximation

The approximation states

$$\frac{1}{(s-M^2)^2+M^2\Gamma^2} \to \frac{\pi}{M\Gamma}\delta(s-M^2)$$

as Γ tends to zero.

In order to prove it, one needs to take this definition of the Dirac's delta distribution:

$$\delta(x) = \frac{1}{\pi}\lim_{\epsilon\to 0}\frac{\epsilon}{\epsilon^2+x^2} \text{ [82]}$$

What we want to demonstrate can be rewritten

$$\frac{M\Gamma}{\pi(y^2+M^2\Gamma^2)} = \delta(y)$$

with $y = s - M^2$. To prove that the narrow width approximation is right, we will have to choose the right expression for ϵ and x. As two δ's have been isolated, one can equal the two other sides of the equality:

$$\frac{M\Gamma}{\pi(y^2+M^2\Gamma^2)} = \frac{1}{\pi}\frac{\epsilon}{\epsilon^2+x^2}$$

which is true if one chooses $\epsilon = M\Gamma$ and $x^2 = y^2 = s - M^2$. Thus, we can write:

$$\frac{1}{\pi}\lim_{\epsilon\to 0}\frac{\epsilon}{\epsilon^2+x^2}\bigg|_{\epsilon=M\Gamma, x^2=s-M^2} = \frac{1}{\pi}\lim_{M\Gamma\to 0}\frac{M\Gamma}{M^2\Gamma^2+(s-M^2)^2}$$

Moreover, $M\Gamma \to 0$ is equivalent to $\Gamma \to 0$ as the mass is fixed and different from 0.

Appendix D

Glashow resonance cross section

The quantum process of the Glashow resonance consists in an incident electron antineutrino that will interact with an electron through a weak boson, and produce a pair of particles which can be an electron-positron pair, a muon-antimuon pair, etc.

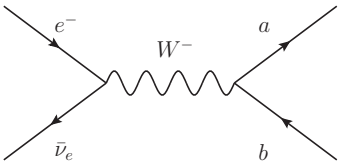

Figure D.1: Glashow Resonance. The boson is a negative weak boson, which implies that Weak Interaction is considered. x and y are unspecified particles and antiparticles.

In this appendix will be presented the general outlines of the computation of the cross section of this process. The different properties that are used will be explained, whereas the simple computation that do not require any particular subtleties will be skipped.

To compute the cross section, one needs the vertex that corresponds to two fermionic lines and one bosonic line in the weak interaction framework, as well as the Proca propagator, which corresponds to the propagation of a massive boson. Their expression can be seen in appendix A. For the propagator, the second part of the numerator will be dropped, since its contribution will be zero. It will be shown during the mathematical derivations. One also needs to introduce the γ_5 matrix, which is defined using the 4 Dirac's gamma matrices:

$$\gamma_5 \;=\; i\gamma_0\gamma_1\gamma_2\gamma_3$$

This new matrix has several properties: $(\gamma_5)^\dagger = \gamma_5, \quad (\gamma_5)^2 = \gamma_5, \quad \gamma_5, \gamma_\mu = 0.$

First, we need to compute the amplitude of the process. In the following, these notations will be used: p and k will correspond to the electron and antineutrino 4-momentum, p' and k' to the outgoing unspecified x and y particles, and q to the 4-momentum of the boson. The diagram of the "squared" amplitude is then:

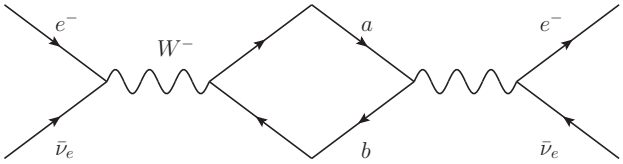

Figure D.2: Squared processed of the Glashow Resonance. It consists in putting the conjugate of the process after the real one, which allows to compute the cross section.

One must compute the traces of all the fermionic loops. First, let us compute the one that expands on both edges. One has

$$Tr(\gamma_\alpha(1-\gamma_5)\ \gamma\cdot p\ \gamma_\nu\ (1-\gamma_5)\ \gamma\cdot k)(\frac{iA}{2})^2 \tag{D.1}$$

Before going further, it can be shown why the second term of the propagator can be dropped. It contains $q_\mu q_\nu$ with $q = p + k$. Let us look at what would be the contribution of q_μ. It would mean multiplying the trace by k_μ, by p_μ and then summing the 2. The first term would then be $Tr(\gamma\cdot\ k\ ...\ \gamma\cdot k)$. As it is cyclic, it can be rewritten $Tr(...\ \gamma\cdot\ k\ \gamma\cdot k) = k^2 Tr(...) = 0$ since $k^2 = 0$. The same can be said if the trace were multiplied by p_μ. Moreover, the same contribution would be obtained by multiplying the trace by q_ν. Thus, since the contribution of the second part of the propagator is null, it can be dropped, as it was stated above.

By distributing and using $Tr(A + B) = Tr(A) + Tr(B)$, only two different traces need to be computed. These are the following:

$$Tr(\gamma_\alpha\ \gamma\cdot p\ \gamma_\nu\ \gamma\cdot k) = 4(k_\alpha p_\nu + p_\alpha k_\nu - p\cdot k g_{\alpha\nu}) \tag{D.2}$$

$$Tr(\gamma_\mu\ \gamma\cdot p\ \gamma_\nu\ \gamma_5\ \gamma\cdot k) = p^\gamma k^\delta 4i\epsilon_{\alpha\gamma\nu\delta} \tag{D.3}$$

using

$$Tr(a\cdot\gamma\ b\cdot\gamma\ c\cdot\gamma\ d\cdot\gamma) = 4(a\cdot b\ c\cdot d + a\cdot d\ b\cdot c - a\cdot c\ b\cdot d)$$
$$Tr(\gamma^5\gamma^\mu\gamma^\nu\gamma^\tau\gamma^\sigma) = -4i\epsilon^{\mu\nu\tau\sigma}$$

The trace is then:

$$2A^2(k_\alpha p_\nu + p_\alpha k_\nu - p\cdot k\ g_{\alpha\nu} - i\epsilon_{\alpha\gamma\nu\delta}p^\gamma k^\delta) \tag{D.4}$$

The other trace corresponding to the other fermionic loop must be computed as well. Here, one has:

$$Tr(\gamma^\beta(1-\gamma^5)\ \gamma\cdot k'\ \gamma^\mu\ (1-\gamma^5)\ \gamma\cdot p')(\frac{iA}{2})^2$$

By doing the same process as for the first trace, one also obtains 4 traces to compute, where only 2 are different. These are:

$$Tr(\gamma^\beta\ \gamma\cdot k'\ \gamma^\mu\ \gamma\cdot p') = 4(p'^\beta k'^\mu + k'^\beta p'^\mu - p'\cdot k' g^{\mu\beta}) \tag{D.5}$$

$$Tr(\gamma^\beta\ \gamma\cdot k'\ \gamma^\mu\ \gamma_5\gamma\cdot p') = p'_\rho k'_\sigma 4i\epsilon^{\beta\rho\mu\sigma} \tag{D.6}$$

Once it has been multiplied by $g^{\mu\nu}g^{\alpha\beta}$, *i.e.* when the indices are propagated, the trace of the second loop is then:

$$2A^2(p'^\nu k'^\alpha + p'^\alpha k'^\nu - p'\cdot k' g^{\alpha\nu} - i\epsilon^{\nu\rho\alpha\sigma}p_\rho k_\sigma) \tag{D.7}$$

In order to obtain the square amplitude, we need to multiply the two traces and the propagator[1]. First, let us do the product of the traces. Tr_A will refer to the first trace that was computed, whereas Tr_B will refer to the second one.

$$Tr_A\ Tr_B\ = 4A^4(2k\cdot k'\ p\cdot p'\ +\ 2k\cdot p'\ p\cdot k'\ - p^\gamma k^\delta k'_\sigma p'_\rho \epsilon_{\alpha\gamma\nu\delta}\epsilon^{\nu\rho\alpha\sigma}) \tag{D.8}$$

To obtain this expression, several terms have vanished. Indeed, the terms that contained $g_{\alpha\nu}\epsilon^{\nu\omega\mu\alpha}$ (or anything similar) are equal to zero, because $g_{\alpha\nu}$ is different than zero only if $\alpha = \nu$, which imply that the 4 dimensional Levi-Civita symbol is equal to zero, as 2 of its indices are then equal. Moreover, the four terms that contain a Levi-Civita symbol compensate two by two. It can be shown for two of them:

$$\begin{aligned} k_\alpha p_\nu k'_\sigma p'_\rho \epsilon^{\nu\rho\alpha\sigma}\ +\ k_\nu p_\alpha k'_\sigma p'_\rho \epsilon^{\nu\rho\alpha\sigma} &= k_\alpha p_\nu k'_\sigma p'_\rho \epsilon^{\nu\rho\alpha\sigma}\ +\ k_\alpha p_\nu k'_\sigma p'_\rho \epsilon^{\alpha\rho\nu\sigma} \\ &= k_\alpha p_\nu k'_\sigma p'_\rho \epsilon^{\nu\rho\alpha\sigma}\ -\ k_\alpha p_\nu k'_\sigma p'_\rho \epsilon^{\nu\rho\alpha\sigma} \\ &= 0 \end{aligned}$$

by renaming the indice μ and ν in the second term in the first equality, and using the fact that the Levi-Civita symbol is anti-symmetric ($\epsilon_{\mu\nu\tau\sigma} = -\epsilon_{\nu\mu\tau\sigma}$).

Using the following relation involving the product of 2 Levi-Civita:

$$\epsilon_{\mu\nu\tau\sigma}\ \epsilon^{\mu\nu\omega\alpha}\ =\ 2(\delta_{\tau\omega}\delta_{\sigma\alpha}\ -\ \delta_{\alpha\tau}\delta_{\omega\sigma}),$$

the last term of the product of the traces becomes:

$$p^\tau k^\sigma k'_\omega p'_\alpha \epsilon_{\mu\nu\tau\sigma}\epsilon_{\nu\omega\mu\alpha} = p^\tau k^\sigma k'_\omega p'_\alpha 2(\delta_{\tau\omega}\delta_{\sigma\alpha}\ -\ \delta_{\alpha\tau}\delta_{\omega\sigma}) \tag{D.9}$$

$$= 2(p\cdot k'\ p'\cdot k - p\cdot p'\ k\cdot k') \tag{D.10}$$

Injecting this into the product of the two traces yields:

$$Tr_A Tr_B\ =\ 16A^4\ p\cdot k'\ k\cdot p' \tag{D.11}$$

The total square amplitude averaged on the spin is then the product of the two traces, multiplied by the two propagators, multiplied by a factor 1/2. The factor comes from the fact that we average over all possible electron spin. We don't average over the antineutrino since there is only one chirality.

$$|\overline{M}|^2 = \frac{1}{2}16A^4\ p\cdot k'\ k\cdot p'\ \left|\frac{1}{q^2 - M^2 + iM\Gamma}\right|^2 \tag{D.12}$$

To go further, the Mandelstam invariants must be introduced. They are noted s, t and u and are defined as follows:

$$s = (p+k)^2 = 2p\cdot k\ (\text{as } p\cdot p = 0 \text{ for all 4-momentum}) = 2p'\cdot k' \tag{D.13}$$

$$t = (p-p')^2 = (k-k')^2 = -2p\cdot p' = -2k\cdot k' \tag{D.14}$$

$$u = (p-k')^2 = (p'-k)^2 = -2p\cdot k' = -2p'\cdot k \tag{D.15}$$

Also, by choosing the frame of reference to be in the center-of-mass frame, one has the following

[1] Actually, we have already partly included the propagators as we propagated the indices using the g tensor.

decomposition:

$$
\begin{aligned}
p &= \left(\frac{\sqrt{s}}{2}, 0, 0, \frac{\sqrt{s}}{2}\right) \\
k &= \left(\frac{\sqrt{s}}{2}, 0, 0, \frac{\sqrt{s}}{2}\right) \\
p' &= \left(\frac{\sqrt{s}}{2}, \frac{\sqrt{s}}{2}\sin\theta\cos\phi, \frac{\sqrt{s}}{2}\sin\theta\sin\phi, \frac{\sqrt{s}}{2}\cos\theta\right) \\
k' &= \left(\frac{\sqrt{s}}{2}, -\frac{\sqrt{s}}{2}\sin\theta\cos\phi, -\frac{\sqrt{s}}{2}\sin\theta\sin\phi, \frac{\sqrt{s}}{2}\cos\theta\right)
\end{aligned}
$$

One can then write

$$p \cdot k' = k \cdot p' = \frac{s}{4}(1 + \cos\theta)$$

By considering this, one can write

$$|\overline{M}|^2 = \frac{1}{2} 16 A^4 \; p \cdot k' \; k \cdot p' \; \left| \frac{1}{q^2 - M^2 + iM\Gamma} \right|^2 \tag{D.16}$$

$$= \frac{1}{2} A^4 \; s^2 \; (1 + \cos\theta)^2 \frac{1}{(s - M^2)^2 + M^2\Gamma^2} \tag{D.17}$$

Once this expression has been obtained, the differential cross section can be as well. For a $2 \to 2$ process, in the center-of-mass frame of reference, the general expression for the differential cross section is:

$$\frac{d\sigma}{d\Omega} = \frac{1}{64\pi^2 s} |\overline{M}|^2 \tag{D.18}$$

To obtain the total cross section, D.18 must be integrated over all solid angles:

$$\sigma = \int \frac{d\sigma}{d\Omega} d\Omega \tag{D.19}$$

$$= \int \frac{d\sigma}{d\Omega} d\phi d(\cos\theta) \tag{D.20}$$

$$= \frac{1}{64\pi^2} \frac{A^4}{3} \frac{s}{(s - M)^2 + M^2\Gamma^2} \frac{8}{3} 2\pi \tag{D.21}$$

$$= \frac{g^4}{48\pi} \frac{1}{2} \frac{s}{(s - M^2)^2 + M^2\Gamma^2} \tag{D.22}$$

by replacing $A = g/\sqrt{2}$.

Considering that the Fermi coupling constant is defined by $G_F = \frac{\sqrt{2}}{8} \frac{g^2}{M^2}$ [83] in natural units, and that one has $s = 2p \cdot k = 2mE_\nu$, the cross section of the Glashow resonance is given by

$$\sigma = \frac{4}{3} \frac{G_F^2 m E_\nu}{2\pi} \frac{M^4}{(M^2 - 2mE_\nu)^2 + M^2\Gamma^2} \tag{D.23}$$

Bibliography

[1] IceCube Collaboration. Icecube pushes neutrinos to the forefront of astronomy. https://icecube.wisc.edu/news/view/171. Visited on 30/04/2020.

[2] IceCube Collaboration. Research highlights: Neutrino astronomy and multimessenger astrophysics. https://icecube.wisc.edu/science/highlights/neutrino_astronomy. Visited on 30/04/2020.

[3] Neutrinos! http://www.astro.wisc.edu/~larson/Webpage/neutrinos.html. Visited on 15/11/2019.

[4] J.-R. Cudell. SPAT0021-1 Introduction to astroparticles. 2018-2019.

[5] Nobel-winning discovery of neutrino oscillations, proving that neutrinos have mass. https://phys.org/news/2015-12-nobel-winning-discovery-neutrino-oscillations-neutrinos.html. Visited on 15/11/2019.

[6] Super-kamiokande finds neutrino mass. https://physicsworld.com/a/super-kamiokande-finds-neutrino-mass/. Visited on 15/11/2019.

[7] Kit - katrin - neutrino physics. https://www.katrin.kit.edu/67.php. Visited on 07/11/2019.

[8] Standard model of fundamental particles and interactions. https://web.archive.org/web/20160304133522/https://www.pha.jhu.edu/~dfehling/particle.gif. Visited on 14/12/2019.

[9] A first look at how the earth stops high-energy neutrinos in their tracks. https://icecube.wisc.edu/news/view/546. Visited on 16/12/2019.

[10] U.F. Katz and Ch. Spiering. High-Energy Neutrino Astrophysics: Status and Perspectives. 2011.

[11] Abtin Narimani. Freeze-Out of Particles. 2016.

[12] Neutrinos from the Sun. http://www.sns.ias.edu/~jnb/Papers/Popular/Scientificamerican69/scientificamerican69.html. Visited on 24/09/2019.

[13] Radioactivity: Solar neutrinos. https://www.radioactivity.eu.com/site/pages/Solar_Neutrinos.htm. Visited on 20/05/2020.

[14] Neutrinos from Supernovae. http://hep.bu.edu/~superk/gc.html. Visited on 24/09/2019.

[15] The Dawn of a New Era for Supernova 1987a. https://www.nasa.gov/feature/goddard/2017/the-dawn-of-a-new-era-for-supernova-1987a. Visited on 24/09/2019.

[16] Thomas K. Gaisser, Francis Halzen, and Todor Stanev. Particle Astrophysics with High Energy Neutrinos. 1994.

[17] Aya Ishihara. Extremely high energy neutrinos in six years of IceCube data. *J. Phys.: Conf. Ser.718 062027*, 2016.

[18] Shawn Westerdale. Neutrino Mass Problem: Masses and Oscillations. 2010.

[19] Antonio Ereditato. *The State of the Art of Neutrino Physics - A Tutorial for Graduate Students and Young Researchers*, pages 72–73. World Scientific, 2018.

[20] Lecture notes on neutrino oscillations in matter. https://hepwww.pp.rl.ac.uk/users/Ricciardi/Lectures/MSW-1.pdf. Visited on 19/11/2019.

[21] v4.1: Three-neutrino fit based on data available in July 2019 | NuFIT. http://www.nu-fit.org/?q=node/211. Visited on 08/11/2019.

[22] Neutrino mass, mixing, and oscillations. http://pdg.lbl.gov/2016/reviews/rpp2016-rev-neutrino-mixing.pdf. Visited on 01/10/2019.

[23] L. Wolfenstein. Neutrino oscillations in matter. 1978.

[24] Carlo Giunti and Chung W. Kim. *Fundamentals of Neutrino Physics and Astrophysics*, pages 135–179. OXFORD, 2007.

[25] Neutrino mass hierarchy : Hyper-kamiokande. http://www.hyper-k.org/en/physics/phys-hierarchy.html. Visited on 15/11/2019.

[26] Is the neutrino its own antiparticle? https://www.sciencedaily.com/releases/2016/01/160129091842.htm. Visited on 15/11/2019.

[27] Ivan Esteban, M. C. Gonzalez-Garcia, Alvaro Hernandez-Cabezudo, MicheleMaltoni, and Thomas Schwetz. Global analysis of three–flavour neutrino oscillations: synergies and tensions in the determination of θ_{23}, δ_{CP}, and the mass ordering. 2018.

[28] Structure evidence from deep inelastic scattering. http://hyperphysics.phy-astr.gsu.edu/hbase/Nuclear/scatele.html. Visited on 14/12/2019.

[29] Francesco Blanco, P.La Rocca, and Francesco Riggi. Cosmic rays with portable Geiger counters: From sea level to airplane cruise altitudes. 2009.

[30] Matthew G. BARING. DIFFUSIVE SHOCK ACCELERATION: THE FERMI MECHANISM. 1997.

[31] A. Gallo Rosso, C. Mascaretti, A. Palladino, and F. Vissani. Introduction to neutrino astronomy. 2018.

[32] Cosmic rays energues | cosmos. http://astronomy.swin.edu.au/cosmos/C/Cosmic+Ray+Energies. Visited on 16/12/2019.

[33] Active Galaxies and Quasars - Introduction. https://imagine.gsfc.nasa.gov/science/objects/active_galaxies1.html. Visited on 24/09/2019.

[34] Steve Boyd. *Neutrino Detectors and Sources*, page 26. 2016.

[35] Antonio Ereditato. *The State of the Art of Neutrino Physics - A Tutorial for Graduate Students and Young Researchers*, page 332. World Scientific, 2018.

[36] Tadej Novak. Detection of high-energy neutrinos in the IceCube experiment. 2015.

[37] P. Mészáros. Gamma Ray Bursts as Neutrino Sources. 2015.

[38] Antonio Ereditato. *The State of the Art of Neutrino Physics - A Tutorial for Graduate Students and Young Researchers*, page 350. World Scientific, 2018.

[39] Antonio Ereditato. *The State of the Art of Neutrino Physics - A Tutorial for Graduate Students and Young Researchers*, page 361. World Scientific, 2018.

[40] A. Mücke, J.P. Rachen, R. Engel, R.J. Protheroe, and T. Stanev. Photomeson production in astrophysical sources. 1999.

[41] Eli Waxman and John Bahcall. High Energy Astrophysical Neutrinos: the Upper Bound is Robust. 2000.

[42] Eli Waxman and John Bahcall. High Energy Neutrinos from Astrophysical Sources: An Upper Bound. 1998.

[43] IceCube South Pole Neutrino Observatory – Detector. https://icecube.wisc.edu/science/icecube/detector. Visited on 03/09/2019.

[44] Thorsten Gluesenkamp. On the Detection of Subrelativistic Magnetic Monopoles with the IceCube Neutrino Observatory. 2010.

[45] A. Karle et al. IceCube - the next generation neutrino telescope at the South Pole. *arXiv:astro-ph/0209556v1*, 2002.

[46] HyperPhysics - Leptons. http://hyperphysics.phy-astr.gsu.edu/hbase/Particles/lepton.html. Visited on 16/09/2019.

[47] Aidan Bohenick. Kinematics of Tau Lepton Decays. 2019.

[48] Leptons. http://hyperphysics.phy-astr.gsu.edu/hbase/Particles/lepton.html. Visited on 20/05/2020.

[49] The detection of neutrinos in icecube. https://masterclass.icecube.wisc.edu/en/learn/detecting-neutrinos. Visited on 04/10/2019.

[50] The tau neutrino hunt is now in full swing. https://icecube.wisc.edu/news/view/363. Visited on 04/10/2019.

[51] Raj Gandhi, Chris Quigg, Mary Hall Reno, and Ina Sarcevic. Ultrahigh-energy neutrino interactions. *Astroparticle Physics 5 81-110*, 1996.

[52] U.F Katz and Ch. Spiering. High-Energy Neutrino Astrophysics: Status and Perspectives. 2011.

[53] Andreas Höcker and Vakhtang Kartvelishvili. SVD Approach to Data Unfolding. 1995.

[54] Unfolding of atmospheric neutrino spectrum with ic9 data unblinding proposal. https://icecube.wisc.edu/~zornoza/unfolding-unblinding/. Visited on 26/11/2019.

[55] M.G. Aaarsten et al. Energy Reconstruction Methods in the IceCube Neutrino Telescope. 2014.

[56] M.G. Aaarsten et al. Evidence for High-Energy Extraterrestrial Neutrinos at the IceCube Detector. 2013.

[57] Markus Ahlers and Francis Halzen. Opening a New Window onto the Universe with IceCube. 2018.

[58] Atri Bhattacharya, Raj Gandhi, Werner Rodejohann, and Atsushi Watanabe. The Glashow resonance at IceCube: signatures, event rates and pp vs. $p\gamma$ interactions. 2011.

[59] Anne Schukraft. Search for a diffuse flux of extragalactic neutrinos with the IceCube Neutrino Observatory. 2013.

[60] Search for contained neutrino events at energies above 30 TeV in 2 years of data (released 21 Nov 2013). `https://icecube.wisc.edu/science/data/HE-nu-2010-2012`. Visited on 24/09/2019.

[61] The IceCube Collaboration. Characterization of the Astrophysical DiffuseNeutrino Flux with IceCube High-Energy StartingEvents. 2019.

[62] Soumya Sadhukhana Subhendra Mohanty, Ashish Narang. Cutoff of IceCube Neutrino Spectrum due to t-channel Resonant Absorption by $C_\nu B$. 2019.

[63] Daniele Fargion, Pietro Oliva, Pier Giorgio De Sanctis Lucentini, Daniele D'Armiento, and Paolo Paggi. UHECR narrow clustering correlating IceCube through-going muons. 2017.

[64] Sheldon L. Glashow. Resonant Scattering of Antineutrinos. 1959.

[65] W. Hollik. Quantum field theory and the Standard Model. 2010.

[66] Dhiman Chakraborty. PHYS 684 Introduction to High Energy Physics. 2010.

[67] Lu Lu, Christian Haack, and Tianlu Yuan. Icecube recent results : Hint of first glashow resonance & the possible first neutrino source. `https://indico.in2p3.fr/event/17063/contributions/64241/attachments/50397/64308/UHECR_Paris_Lu_upload.pdf`. Visited on 30/03/2020.

[68] Hans Niederhausen. Diffuse high energy neutrino fluxes results from icecube. `https://indico.cern.ch/event/768000/contributions/3274999/attachments/1814679/2965380/NuTel19_IceCube_Diffuse_Niederhausen.pdf`. Visited on 30/03/2020.

[69] C. Haack and C. Wiebusch. A measurement of the diffuse astrophysical muonneutrino flux using eight years of icecube data. `https://pos.sissa.it/301/1005/pdf`. Visited on 30/03/2020.

[70] Pierre MAGAIN. PHYS0931-1 Traitement des données. 2019-2020.

[71] J.Bernabéu, S.Palomares-Ruiz, A.Pérez, and S.T.Petcov. The earth Mantle-Core effect in charge-asymmetries for atmospheric neutrino oscillations. 2002.

[72] A. Yu. Smirnov. The msw effect and neutrino astrophysics. `http://www1.na.infn.it/wsubnucl/cosm/icarus/seminars/smirnovMSW.pdf`. Visited on 30/03/2020.

[73] Atri Bhattacharya, Sandhya Choubey, Raj Gandhi, and Atsushi Watanabe. Ultra-high energy neutrino fluxes as a probe for - Interplay astrophysical of energy neutrino dependent flavor ratios and new physics effects non-standard physic. 2010.

[74] Atri Bhattacharya, Sandhya Choubey, Raj Gandhi, and Atsushi Watanabe. Diffuse ultra-high energy neutrino fluxes and physics beyond the Standard Model. 2010.

[75] Mikhail Bilenky and Arcadi Santamaria. Bounding Effective Operators at the One-Loop Level:The Case of Four-Fermion Neutrino Interactions. 1994.

[76] Mikhail Bilenky and Arcadi Santamaria. "SECRET" NEUTRINO INTERACTIONS. 1999.

[77] Philipp Baerwald, Mauricio Bustamante, and Walter Winter. Neutrino decays over cosmological distances and the implications for neutrino telescopes. 2012.

[78] Celio A. Moura and Marcelo M. Guzzo. New analyses of double-bang events in the atmosphere. 2008.

[79] Jorge Crispim Romão. Advanced Quantum Field Theory. page 384, 2015.

[80] J.-R. Cudell. SPAT0162-1 Quantum Field Theory. 2018-2019.

[81] H.Athar, M. Jezabek, and O. Yasuda. Effects of neutrino mixing on high-energy cosmic neutrino flux. 2000.

[82] Delta function – from wolfram mathworld. `https://mathworld.wolfram.com/DeltaFunction.html`. Visited on 17/08/2019.

[83] Michael E. Peskin and Daniel V. Schroeder. *An Introduction to Quantum Field Theory*, page 559. Addison-Wesley Publishin Company, 1995.